Some Transport Properties of Sodium Chloride

A thesis submitted
in supplication for the
Degree of Doctor of Philosophy

by

Kenneth George McQuhae
B.A.Sc. (British Columbia 1965)

March 1969

Department of Metallurgy
Imperial College of Science and Technology
University of London

Abstract

The conductance of cations 'injected' into tilt boundaries in NaCl is measured and the activation energies of motion for Na^+, K^+ and Cs^+ ions calculated to be 0.32 ± .03 eV, 0.55 ± .03 eV and 0.65 ± .03 eV respectively. Purification of the NaCl before the growth of bicrystals ensured that the effect did not arise from impurity segregation.

The enhanced conductance indicates a high vacancy density in the boundary region while the dependence of the energy of motion on the ion size indicates a structure with discrete sites rather than a 'liquid' grain boundary structure. The lack of dependence of the energy of motion with the angle of misorientation is interpreted as arising from a common vacancy mechanism of motion. The anisotropic behaviour of the conductance for low angle boundaries, dependent on the direction within the boundary plane, is interpreted in terms of a columnar dislocation structure, while an 'island' structure model is more appropriate for high angle boundaries.

The energy of motion for Na^+ ions is compared with the literature on motion in dislocations, and on motion in grain boundaries and dislocations in LiF.

Surface potential profile experiments indicate the absence of surface layers of enhanced resistivity, which were previously reported. The previous results are interpreted in terms of effects arising from the measuring circuit. Conductivity measurements on bicrystals exhibited no anomalous polarization arising from the grain boundary.

Table of Contents

Table of Contents

Table of Contents

CHAPTER 1

INTRODUCTION AND LITERATURE REVIEW

1-1 General Introduction

Diffusion, conductivity and more recently, nuclear magnetic resonance techniques have been used to investigate the transport of matter in ionic crystals. The earlier investigators of sodium chloride, using polycrystalline material or natural single crystals of rock salt, recognised that the specimens exhibited intrinsic behaviour at elevated temperatures but were structure sensitive at lower temperatures. Theoretical calculations indicated for many NaCl-type alkali halides that ion transport was dependent on point defects. These were confirmed to be Schottky defects, pairs of cation and anion vacancies. Further, cation vacancy motion was established as the predominant charge carrier, anion motion contributing only at higher temperatures and electrons contributing only slightly to the total conduction. Diffusion data for cation and anion motion confirmed the greater mobility of cation vacancies. In recent years, the growth of artificially 'doped' as well as high purity single crystals has enabled researchers to investigate the defect structure more fully and to resolve the predominant structure in various temperature regions. Activation energies for the formation and motion of the defects affecting the mobility of ions are well documented, even if somewhat uncertain.

In many of the previous studies, little attention has been paid to the effect of free surfaces or grain boundaries on the measured parameters. Some effect was often suspected, but for the most part it was ignored or considered negligible. Surface and grain boundary diffusion in metals has received more attention than in ceramic or ionic systems. Few

investigations have been made of surface or grain boundary conductivity. As an instance of the importance of surface conductivity in ceramics, a recent study[1] was made on Al_2O_3, taking care to eliminate or subtract out the bulk and atmospheric contributions. The resultant curves for the temperature dependence of the surface conductivity showed a striking resemblance to the curves often previously reported to be bulk conductivity. Further studies[2], eliminating surface effects, gave a very different result for bulk conductivity. As conductivity in NaCl is ionic rather than electronic (as in pure Al_2O_3), and as the bulk current is much larger, surface effects are not expected to cause such large discrepancies.

Various researchers have postulated models for ionic crystals in which surface layers exhibit different electrical properties than the bulk. That is, the defects responsible for ion transport or other defects that can affect ion mobility are concentrated in surface regions. Grain boundary conduction effects are most often attributed to 'pipe' diffusion in the 'dislocation array' forming the boundary, but this analysis breaks down for large angle boundaries. Much more work is necessary to resolve the operative mechanisms.

This thesis then, will describe the experiments carried out by the author on the charge transport properties of grain boundary and surface regions. The remainder of this chapter will discuss briefly the structure of surface regions and grain boundaries and in more detail, the literature on ion transport in boundary regions. As the primary method of investigation was electrical conductivity, brief sections are included on the theoretical considerations of ion and charge transport.

1-2 Defects in Sodium Chloride

The Perfect Lattice

The NaCl-type of crystal lattice consists of two interpenetrating fcc lattices, one for cations and the other for anions. A unit cell of the perfect structure is shown in Figure 1. The bonds in alkali halides are almost entirely ionic, meaning that a transfer of electrons has occurred and that the resultant ions have an electrostatic attraction for each other. Transport of matter is associated with transport of charge because of the charged nature of the diffusing species. The large band gap between the energies of the valence and conduction bands preclude any major contribution to the transport of charge from electron motion.

In the perfect lattice the transport of ions would mean that two ions on adjacent lattice sites must exchange places. These ions would have to squeeze past each other, passing through spatial positions of large electrostatic repulsion. Further, the exchange can only occur between species of the same polarity as the repulsive forces prohibit an exchange into the sublattice of the other ion. The mechanism of movement then can only be explained in terms of the presence and movement of defects or imperfections in the lattice structure.

Point Defects

Van Bueren[3] gives an excellent summary of imperfections in all types of crystal systems. Frenkel defects, a vacancy on a lattice site and an interstitial atom, are present in many systems. Schottky disorder however, predominates in

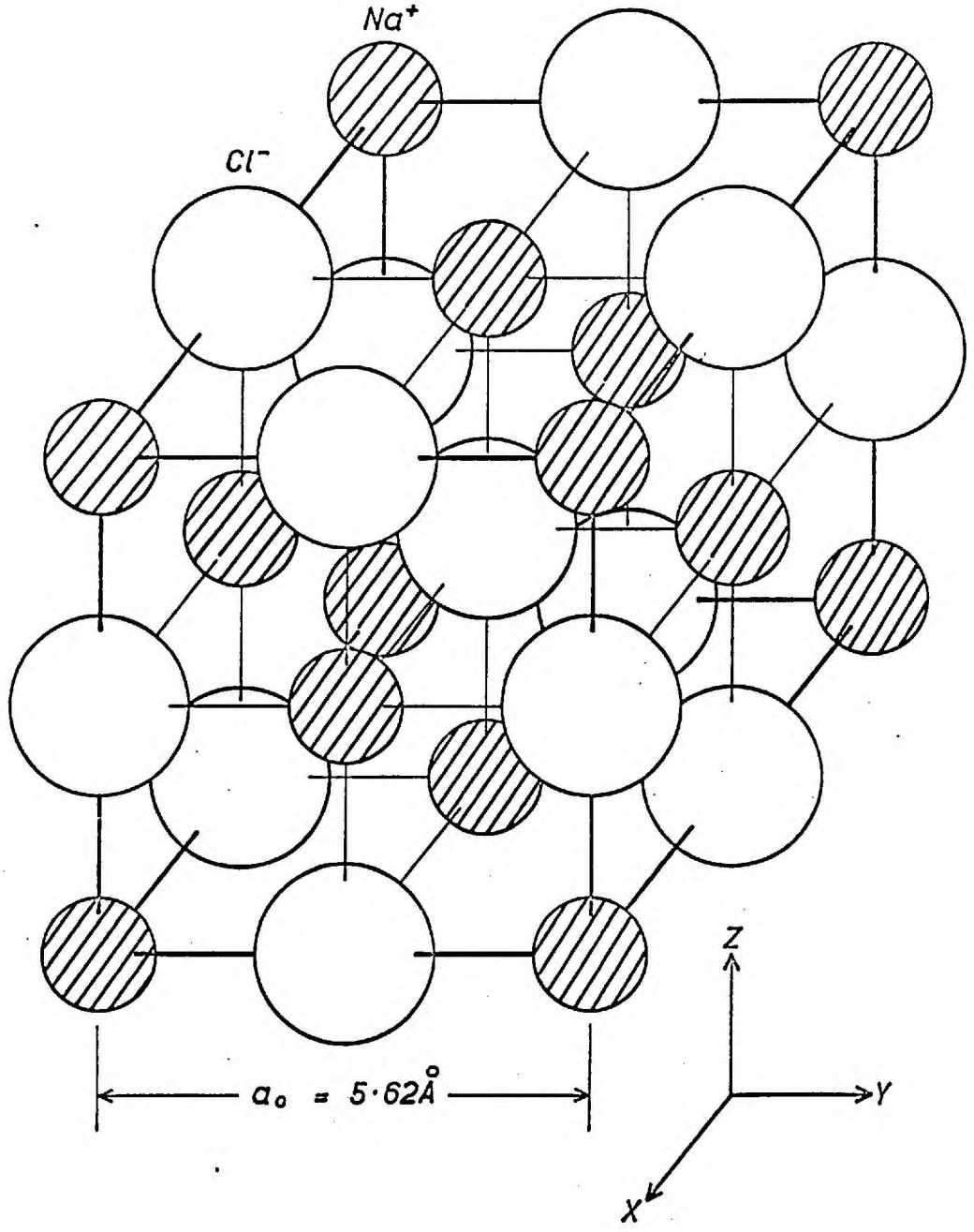

Fig. 1. UNIT CELL OF NaCl

the alkali halides due to the lower energy of formation. Many sources give rigorous calculations for the equilibrium number of vacancies present in a crystal. A brief account will be presented here. Consider an ionic system with N cation and N anion sites, and let n_{vc} and n_{va} be the number of vacant cation and anion sites respectively. The vacancies can be arranged in $\binom{N!}{n!}$ different ways and the introduction of these vacancies will increase the configurational entropy of the system by

$$\Delta S_c = k \ln \frac{N!}{(N-n_{vc})!n_{vc}!} \frac{N!}{(N-n_{va})!n_{va}!} . \qquad (1)$$

At equilibrium, consider that the overall charge balance must be zero and $n_{vc} = n_{va}$. Equation 1 may be rewritten,

$$\Delta S_c = 2 k \ln \frac{N!}{(N-n)!n!} , \qquad (2)$$

where n now represents the number of vacancy pairs. ΔS_c can also be considered to be the entropy of mixing a dilute (ideal) solution of vacancies in the system. The enthalpy increase of the system is given by

$$\Delta H = n \Delta E_v , \qquad (3)$$

where ΔE_v is the formation energy of a pair of vacancies, the small contribution to the enthalpy of the volume change being neglected. The change of free energy of the system is

$$\Delta G = \Delta H - T\Delta S \ . \tag{4}$$

Equations 2, 3 and 4 can be combined to give

$$\Delta G = n\Delta E_v - 2kT \ln \frac{N!}{(N-n)!n!} \ . \tag{5}$$

By definition, the free energy is a minimum at equilibrium. Differentiating Equation 5 with respect to n and setting the derivative equal to zero (assuming $N \sim N-n$),

$$\frac{n}{N} = \exp - \frac{\Delta E_v}{2kT} \ . \tag{6}$$

As n represents the number of vacant lattice sites and N the number of lattice sites, the term n/N is an expression of site or atom fraction. Letting X_o represent this site fraction and squaring Equation 6 yields

$$X_o^2 = \exp - \frac{\Delta E_v}{kT} \ . \tag{7}$$

As the derivation assumed that $n_{va} = n_{vc}$ (and thus $X_{va} = X_{vc}$), evidently $X_o = X_{vc} = X_{va}$, and

$$X_{vc} \, X_{va} = \exp - \frac{\Delta E_v}{kT} \ . \tag{8}$$

This equation states that the product of the site fractions of vacancies is constant for constant temperatures. Although

the equation has been derived for the condition of equal vacancy numbers for simplicity, the expression is more general and holds true for differing values of X_{vc} and X_{va}. Further, the total entropy change was assumed to be only the entropy of mixing. This is not strictly true as another small contribution arises from the change in the vibrations of ions near a vacancy. Adding an entropy term $T\Delta S_v$ to the enthalpy term of Equation 8, a free energy term is obviously more appropriate and

$$X_o^2 = X_{vc}\, X_{va} = \exp - \frac{\Delta G_s}{kT} , \qquad (9)$$

where ΔG_s is the Gibbs free energy of formation of a Schottky defect. The number of vacancies increases with increasing temperature, the quantity being dependent on the thermal energy necessary to create them. An ion situated next to a vacancy now can move into that lattice site without the problems associated with large repulsive energy barriers.

Another type of point defect is the impurity ion. These are generally in lattice sites, as they are too large to fit in interstitial sites in alkali halides. If a divalent cation impurity is considered (a frequent impurity in NaCl), one can see intuitively that for overall charge balance, either another cation vacancy must be created or an anion must take an interstitial site. As the former process is known to occur due to the more favourable free energy change, the relation between atoms fractions of impurities and vacancies can be written

$$X_{++} + X_{va} = X_{vc}. \qquad (10)$$

X_{++} is the atom fraction of cation sites occupied by divalent impurities. These ions have a net positive charge as the normal lattice site requires a monovalent ion. The anion vacancies have an effective positive charge (a lack of negative charge) and the two must equal the defects with an effective negative charge. Combining Equations 9 and 10,

$$(X_{vc})(X_{vc} - X_{++}) = \exp - \frac{\Delta G_s}{kT} = X_o^2 , \qquad (11)$$

assuming all defects are randomly distributed. Rearranging and solving the quadratic equation for the positive root,

$$X_{vc} = \frac{X_{++}}{2}\left[1 + \left(1 + \frac{4X_o^2}{X_{++}^2}\right)^{\frac{1}{2}}\right] . \qquad (12)$$

When $X_o \gg X_{++}$, then $X_{vc} = X_o$, as in the case for pure Schottky disorder. But when $X_{++} \gg X_o$, then $X_{vc} = X_{++}$. At high temperatures, the number of cation vacancies varies exponentially but at lower temperatures the number is fixed by the ever present cation impurities.

Other more complex point defects can exist in NaCl. Some association takes place between the divalent impurities and vacancies as a result of electrostatic attraction. Cation and anion vacancies can also associate to form vacancy pairs, again forming a neutral complex. These associated species contribute to mass transfer but not to charge transfer.

At even lower temperatures, defects may precipitate or segregate to other imperfections, thus not contributing to either mass or charge transfer.

Dislocations

Dislocations are a line defect. A good introduction to dislocations and dislocation theory is given by Read[4]. For a more detailed discussion of dislocations, especially in ionic crystals, the reader is referred to 'Theory of Dislocations' by Hirth and Lothe[5]. An edge dislocation in an ionic crystal is shown in Figure 2. Edge and screw dislocations can allow the transport of matter and thus charge along the length due to the disorder associated with the 'core'. In many systems ions diffuse much more readily along dislocation cores than in the bulk material. When sufficient dislocations are available, an enhancement in the measured bulk diffusion is evident. Charge transport along dislocations is readily seen by the increase in the conductivity with compressive deformation.

Surfaces and Boundaries

Free surfaces and grain boundaries can also be considered as imperfections in that they disrupt the periodicity of the lattice. Surface conductivity implies the movement of charge along the surface, but surface regions could also affect bulk measurements by impeding or enhancing charge flow through the region; that is, from the surface into the bulk region. Grain boundaries can be considered as thin regions or 'slabs' of 'disordered' material between ordered regions. Again, transport of charge through the region could affect bulk measurements, or ionic conductivity in the plane of the boundary can be studied.

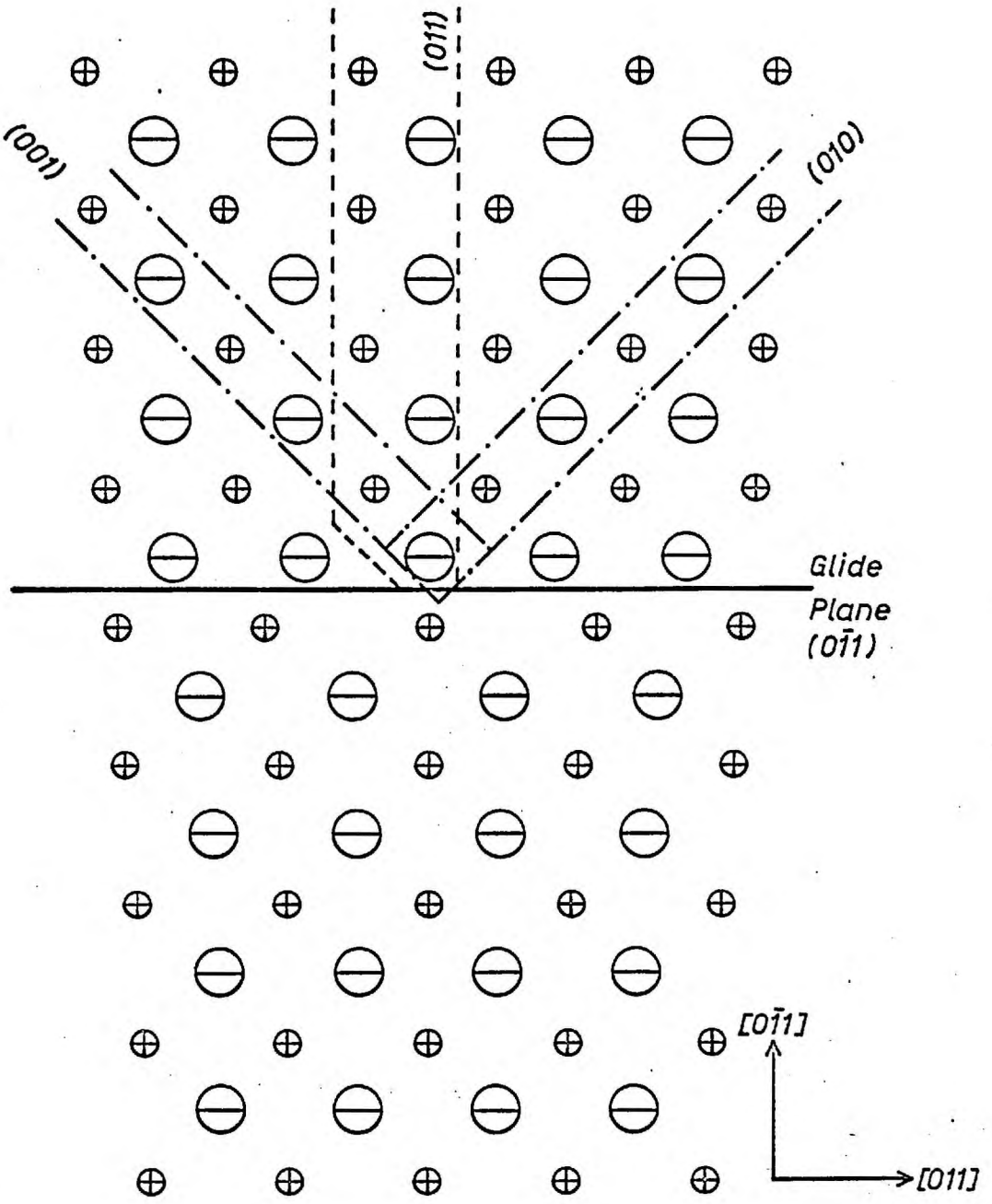

Fig. 2. EDGE DISLOCATION IN NaCl

1-3 Transport Properties of Single Crystals

Diffusion Theory

Shewmon[6] gives a good introductory analysis of diffusion in solids. Fick's First Law of Diffusion states

$$J = - D \frac{dc}{dx} , \tag{13}$$

where J is the flux of matter (per unit area per unit time), D is the diffusion coefficient and dc/dx is the concentration gradient. For non-steady-state phenomena and where D is not a function of position, Fick's Second Law is more useful

$$\frac{\partial c}{\partial t} = D \frac{\partial^2 c}{\partial x^2} , \tag{14}$$

where D is the diffusion coefficient at a given temperature and c is the concentration of the diffusing species at a distance (x) from the initial source. Integrating Equation 14 under the boundary conditions of constant concentration at the initial source (i.e. a surface) and of an infinite diffusion front with respect to the depth of penetration,

$$c = \frac{c_o}{\sqrt{\pi D t}} \exp - \frac{x^2}{4Dt} . \tag{15}$$

In this equation c_o is the initial concentration at $t = 0$ and $x = 0$.

A further implicit assumption is that the diffusion medium is homogeneous. Generally, diffusion measurements are made using radioactive tracers and the concentration of the tracer species is proportional to the radioactive count (A) at any point. Thus,

$$\ln A = \text{Constant} - \frac{x^2}{4D_t t}, \tag{16}$$

where D_t refers to the tracer, for any given experiment of known duration and constant temperature. The diffusion coefficient is given by

$$D_t = \frac{x_2^2 - x_1^2}{4t \ln A_1/A_2} . \tag{17}$$

If experiments are conducted over a range of temperatures, an equation for the temperature dependence of D_t can be deduced, and

$$D_t = D_{ot} \exp - \frac{Q}{kT}, \tag{18}$$

where D_{ot} is a frequency factor (diffusion constant), k is Boltzman's constant, and Q is an effective activation energy that remains constant over certain temperature intervals.

An important consideration in tracer diffusion measurements is the manner in which motion takes place. True self-diffusion coefficients are derived from considerations of completely random motion. While vacancies do move in a random fashion, a jump by a tracer ion is correlated to the immediately preceeding jump. Since a vacancy has an equal

probability of exchanging with any of its neighbours, a tracer ion which has just jumped to a vacant site has a finite possibility of a jump in the reverse direction. Thus a certain percentage of random jumps do not cause any motion in the general diffusion direction. This effect can be defined by a correlation factor

$$f = \frac{D_t}{D} . \tag{19}$$

This factor depends on the type of crystal lattice and on the diffusion mechanism, but has been calculated for most systems and mechanisms. A second consideration arises from the site fractions of vacancies X_v and tracer ions X_t. Thus for the fcc - type sublattice of NaCl where diffusion proceeds via jumps into vacant lattice sites,

$$D_v = \frac{X_t D_t}{X_v f} , \tag{20}$$

where f = 0.7815 and the subscript v refers to the vacancies. The more general form of Equation 18 for self-diffusion is

$$D = D_o \exp - \frac{Q}{kT} , \tag{21}$$

which applies to any single diffusion process in an homogeneous medium. To gain some insight into the origins of D_o and Q consider the following analysis. The NaCl-type

lattice is composed of two sublattices, diffusion on one proceeding independently of the second. Consider diffusion by the vacancy mechanism on the cation sublattice containing a site fraction X_{vc} of vacancies. If z is the coordination number and w the probability of a vacancy jump, then the jump frequency will be

$$\nu_v = zw \tag{22}$$

The average jump frequency of an ion (ν) will depend on the probability of a vacancy being a nearest neighbour, which is just X_{vc}. Thus

$$\nu = \nu_v X_{vc} = zwX_{vc} \, . \tag{23}$$

The motion of a vacancy, and thus the probability of its motion (w), is a thermally activated process, and

$$w = \nu_o \exp - \frac{\Delta G_m}{kT} \, , \tag{24}$$

where ν_o is a frequency of vibration of the vacancy in the direction of motion and ΔG_m is the Gibbs free energy necessary for motion. The theory of random walk considers the random motion of a large number of particles moving without mutual or external influence and yields a diffusion coefficient

$$D = (r^2)_{avg} \frac{\nu}{6} \, , \tag{25}$$

where $(r^2)_{avg}$ is the average mean square displacement of the

particles which undergo an average of v displacements per unit time. In the system considered here the jump distance is always the nearest neighbour distance (d) or, in terms of the unit cell parameter (a_o), is $a_o/\sqrt{2}$ for the fcc lattice. Rewriting Equation 25,

$$D = \frac{a_o^2 v}{12} \quad . \tag{26}$$

Now as the coordination number (z) is 12 in fcc lattices, conbining Equations 23, 24 and 26 gives

$$D = a_o^2 \, v_o \, X_{vc} \exp - \frac{\Delta G_m}{kT} \quad . \tag{27}$$

Recalling Equation 9, X_{vc} is also temperature dependent in the intrinsic region. Assuming the free energy of formation of a cation vacancy (ΔG_f) is one-half ΔG_s, and writing $\Delta G = \Delta H - T\Delta S$, Equation 27 becomes

$$D = a_o^2 v_o \exp \frac{\Delta S_s/2 + \Delta S_m}{k} \exp - \frac{\Delta H_s/2 + \Delta H_m}{kT} \quad . \tag{28}$$

A comparison of Equations 21 and 28 reveals

$$D_o = a_o^2 \, v_o \exp \frac{\Delta S_s/2 + \Delta S_m}{k} \quad , \text{ and}$$

$$Q = \Delta H_s/2 + \Delta H_m \quad . \tag{29}$$

Ionic Conductivity Theory

Lidiard[7] has compiled a comprehensive review of the knowledge of ionic conductivity. Fick's First Law defines a flux of matter (J) in terms of D and a concentration gradient. Electric current is a flux of charge (I) in a potential gradient (dp/dx) and an analogous expression may be written

$$I = - \sigma \frac{dp}{dx} . \qquad (30)$$

The conductivity (σ) can be written as

$$\sigma = c \mu q , \qquad (31)$$

where c is the concentration of charge carriers (number per unit volume), μ is the mobility of the moving species and q is the charge per carrier. In the NaCl-type structure there are two possible charge carriers and the total current will be the sum of both contributions. For NaCl however, anion motion is often neglected at low temperatures when the mobility of anions is comparatively small and when the divalent cation impurities depress the number of anion vacancies. Neglecting anion motion will cause some error at higher temperatures when Schottky disorder predominates. Nevertheless, consider that the total current arises only from cation vacancy motion and the concentration of charge carriers is the product of the site fraction vacant (X_{vc}) and the number of sites per unit volume (N_c),

$$c = N_c X_{vc} . \qquad (32)$$

The mobility of vacancies depends on the jump frequency (v_v) and is given by

$$\mu = \frac{a_o^2 v_o q}{kT} \exp - \frac{\Delta G_m}{kT} . \qquad (33)$$

The charge (q) is simply the charge of one electron for monovalent species, so combining Equations 31, 32 ans 33 yields

$$\sigma = \frac{a_o^2 v_o e^2 N_c X_{vc}}{kT} \exp - \frac{\Delta G_m}{kT} . \qquad (34)$$

Recalling Equations 9 and 29,

$$\sigma = \frac{D_o e^2 N_c}{kT} \exp - \frac{Q}{kT} . \qquad (35)$$

If D in Equation 25 is calculated for vacancies, then the foregoing arguments can be combined to give the NERNST-EINSTEIN Equation,

$$\frac{\sigma}{D_v} = \frac{N_c X_{vc} e^2}{kT} , \qquad (36)$$

where σ and D_v both refer to measurements of cation vacancy motion only. When comparing σ to D_t of course, the correlation factor must be used. Equation 35 is usually expressed as

$$\ln \sigma T = \text{constant} - \frac{Q}{kT} , \qquad (37)$$

commonly known as an Arrhenius equation. A plot of ln σT versus 1/T will give a slope of -Q/k and the effective activation energy of the process can be calculated. Although the assumption of negligible anion contribution is a good approximation[7], recent studies by Kirk[8] and by others[9-11] indicate as much as 10 to 20 percent anion contribution to the total conductivity above 550°C.

For nominally pure single crystals Equation 12 shows that $X_{vc} = X_o$. Thus Equation 35 is valid and Q in Equation 37 is given by

$$Q_I = \Delta H_s/2 + \Delta H_m \qquad (38)$$

for the intrinsic region. At lower temperatures $X_{vc} = X_{++}$, and the slope of the Arrhenius plot changes to

$$Q_{II} = \Delta H_m \ , \qquad (39)$$

for the extrinsic or structure sensitive region. The change from intrinsic to extrinsic behaviour occurs at the 'knee' temperature. At even lower temperatures, association of impurity ions and vacancies occurs followed by agglomeration and precipitation, so that the slope of the conductivity plot changes further. These latter mechanisms are not of great interest to the present study and will not be discussed in any detail.

Previous Works

Dreyfus and Nowick[12], Mapother, Crooks and Maurer[13] and many others have measured the enthalpy and entropy of the formation and motion of vacancies for NaCl and KCl crystals. More recently, Kirk[8] reported smaller values for ΔH_m. Guccione, Tosi and Asdente[14] have made theoretical calculations of the migrational barriers for ion motion, while Fumi and Tosi[15] and more recently, Boswarva and Lidiard[16], have considered the formation energies of Schottky defects in alkali halides. Barr, Morrison and Schroeder[17] resolved two mechanisms of anion diffusion; a single vacancy mechanism and a vacancy pair mechanism. Both contribute in the intrinsic region but the former predominates at lower temperatures. Table 1 gives some theoretical and measured values of enthalpies associated with cation and anion vacancies.

	ΔH_m	ΔH_s	Ref.
NaCl-Na^+-measured	0.80eV	2.12eV	12,13
-Na^+-measured	0.70	2.30	8
-Na^+-theoretical	0.87	2.12	14,15
-Cl^--measured-single vacancy	0.9	2.0	17
vacancy pair	1.0	-	17
-theoretical-single vacancy	1.11	2.12	14,15
-vacancy pair	1.07	2.12	15
KCl-K^+-measured	0.84	2.22	12
theoretical	1.13	2.21	14,15
-Cl^--measured	-	-	-
theoretical	1.18	2.21	14,15

Table 1 Measured and Theoretical Activation Energies

A few investigations of impurity diffusion have been made in NaCl. Stoebe[9] summarised these results, which are given in Table 2.

Ion	radius (Å)	ΔH_m (eV)
Zn^{++}	0.74	0.46
Mn^{++}	0.80	0.66
Ca^{++}	0.99	0.96
Sr^{++}	1.13	1.00

Table 2 Impurity Diffusion in NaCl

The theory of conductivity predicts no dependence of the vacancy mobility with impurity cation. Kao, Giles and Calderwood[18] recently reported some results of Mg, Ca, Sr and Ba doped NaCl crystals. Although the activation energy of cation vacancy motion did not vary, the mobility was dependent on the impurity ion size. This effect must arise from an association reaction with the vacancies, indicating that there is always some association in region II for relatively high impurity concentrations.

1-4 Electrical Phenomena at Surfaces

Polarization

An important consideration when measuring ionic conductivity is the effect of polarization. Joffé[19] expounded a space charge polarization theory. A region of space charge develops with time at one or both electrodes, due to the finite rate of discharge (or zero discharge) of the charge carriers in a crystal in a d.c. field. At high temperatures (in the intrinsic region), a polarization effect with a long time constant is evident. This effect is manifested as a time dependence of the d.c. current[10] or as a frequency dependence of the a.c. capacity[20]. Jacobs and Maycock[21] studied the frequency dependence of the a.c. capacity and concluded that for KCl at least, both charge carriers (cation and anion vacancies) would be blocked at the electrodes. However, for both KCl and NaCl, cation diffusion measurements agree well with a.c. conductivity measurements assuming some anion contribution. Blocking of cation vacancies in KCl then, must play a relatively minor role at higher temperatures. Electrode polarization is virtually absent (for KCl and NaCl) in the extrinsic region as the bulk conductivity is low, and the charge carriers can discharge at the electrodes as fast as they arrive.

A second theory of dielectric relaxation ascribes the decay of d.c. conductivity with time to a time dependent change in the macroscopic dielectric constant of the material. Sutter and Nowick[22] studied the time dependent polarization of NaCl between 50°C and 200°C and concluded that it resulted from the displacement of charge carriers from clusters of defects, from

charged jogs on dislocations or from impurity aggregates. Dreyfus[23] showed for lower temperatures, -60°C to 0°C, that dielectric relaxation due to the rotation of divalent ion-cation vacancy dipoles takes place.

Wimmer and Tallan[24] studied polarization effects in NaCl between 300°C and 400°C (extrinsic and association regions) and found excellent agreement between their observations and Volger's[25] theoretical analysis of an interfacial polarization model. This model considers that bulk material, having a particular set of electrical properties, is 'sandwiched' between thin surface layers having a different set of electrical properties. Although experimental evidence of such layers exists, their origin is unknown. The thickness of the layer was calculated from their data as 20 microns. Further studies, involving the measurement by a surface probe of the potential profile on a specimen 2.4 mm. thick, showed that 25 percent of the applied potential dropped in a layer 30 microns thick next to each electrode. The results of this experiment are shown schematically in Figure 3.

Surface layers with properties different than those of the bulk could be related to the enhanced grain boundary diffusion noted by Laurent and Bénard[26,27], by Cabané[28] and by others[29,30], but a correlation between the boundary diffusion parameters and the electrical properties of the surface regions will be extremely difficult. However, dielectric measurements[24] and an interpretation based on the surface layer model may be helpful in estimating the effective thickness of grain boundary regions.

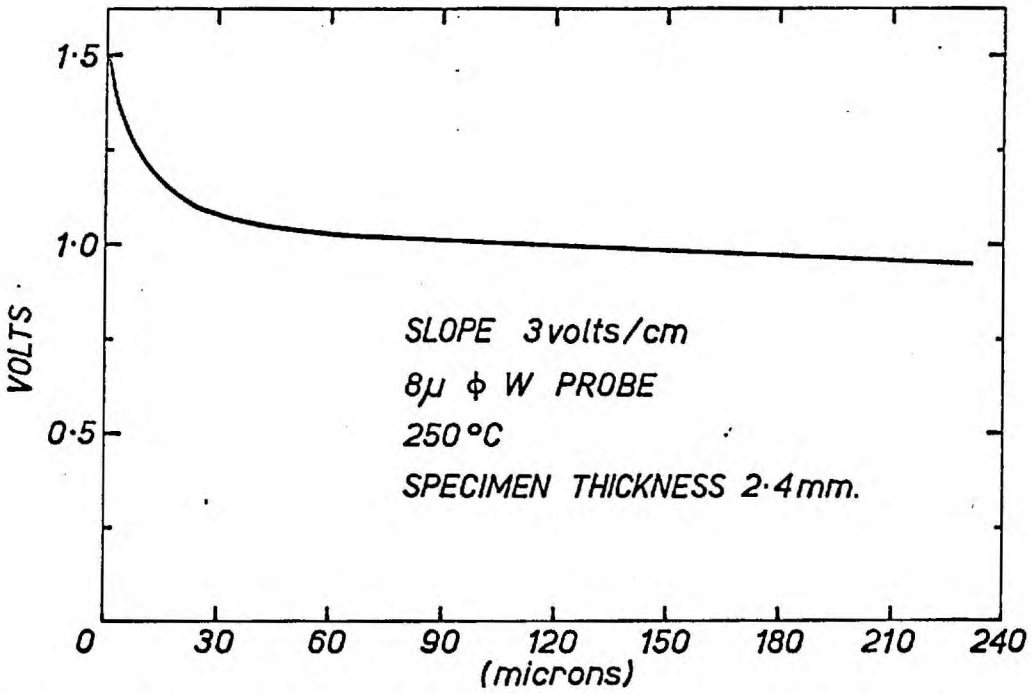

Fig. 3. POTENTIAL PROFILE APPROACHING ONE ELECTRODE [24]

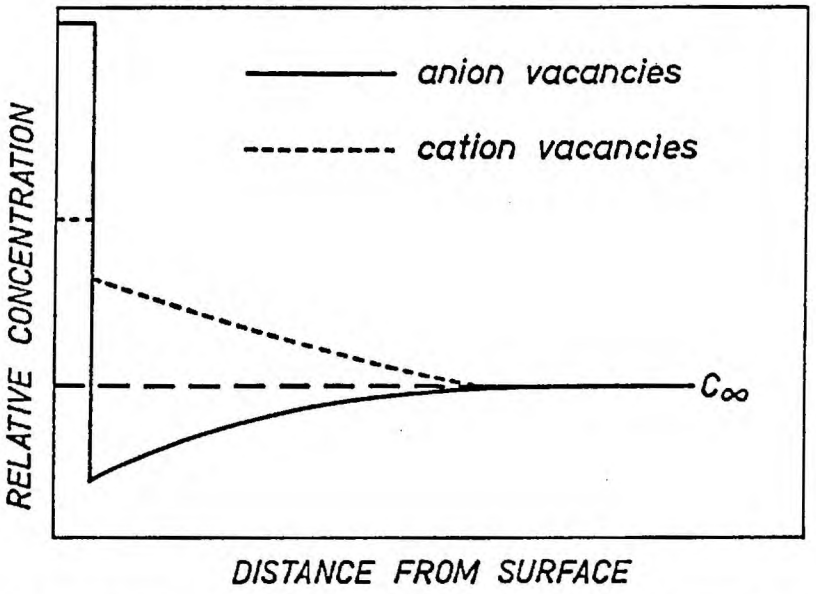

Fig. 4. DISTRIBUTION OF VACANCIES IN THE SURFACE AND NEAR SURFACE REGION [35]

Vacancy Distribution

Frenkel[31] pointed out that a double charge layer should exist at surfaces because of an equilibrium gradient of defects in the crystal. This can arise in ionic crystals if the formation energies of anion and cation vacancies differ. For pure, stoichiometric ionic crystals, Lehovec[32] specified that this net surface charge is positive with a negative compensation space charge under the surface. The thickness of this layer has been calculated as 0.1 micron at 400°C. The layer could give rise to the interfacial polarization effect, although there is disagreement in the thickness of the calculated charged layer and the measured surface polarization layer[24].

Eshelby, Newey, Pratt and Lidiard[33] predicted that the introduction of divalent cations into an alkali halide crystal leads to a negative surface charge at lower temperatures, a positive charge at higher temperatures, and an 'isoelectric' temperature at which the surfaces are uncharged. Schwensfeir and Elbaum[34] measured the migration of low-angle boundaries under an applied electric field and confirmed this prediction, the isoelectric temperature being between 560°C and 640°C. More recently, Lifshits and Geguzin[35], and Lifshits, Kosevich and Geguzin[36] proposed a different model in which the free energy to form a vacancy pair rather than an isolated vacancy is considered. A schematic diagram of the vacancy distribution in the near-surface region is shown in Figure 4. Such a distribution is not expected to affect bulk conductivity measurements on single crystals but it could retard or enhance diffusion along grain boundary regions. A further point is that the surface charge can vary with the

state of the surface, with temperature or with impurity content, making an analysis of any effect on surface region conductivity extremely difficult.

Interaction of Dislocations with Surfaces

Since Eshelby et al. extended the theory of Lehovec on charged surfaces to dislocations many publications on the subject have followed. The number is too large to deal with here and the reader is referred to a few of the publications of Whitworth[37-39]. An excess of half-jogs or isolated vacancies of one sign in the core of an edge dislocation will result in an effective charge. Glide motion of such a dislocation will result in charge flow (Stepanov effect) in the direction of the Burgers vector. By measuring the charge increase at free surfaces of a specimen undergoing plastic deformation, the sign of the effective charge can be determined. Unfortunately there is little agreement in the literature. The sign of the charge can also be deduced by observing the motion of dislocations under the influence of an electric field. Using this technique, Zagoruiko[40] reported that dislocations have a net positive charge. Turner and Whitworth[41], using both techniques, reported a net negative charge on edge dislocations, the charge being -3.8×10^{-13} coulomb/cm or the equivalent of one positive ion vacancy for every eight sites in the core. The ambiguity of the literature could be explained by the effects of surface states, temperature and impurities that affect the concentration and distribution of vacancies. Hikata, Elbaum, Chick and Truell[42] demonstrated experimentally that only edge and not screw dislocations transport charge. Hirth and Lothe[5] point out however, that

at elevated temperatures sessile jogs on screw dislocations can be thermally activated. Further, an absorbed vacancy can decompose into a series of four charged jogs and kinks. The screw can then transport charge when it moves by jog drag.

Colour Centre Distribution

The most common colour centre in alkali halides is the F-centre, an electron trapped in an anion vacancy. Irradiation produces F-centres and the relative numbers formed can be measured by observing the F-band absorption in the visible wavelengths. The initial stages of formation are known to be structure sensitive, being affected by dislocations and impurities. Photodielectric studies by Macdonald[43] on coloured KBr crystals indicated an absence of centres in thin surface layers, leading to higher electrical resistivity in the surface regions. Again this effect can be explained in terms of the distribution of vacancies.

1-5 Grain Boundary and Dislocation Studies

Grain Boundary Models

Grain boundaries have long been recognized in metals as having a controlling influence on such properties as the yield point, hardenability, ductility and recrystallization rates. In ceramics, grain boundaries are partially responsible for the lack of ductility due to the interaction of dislocations with boundaries. Optical transparency often depends on the state of the boundary regions. Permanent ceramic magnets depend on boundaries to inhibit domain rotation. High strength and creep resistance in ceramics depend upon low porosity and a small grain size. Impurities concentrated at grain boundaries can control grain size in the sintering process. Low porosity depends on the relative rate of volume to grain boundary diffusion.

To aid the understanding of grain boundaries Burgers[44] proposed a dislocation model for low angle boundaries. Other earlier works[45-47] and a recent summary of the knowledge of low angle boundaries by Amelinckx and Dekeyser[48], as well as proposed models for high angle boundaries[49-53] have been reviewed by McGee[54]. Kronberg and Wilson[55] proposed a coincidence model for two grains of specific axes and angles of misorientation (separated by a boundary) which share some common lattice sites. A twin boundary is a simple example of a coincidence boundary. Recently, Brandon[56] extended and combined the coincidence model with the dense dislocation array model proposed by Read and Shockley[57], to propose a model of high-angle boundaries consistent with observed properties. Recent calculations on high-angle boundaries include those of Gifkins[58] and of Bolling[59].

Grain Boundary Structure in Sodium Chloride

Many ceramic materials have the NaCl crystal structure. The alkali halides offer an excellent opportunity to study the basic properties of grain boundaries in cubic ionic systems. Martin, Fehr and McGee[60] showed by transmission electron microscopy that for misorientations up to 12° in NaCl bicrystals, the tilt boundaries are made up of a dislocation array and that the spacing of dislocations conforms to that predicted by the dislocation model. Observations on the relative energies of grain boundaries confirmed the angular dependence of the energy as predicted by the model. Gimpl, McMaster and Fuschillo[61,62] investigated the structure of twist boundaries in NaCl. Optical microscopy showed agreement with Mott's model[50] of 'islands' of good atomic matching surrounded by areas of mismatch, but on a macroscopic rather than an atomic scale. These boundaries were mechanically weak under a shear stress and could account for the low ductility of polycrystalline NaCl. Optical and electron microscopy studies by Fuschillo, Gimpl and McMaster[63] on tilt boundaries revealed no visible fine structure. They observed however, that the mechanical strength of tilt boundaries was good (inferring good bonding across the boundary) and that the rates of dissolution of both dislocations etch pits and grain boundaries were equal (inferring equal free energy per unit volume). Observations of birefringence in NaCl bicrystals under four point loading by Long and McGee[64], indicated that plastic deformation could pass through the boundary. The stress required for deformation increased with increasing mismatch and was consistent with that predicted by the dislocation model. Twist boundaries were found to be more resistant to ductile deformation than tilt boundaries.

Ion Transport in Grain Boundaries

Enhanced grain boundary diffusion has long interested researchers. Earlier experiments were generally on metals, and Turnbull and Hoffman[65] investigated the effect of relative crystal and grain boundary orientations on grain boundary diffusion rates in silver. They found that the grain boundary diffusion coefficient (D') was several orders of magnitude larger than the bulk diffusion coefficient (D_b), and that the activation energy of motion (Q_m) was independent of the angle of misorientation up to 28°. Working with MgO, Wuensch and Vasilos[66] confirmed enhanced grain boundary diffusion for nickel and cobalt ions. However, the effect was due to impurity segregation at the grain boundaries (Ca, Si, Fe) and was thus an extrinsic rather than an intrinsic property.

Fisher[67] made a mathematical analysis of diffusion down a grain boundary perpendicular to the diffusion surface and parallel to the diffusion direction. His relatively simple analysis is useful for large ratios of D'δ to D_b where δ is the 'effective' width of the boundary. Whipple[68] made a more precise analysis of diffusion in the region of grain boundaries. At any point (x,y), the concentration of the tracer depends on two sources; direct diffusion from the surface (c_1) and 'sideways' diffusion from the grain boundary (c_2). Assuming $D' > D_b$,

$$c = c_o \operatorname{erfc} \frac{\alpha}{2} + \frac{\alpha c_o}{\sqrt{\pi}} \int_0^1 \exp \frac{-\alpha^2 \varepsilon^2}{4} \operatorname{erfc} \frac{1}{2}\left[\frac{1}{\varepsilon^2 \partial} - \frac{1}{\partial} + \gamma\right] d\varepsilon \quad , \quad (40)$$

where $$\gamma = \frac{y}{\sqrt{D_b t}} \quad , \quad \alpha = \frac{x}{\sqrt{D_b t}} \quad , \text{ and } \partial = \frac{1}{2} \frac{D'\delta}{D_b \sqrt{D_b t}} \frac{1}{\sqrt{D_b t}} \quad . \quad (41)$$

In these equations, y is the distance from the boundary, x is the distance from the surface, and ε is a dummy variable of integration. Again, the initial surface concentration (c_o) must remain constant with time (t). From the equation it is apparent that for a constant product $D_b t$, the concentration at any point depends only on the term $D'\delta/D_b$, and increases with it.

Laurent and Bénard[26] investigated the isotropic nature of self-diffusion in NaCl and also the effects of grain boundaries. They found diffusion of Na^+ and Cl^- ions was isotropic for the [100], [110] and [111] directions. Further, they found no difference between Na^+ ion diffusion in single crystals or polycrystals, but they did find an increase in the diffusion coefficients of Cl^- ions for polycrystals. This bulk, polycrystalline diffusion coefficient (D_{bp}) increased with decreasing grain size, but the activation energy in all samples remained constant. Therefore, it was the diffusion constant (D_{op}) that was affected by grain boundaries. The results are reproduced in Figure 5. Later, Laurent and Bénard[27] studied the effect of grain size on self-diffusion in the potassium halogen and in the alkali chloride series of ionic compounds. The results indicated that in the temperature region studied, 450°C to 700°C;

1. The activation energy of motion for anions was the same as for single crystals, indicating a common mechanism.
2. The presence of grain boundaries enhanced only the diffusion constant (D_{op}) and only for anions (excepting the case of Cs in CsCl and CsF).
3. D_{op} for anions increased with decreasing grain size, and thus increased as the ratio of grain boundary 'volume' to bulk volume increased.

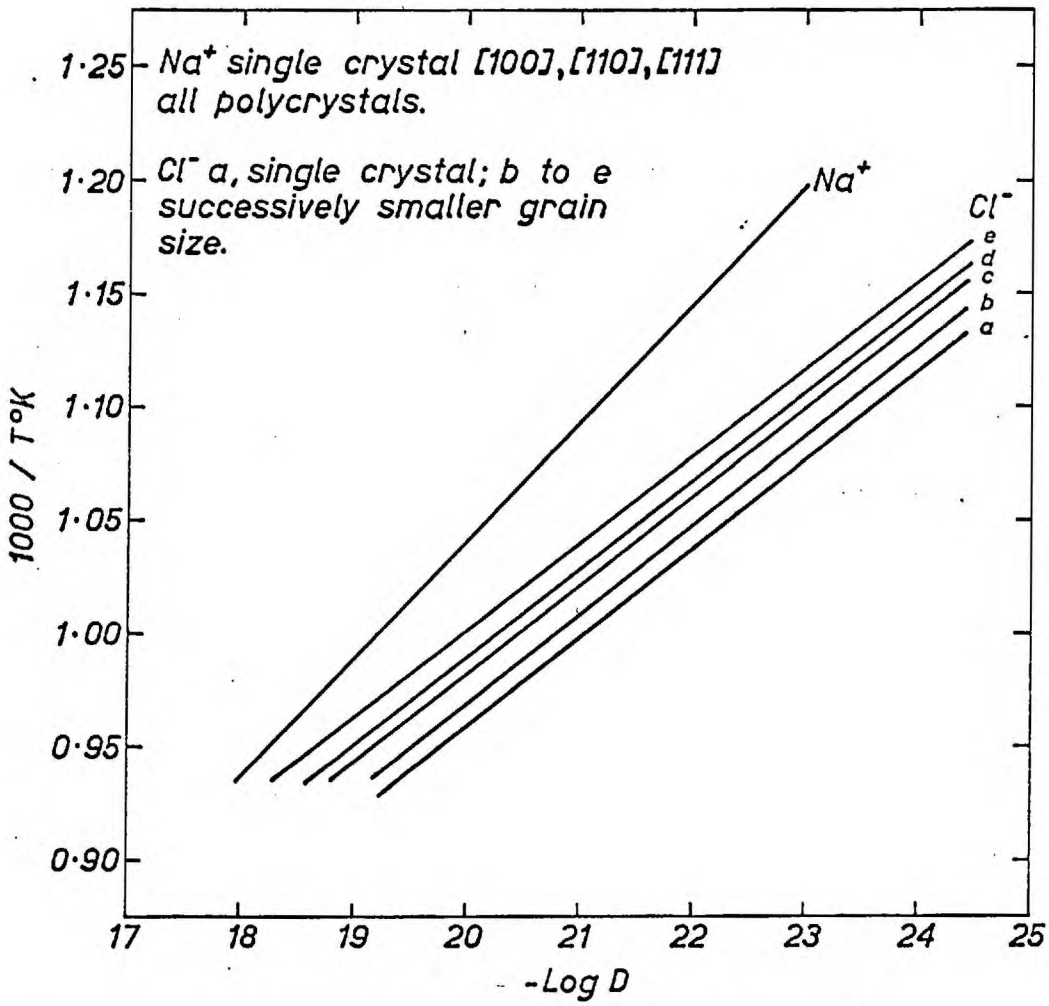

Fig. 5. DIFFUSION IN POLYCRYSTALLINE NaCl.[26]

Using the fact that the increase in diffusivity had a similar temperature dependence, an apparent diffusion constant (D_a) was defined as the ratio of D_{op} for a particular species and grain size to D_o for the corresponding single crystal, and the relationship to the grain size can be seen in Figure 6. Their hypothesis on the effect of the polarizability of anions can be compared with the results shown in Figure 7, which indicate a linear dependence of D_a on the polarizability of the anion species and on the polarizing ability of the cation species.

Barr, Hoodless, Morrison and Rudham[69], using an isotopic exchange technique, confirmed that dislocations and grain boundaries enhance anion diffusivities. Their results agreed with those of Laurent and Bénard in that increasing densities of these defects did not cause deviations from the kinetics of bulk diffusion.

These experiments, although proving enhanced grain boundary diffusion, did not give any indication of the relative size of D' to D_b. The bulk polycrystalline diffusion coefficients and constants can only be compared with those of single crystals. Further, Laurent and Bénard used a form of Equation 16 based on an homogeneous diffusion medium and a constant surface concentration of tracer ions. Cabané[28] later pointed out that polycrystals are <u>not</u> a homogeneous medium and that, because of the long duration of diffusion anneals, the final surface concentration in these experiments was only 0.3 c_o.

Cabané investigated the methods used to prepare polycrystalline specimens. He found that moisture, divalent impurities and absorbed organic gases all retarded grain growth in specimens annealed at elevated temperatures after being

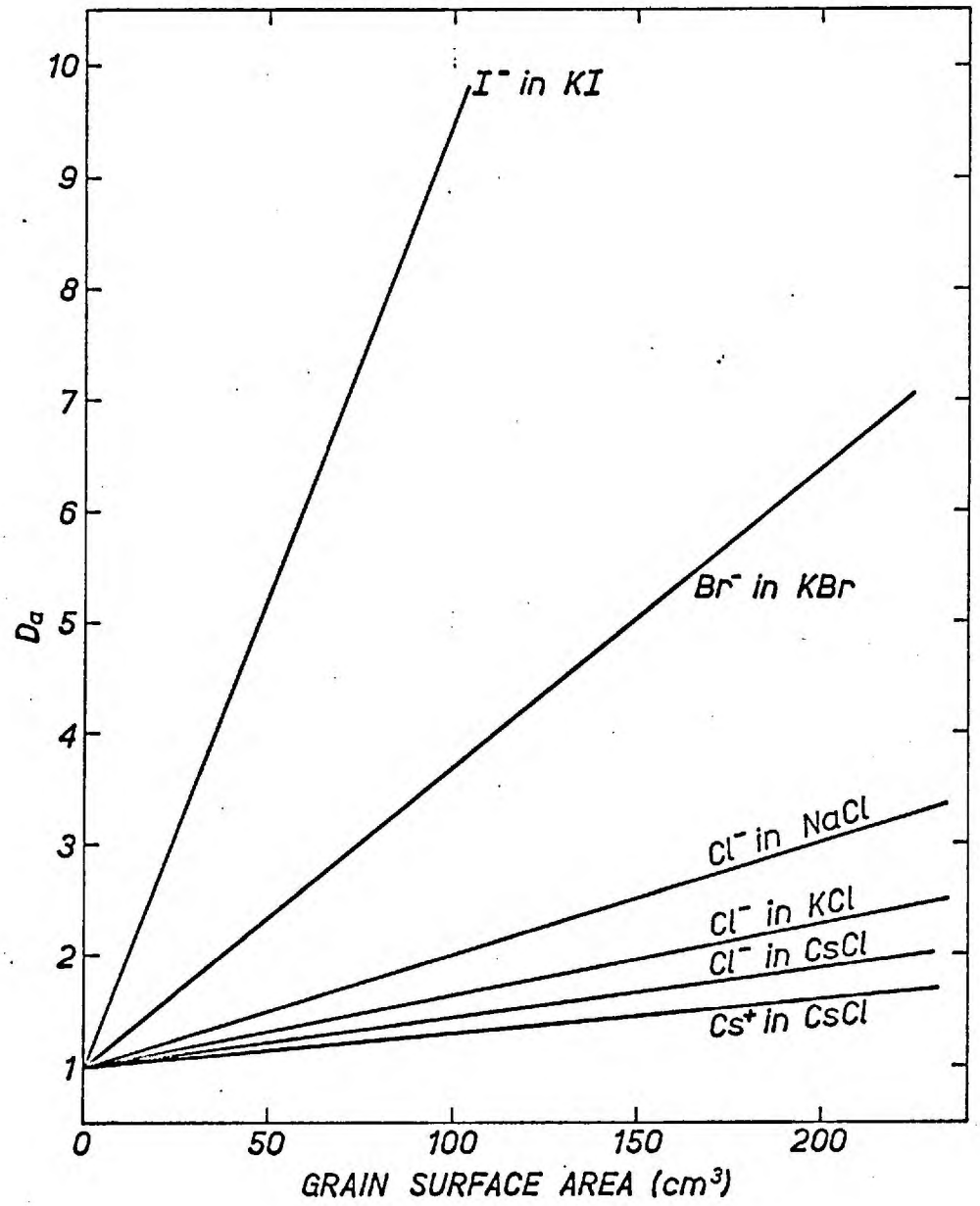

Fig. 6. RELATIVE APPARENT DIFFUSION COEFFICIENTS FOR POLYCRYSTALS [27]

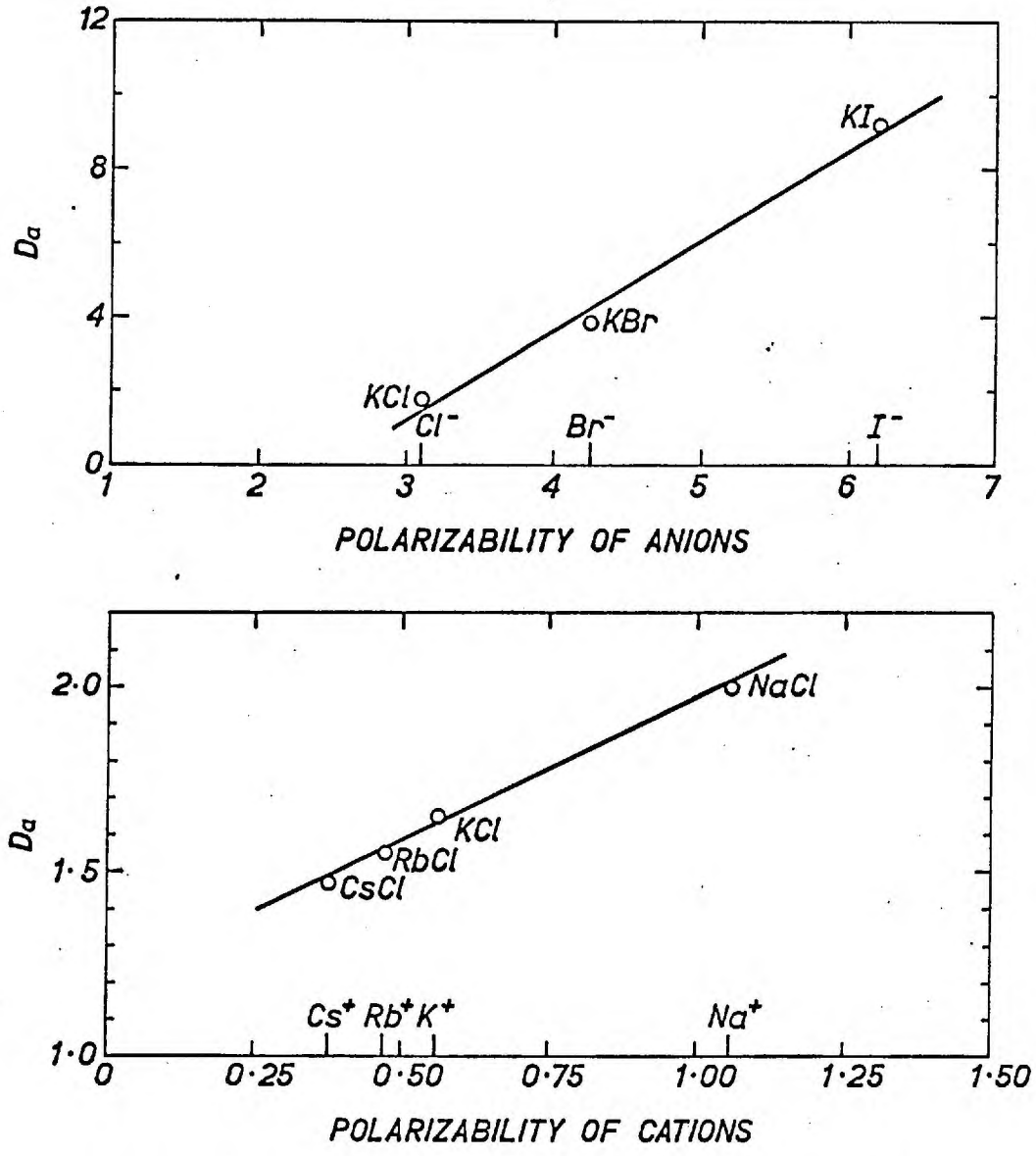

Fig. 7. IONIC POLARIZATION EFFECTS ON APPARENT DIFFUSION COEFFICIENTS [27]

sintered under pressure. Specimens hot-pressed from material previously treated by drying, were transparent and had grain boundaries that were very difficult to detect even after etching. Specimens made from material which had not undergone a drying treatment were opaque, with boundaries that were easily etched by chemical dissolution or by preferential thermal evaporation.

Diffusion experiments similar to those of Laurent and Bénard on polycrystalline specimens of KI and NaCl showed the influence of moisture in the grain boundaries. No specimen displayed enhanced cation motion. Only the opaque specimens showed enhanced anion mobility. Thus, the effect seen by Laurent and Bénard was an extrinsic rather than intrinsic property of grain boundaries; a conclusion similar to that of Wuensch and Vasilos for MgO. Few investigations seem to consider this possibility in NaCl.

Whipple's analysis is for an isolated boundary, but it can be used for polycrystalline material as long as neighbouring boundaries do not interact and if a suitable statistical factor is introduced to account for the total length and random orientation of boundaries. Theoretical curves of penetration[28] for a polycrystal are shown in Figure 8. A consequence of long diffusion anneals can be seen. The law of distribution for the diffusing species approaches that of single crystals. Thus a diffusion coefficient (D_{bp}) for polycrystals can be calculated in the same way as the diffusion coefficient for single crystals, which is what Laurent and Bénard did. But for anneals of very short duration, a definite 'break' should be apparent in the distribution of diffusing species. Using the conventional sectioning and counting technique, Cabané observed this discontinuity in the concentration profile of polycrystalline KI

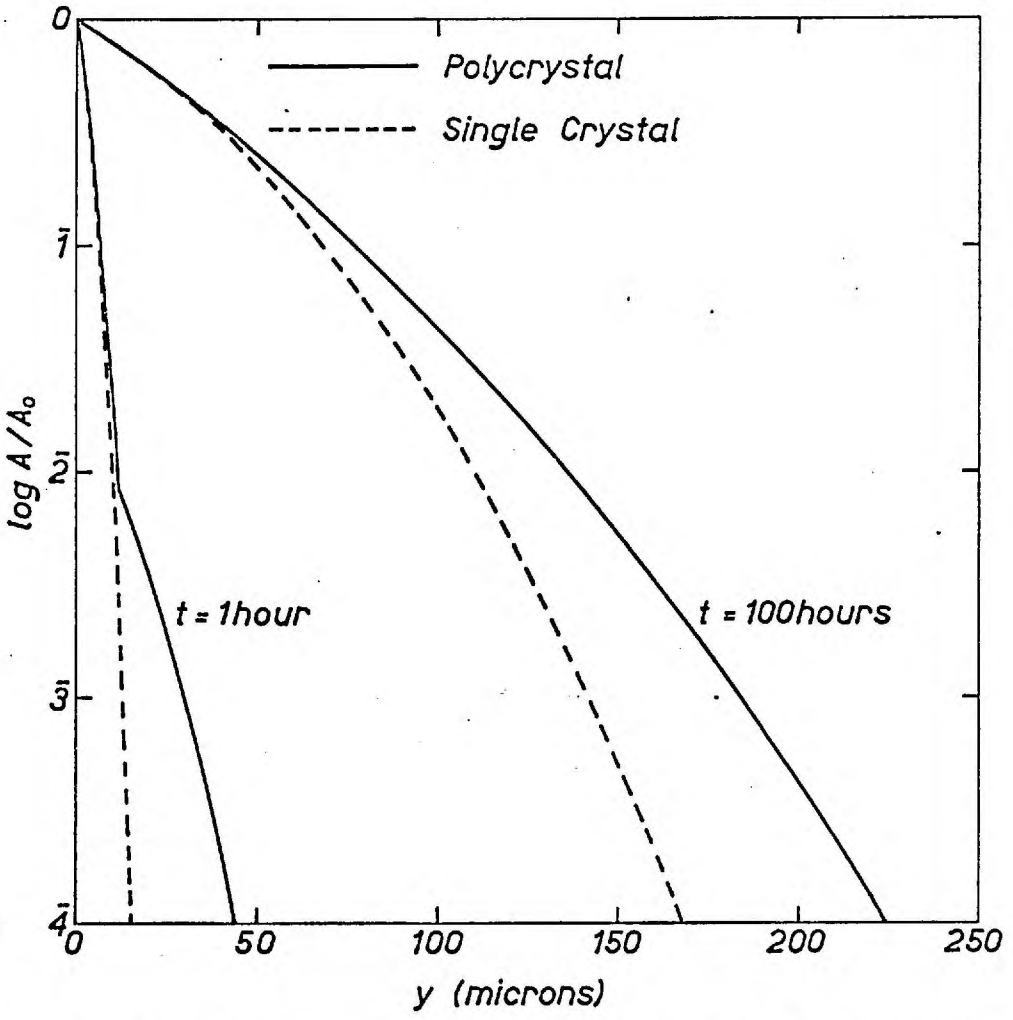

Fig. 8. DIFFUSION PENETRATION CURVES FOR POLYCRYSTALS[28]

and NaCl providing the time of diffusion was short.

The standard method of tracer diffusion analysis, sectioning with a microtome and counting the radioactivity in the removed layer, has a lower limit of detection of $D = 10^{-12}$ cm.^{2} sec.$^{-1}$. Using Whipple's analysis, Cabané showed that an autoradiographic method of analysis should be able to detect a value for the term $D'\delta/D_b$ down to 10^{-5} cm. The bulk diffusion coefficient can be measured in single crystals. $D'\delta$ then can be calculated for very small values of β in Equation 41 by this technique. When β is somewhat larger, the normal slicing and counting technique can be used in conjunction with Whipple's theoretical concentration curves derived from Equation 40 by numerical analysis. Fisher's analysis can be used for $\beta > 100$.

An autoradiographic examination of diffusion of I^- ions in KI polycrystals, in the temperature range 280°C to 525°C, indicated the existence of two diffusion mechanisms. The first, in the opaque specimens, was characterized by an activation energy similar to that of single crystals. The diffusion parameter $D'\delta$ increased with decreasing grain size and had the same temperature dependence as D; a conclusion similar to that of Laurent and Bénard. It could be the result of the association of large anions with defects or impurities in the boundary region. The second mechanism, evident in transparent polycrystals, had an activation energy of about one-half of that found in single crystals. The boundary diffusion parameter $D'\delta$ was therefore less temperature dependent than D_b and was only detectable at lower temperatures when the bulk diffusion coefficient was relatively small. This fact indicated that the boundary width δ was only a few atomic spacings at least for 'pure' boundaries; a conclusion similar to the boundary model

for metals. That anions can diffuse by two mechanisms in bulk material has previously been shown by Barr, Morrison and Schroeder[17]. As opposed to the grain boundary diffusion usually interpreted in terms of a dislocation model, a second mechanism of diffusion might arise as a result of charged surface layers in ionic crystals[24].

Moment and Gordon[29] used the method of Tucker, Laskar and Thompson to investigate the a.c. conductivity phenomena in Na^+ ion-doped grain boundaries of LiF. For the extrinsic temperature range, 250°C to 375°C, they found $\Delta H_m = 0.32$ eV for the Na^+ ions. This value was constant over a large range of tilt misorientations (4° to 53°). The agreement with the results of Tucker et al. for dislocations was good, even for large boundary angles where the dislocation model is not thought to be valid. This fact, plus the fact that high-angle tilt boundaries in LiF have good mechanical strength, seemed to indicate that a 'mushy' core structure (i.e. high vacancy density) rather than an open or hollow core structure exists.

In the experiments described above, the enhanced conductivity was never more than twice the background conductivity which arose from the volume of crystal near the grain boundary. The background current then, must have affected the slope of the conductivity plot. Moment and Gordon overlook this point however, and consider the derived activation energy to be the result of Na^+ ion motion only.

Graham, Tallan and Russell[30] showed for polycrystalline material that bulk conductivity in NaCl does contribute to the enhanced, anion grain boundary conductivity until the ratio of boundary 'volume' to bulk volume becomes large. They investigated the particle size dependence of the conductivity in NaCl, and

postulated that the well known current decay under d.c. field conditions was due to the blocking of anion motion and that the steady-state d.c. current (σ_∞) was due to cation motion alone. The difference between the initial current (σ_o) and the steady state current was then the current due to anions. As a.c. conductivity is equivalent to σ_o the difference $\sigma_{a.c.} - \sigma_\infty$ gives the blocked contribution. Investigating grain sizes from 1-2 microns to greater than 147 microns, an increase in the total conductivity and hence in an anion contribution was found. This contribution increased with decreasing grain size. The effect is illustrated in Figure 9 while Table 3 shows the complete results.

Polycrystalline NaCl Grain size	ΔH_m anions
147 microns	1.27 eV
147 - 74	1.14
74 - 44	1.18
44 - 38	0.97
38	0.98
1 - 2	0.99

Table 3 Results of Graham, Tallan and Russell

The value of about 1 eV compares well with the value of bulk anion diffusion (see Table 1). A correlation between diffusion coefficients for anions in bulk and boundary regions has also been noted by Laurent and Bénard, by Cabané and by Barr et al.

In summary then, anions have greater mobility in boundary regions than in bulk material in alkali halides. Enhanced cation self-diffusion has not been observed, although impurity

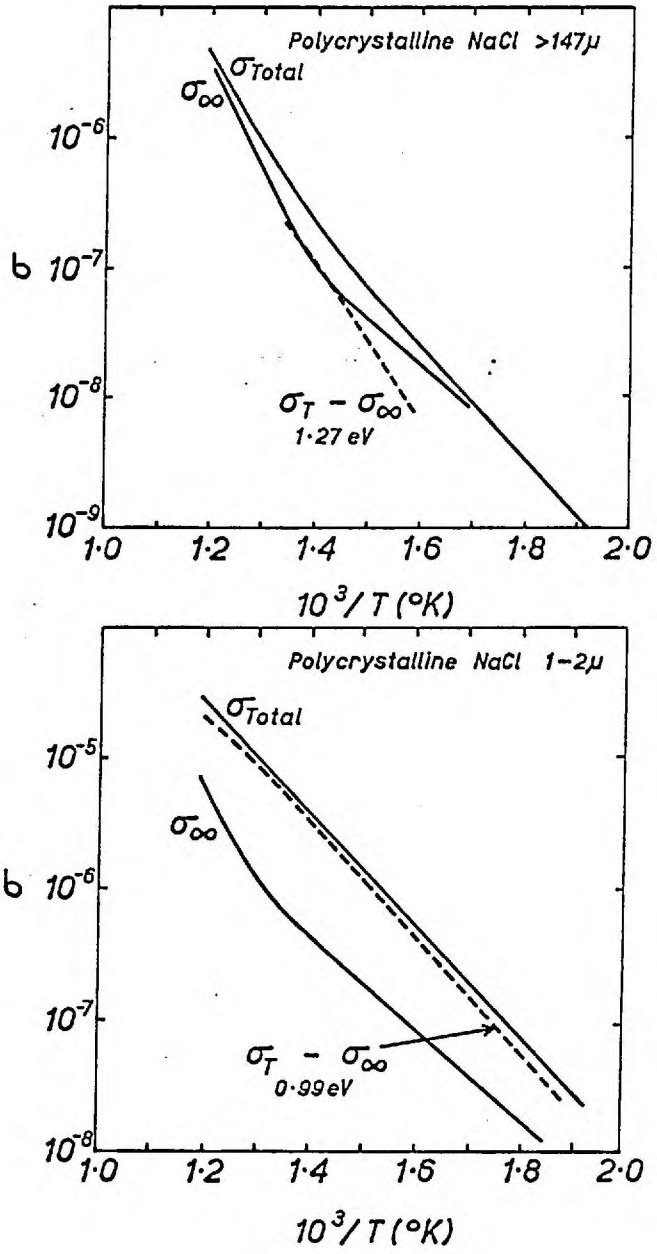

Fig. 9. CONDUCTIVITY FOR POLYCRYSTALS[30]

cation motion in dislocations and in boundaries has been found. Even relatively high-angle boundaries seem to fit the dislocation model usually associated with low-angle boundaries. No studies have been made on the anisotropic behaviour of ion mobility in grain boundaries.

Ion Transport In Dislocations

Because of the way dislocations can be arrayed to form grain boundaries, some investigations of ion transport in dislocations are reviewed here. Tucker et al.[70] measured the conductivity of Na^+ ions in dislocations in LiF by both a.c. and d.c. techniques. NaCl was vacuum evaporated onto a surface of the LiF crystal and the Na^+ ions were 'injected' into the dislocation cores by an applied d.c. field. A small metal electrode was plated onto the opposing face directly opposite the dislocation etch pits. An activation energy of motion and a frequency factor D_o of 0.3 eV and 0.01 $cm.^2$ $sec.^{-1}$ respectively were deduced from a.c. measurements. Optical observations and d.c. measurements confirmed the equality of mass and charge transport. Analysis of the charge effects in the dislocation cores led to a model with a very high vacancy density.

Geguzin and Dobrovinskaya[71] used the conventional tracer technique to study the diffusion of Na^+ ions along screw and edge dislocations in NaCl single crystals of differing dislocation density. The duration of diffusion anneals was arranged to satisfy either the Hart[72] model of overlapping diffusion channels or the Smoluchowski[73] model of independent diffusion 'tubes', and the agreement was good. The results showed

$$D_d S_{edge} = 7 \times 10^{-12} \exp - \frac{0.61 \text{ eV}}{kT}, \quad \text{and} \qquad (42)$$

$$D_d S_{screw} = 8 \times 10^{-10} \exp - \frac{1.1 \text{ eV}}{kT} , \qquad (43)$$

S being the tube area. These experiments were performed between 200°C and 540°C. An interpretation of the activation energy in terms of contributions arising from the energies of formation, motion and association of vacancies in dislocations is extremely difficult. However, accepting that the energy of motion of cation vacancies in the bulk material is 0.7 eV, edge dislocations at least appear to have a high diffusion 'permeability' to cations.

Grain Boundary Segregation

Segregation of impurity solutes to grain boundaries has for long been observed and its effects studied. Westbrook[74] gives a fairly comprehensive review of the subject. In metals, some solutes inhibit, while others encourage grain boundary diffusion. Wuensch and Vasilos[66] found that impurities enhance diffusion in grain boundaries in MgO. All studies on intergranular diffusion, however, really measure the effects on the diffusion parameter D'δ. Whether impurity segregation to grain boundaries affects D', δ or both is not clear. Most investigations of grain boundary diffusion in NaCl do not consider the effect of impurity segregation on the diffusion coefficient.

1-6 Present Work

As the literature contains no direct experimental evidence of enhanced Na^+ ion diffusion in grain boundaries in NaCl, the method of Moment and Gordon[29] is used to investigate the conductivity of Na^+ ions 'injected' into tilt boundaries in bicrystals. The enhanced conductance arising from the motion of other injected alkali metal and halogen ions, including Cl^-, is also investigated in the temperature region 300°C to 400°C. The effect of OH^- ion doping on the enhanced conductance of Na^+ ions is studied to determine whether two mechanisms are evident, as was observed by Cabané[28] for enhanced Cl^- ion diffusion in grain boundaries. The anisotropic structure of tilt boundaries is investigated by observing the enhanced Na^+ ion conductance in the orthogonal direction to the 'dislocation array'.

The surface potential profile experiments on NaCl of Wimmer and Tallan[24] are repeated in order to determine whether the observed, enhanced surface-layer resistivity is also evident at tilt boundaries in bicrystals. This enhanced resistivity is also investigated by observing any anomalous polarization effects in the d.c. conductivity of bicrystal specimens.

The effect of tilt boundaries in NaCl on the formation rate of F-centres is briefly investigated.

CHAPTER 2

PURIFICATION AND CRYSTAL GROWTH

2-1 Purification

Removal of Anionic Impurities

In order to avoid effects associated with impurity segregation, an effort was made to purify the sodium chloride before the growth of bicrystals to be used for grain boundary conductivity experiments. As shown in Table 4, Analar grade NaCl has a variety of aliovalent cation and anion impurities. The actual impurity level varies from batch to batch but is generally lower than the maximum level shown. A spectrographic analysis by Kirk[8] of crystals grown from this material showed 30 molar ppm polyvalent cation content.

Some of the anion impurities can be evaporated off but hydroxyl ions hydrolize the salt at elevated temperatures. Although the OH^- ion is monovalent it is known to affect the electrical and optical properties of the bulk[75, 76] and grain boundary[28] regions in NaCl. To reverse the hydrolization process some investigators bubbled chlorine, hydrogen chloride or phosgene gas through the melt while others reduced the OH^- content by controlling the crystal growth or annealing atmosphere. Otterson[77] removed OH^- ions from crystals by annealing at 730°C in a dry HCl gas atmosphere. Barr, Koffyberg and Morrison[78] found that annealing in moist atmospheres introduced impurities while annealing in dry atmospheres did not. More recently, Agarwal and Kulshreshtha[79] actually reduced the OH^- ion content of molten KCl by treatment in an atmosphere of dry nitrogen. Lower OH^- ion concentrations for crystals grown in dry, inert atmospheres rather than in air have been reported by Etzel and Patterson[76], who also found a significant improvement in the purity of crystals grown from quartz rather than platinum or gold containers.

'Analar' NaCl	Weight percent	Polyvalent Anion (Molar) ppm	Polyvalent Cation (Molar) ppm
Insolubles	.003		
Free Acid (as HCl)	.0018		
Br^- and I^- (as Br^-)	.005		
$CN^=$	.0001	1	
$NO_3^=$	.0005	4	
$PO_4^=$	.0005	3	
$SO_4^=$	.002	12	
NH_4^+	.0005		
K^+	.01		
Ba^{++}	.003		12
Ca^{++} and Mg^{++} (as Ca^{++})	.005		75
Heavy metals (as Pb^{++})	.001		2
Fe^{+++}	.0005		5
As^{+++}	.00004		1
Total			95 ppm

Table 4 Impurities in Analar NaCl

As the crystals used by the author were grown from high purity silica beakers in an atmosphere of high purity argon, no further steps were taken to eliminate OH^- ions. Spectrophotometric analysis in the infrared region did not detect any OH^- bond resonance absorption even for specimens of 10 cm. thickness, indicating less than 10 ppm OH^- ion content. The remainder of this section then, will deal with the removal of polyvalent cation impurities.

Techniques for the Removal of Cationic Impurities

The purification and growth of alkali halide single crystals has been reviewed by Dreyfus[80]. Zone refining can be used for the purification of some alkali halides such as KCl[81]. However, it will not remove Ca^{++} ions from NaCl as the rejection ratio between the solid and the melt is approximately unity. This has led to the use of ion exchange techniques to purify NaCl. An advantage of this method is its insensitivity to varying conditions made possible by its broad safety margins.

Detailed theory and kinetics of ion exchange resins can be found in a variety of sources, notably 'Ion Exchange Separations in Analytical Chemistry' by O. Samuelson[82]. Resins are generally crosslinked, long chain organic polymers containing ionogenic groups and counter ions. These ionogenic groups are acid radicals in the case of cation exchangers and amino or quaternary ammonium groups in the case of anion exchangers. Further, cation exchangers are classified as strongly or weakly acid and anion exchangers as strongly or weakly basic, depending on the degree of dissociation of the ionogenic group. Weakly acid cation exchangers are of little use in this work because the degree of dissociation of the functional group varies with the composition of the external solution (and more especially with the pH), and because these resins have a higher affinity for protons than for other ions. A typical exchange reaction for a strongly acid cation exchanger is given in Equation 44, where (R) represents a crosslinked polymer (i.e. polystyrene crosslinked with divinylbenzene), the ionogenic group is the sulphonic acid radical, and the counter ion (H^+) is being exchanged for another (Na^+) from

the external solution;

$$RSO_3^- H^+ + Na^+ \rightleftharpoons RSO_3^- Na^+ + H^+ . \qquad (44)$$

As the ionogenic groups are generally hydrophilic they tend to dissolve in water and to draw the whole polymer into solution. To prevent dissolution the polymer is crosslinked to form a three-dimensional network, usually in the form of beads. The resultant resin may swell but will not dissolve in water. The exchange capacity of resins (mequiv./gm.) varies slightly with the degree of crosslinking. Increased crosslinking inhibits the exchange rate because of the barrier it provides to ion mobility within the beads, often the controlling factor in exchange rates. Other factors affecting the exchange rates are bead size, solution flow rate, ionic species and pH.

The basis of the exchange in resins is the selectivity coefficient. The main factors are the activity coefficients of the two exchanging species, both in the resin phase and in the external solution. For species of equal valence, the relative amounts of ions in the resin phase are virtually independent of concentration. However, for exchanging species of different charge, the position of equilibrium is displaced in favour of an increased uptake of the higher valence ions. Even though a particular resin may have a similar selectivity coefficient for two ions in a solution, a separation may be made if the degree of crosslinking can inhibit the diffusion of the larger species.

As a rule percolation of the solution through an ion exchange column is necessary to ensure a quantitative uptake

of ions. In batch operation, the resin and solution reach an equilibrium state, with both ion species present in both phases. By the use of columns, equilibrium is prevented until saturation of the resin occurs due to the continuous flow of fresh solution.

The reacting ion in a cation exchange resin does not have to be an H^+ ion. Nor does the use of another ion seriously alter reaction rates. Nachod and Wood[83] found that the exchange rate of Ca^{++} ions for Na^+ ions was almost the same as for H^+ ions in a sulphonated coal resin, Zeocarb. To separate various ions in a solution from one another, the resin must exhibit a preferential selectivity towards one or more of the ions present. Beukenkamp and Rieman[84] demonstrated the selective retention of Mg^{++} ions from a solution also containing Na^+ and K^+ ions by a sulphonated resin, Dowex 50.

Recently, a new group of cation exchange resins has become important in separations of alkalis from alkali earths. These are the chelating resins. Chelating groups are organic radicals with rigidly defined bonding angles and two distinct bonding sites having a negative valence. The positions of the 'arms' of the group are such that the bonding sites are very close together spatially and hence prefer one divalent cation to two monovalent cations. Samuelson and Sjöström[85] synthesized EDTA and acetate to a strongly basic anion exchange resin (Dowex 2) to form chelating resins, and noted the selective retention of Ca^{++} and Mg^{++} ions from a solution containing alkali ions. Olsen and Sobel[86] performed a similar separation by precomplexing the alkali earths with EDTA before passing the solution through a bed of polystyrene resin (Dowex 50W) in the tetramethylammonium form. This resin retained

the alkalis and passed unchanged the preconplexed alkali earths. The kinetics of a commercially available chelating resin (Dowex A1) were investigated by Turse and Rieman[87]. They found that although exchange rates were relatively slow, some cations, namely alkali earths and hydrogen but not alkalis, were capable of a very strong complexing action. Pennington and Williams[88] found that this resin in sodium form was capable of completely removing traces of heavy metals from relatively concentrated salt solutions. Gregor, Taifer, Citarel and Becker[89] have summarized the bases of selectivity of ion exchange resins and the suitability of chelating groups.

Chelating agents do not have to be used in resin form. Gruzensky[90] used alizarin in alcohol to purify an aqueous solution of NaCl. Butler, Russell, Quincy and LaValle[91] successfully extracted impurities from KCl with TTA-Hexone. Uses of liquid-liquid extraction techniques, involving the separable ions in an aqueous phase and the chelating agent in an organic phase immiscible with water, are discussed by Sandell[92] and by Alders[93].

Purification Apparatus and Procedure

Borosilicate glassware was used to reduce the risk of contamination. It was cleaned in a mixture of sulphuric and chromic acids, and then in a commercial cleanser, Decon 75 to deionize the surfaces. Finally, it was rinsed thoroughly in deionized water. Figures 10 to 12 show schematically some of the apparatus used.

A variety of methods for the purification of Analar grade sodium chloride was adopted. These processes were chosen from the literature as being at least partially effective

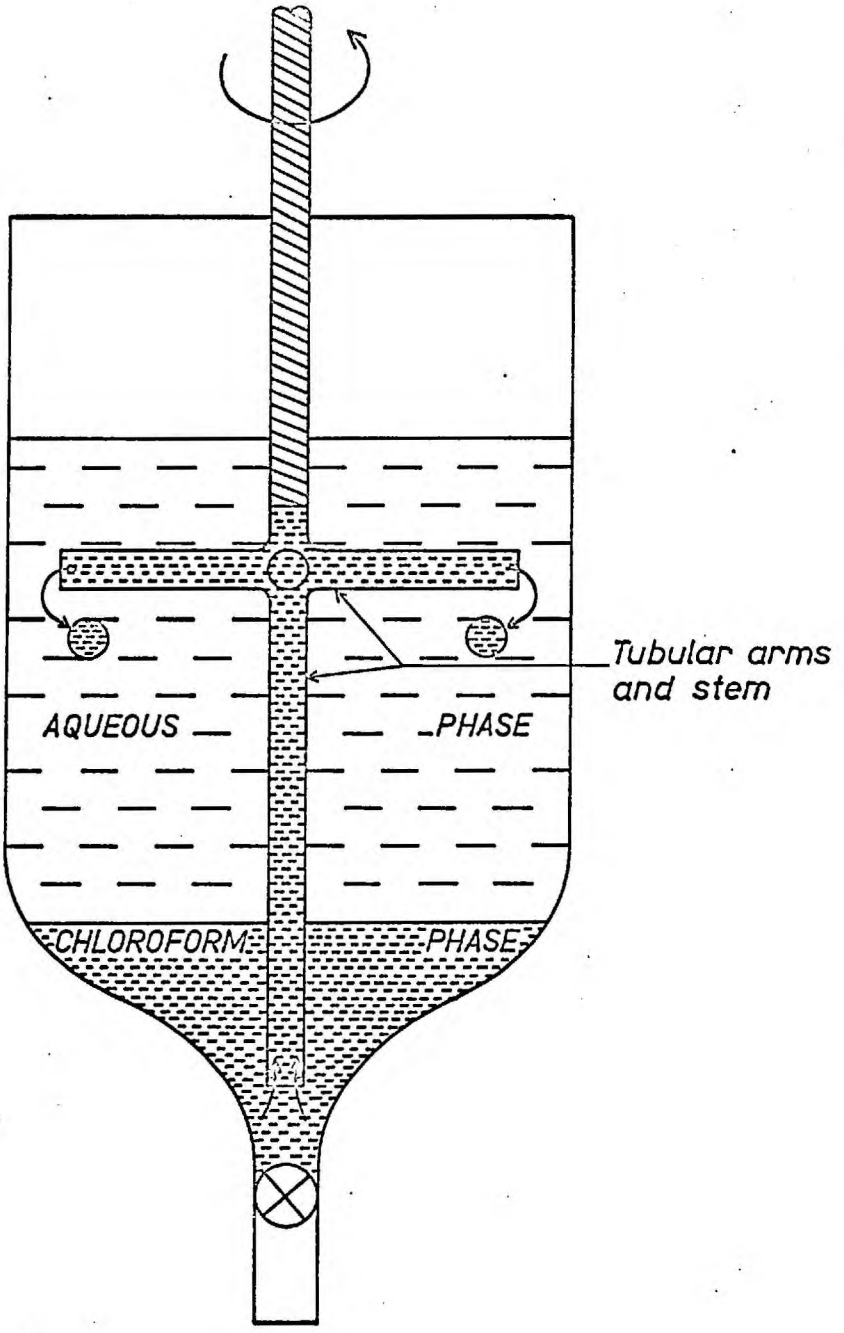

Fig. 10. LIQUID - LIQUID EXTRACTION VESSEL

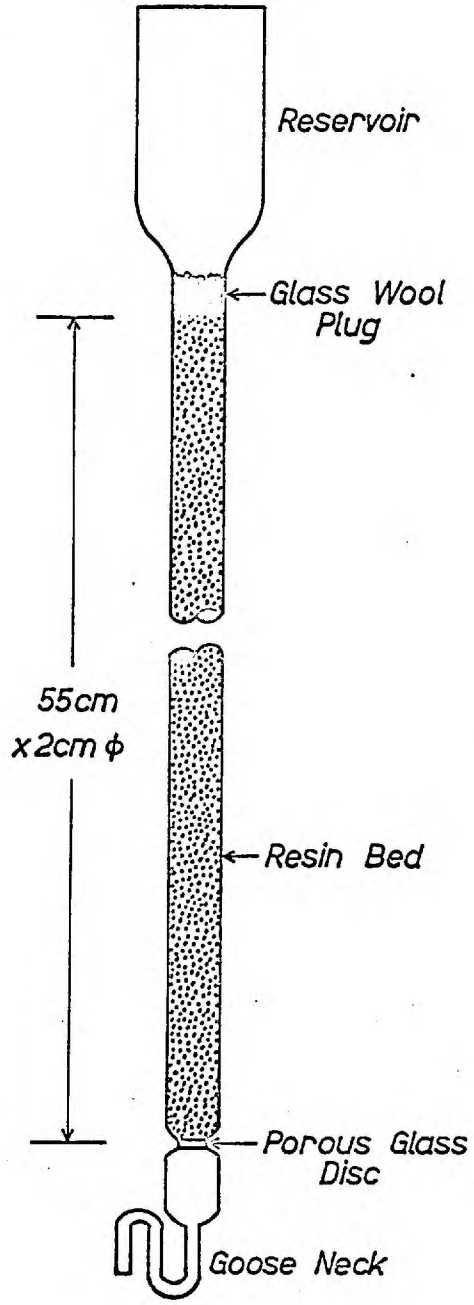

Fig. 11. ION EXCHANGE COLUMN

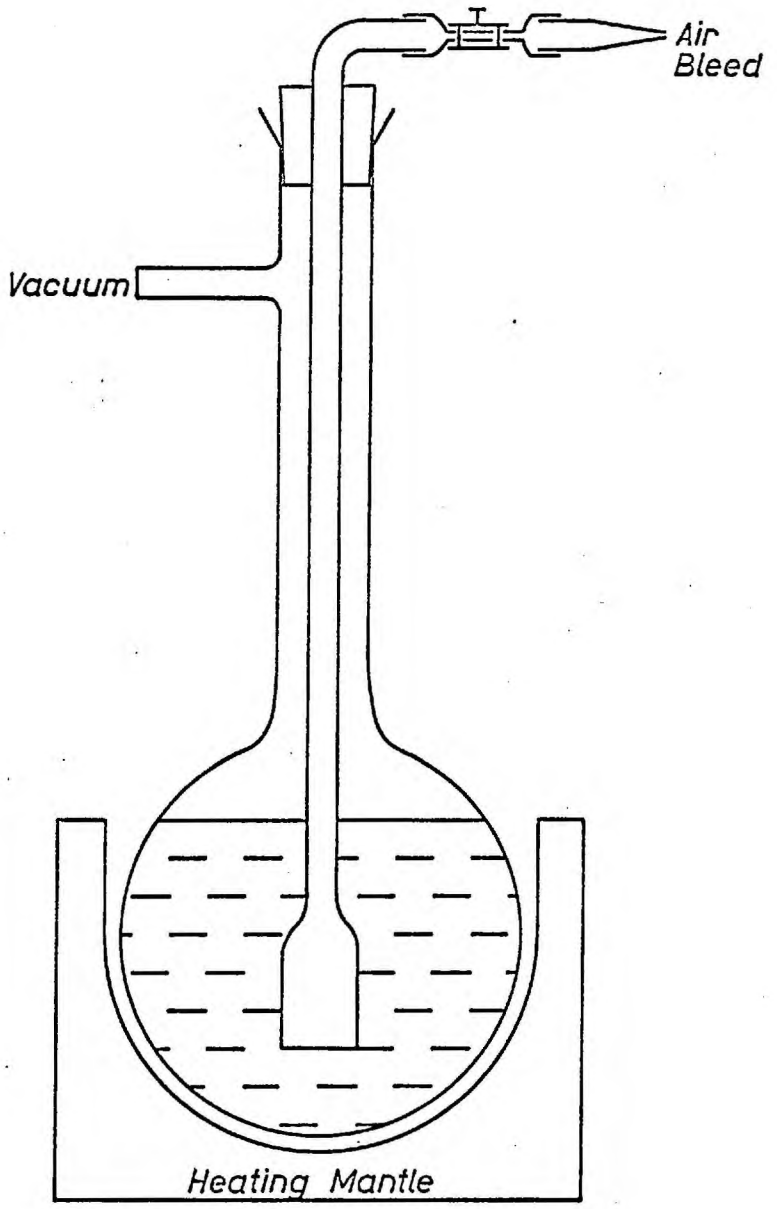

Fig. 12. DISTILLING FLASK FOR RECOVERY OF NaCl

for the removal of polyvalent cation impurities. Figure 13 shows the flow chart for the procedure. For testing purposes, a solution of 100 grams per litre (gpl) NaCl containing added multivalent impurities (in the same proportion and quantity as the specifications) was passed through each stage. A colorimetric analysis using a Parkin-Elmer 450 Spectrophotometer showed qualitatively that each step was effective for multivalent ion removal, at least for the added impurity concentration. Although little could be said about the analysis of a solution without the added impurities, the effectiveness of ion exchange resins is virtually independent of concentration for low levels. Each stage was therefore considered to be at least partially effective for the removal of the smaller impurity concentrations in the Analar NaCl.

One litre portions of a solution of 100 gpl NaCl in deionized water were solvent extracted for 10 minutes with 100 c.c. of chloroform containing 0.01 percent dithizone and 0.05 percent oxine. As the aqueous phase and the heavier chloroform phase were immiscible, the mixing tank in Figure 10 was used. The revolving stirrer drew chloroform up through the glass tube and droplets were thrown out by the tubular arms into the aqueous phase. After allowing the phases to settle and separate the chloroform was removed and discarded. The aqueous phase was then drawn off and vacuum filtered through a Whatman GF/C glass-fibre filter paper of about 10 micron pore diameter. Dithizone and oxine are chelating agents that form complexes with most heavy metals in organic phases. They are particularly effective for Pb, Fe, Ba and Cu but can partially remove Ca and Mg. These complexes are insoluble in water, and were removed with the chloroform phase. Any complexed ions in the

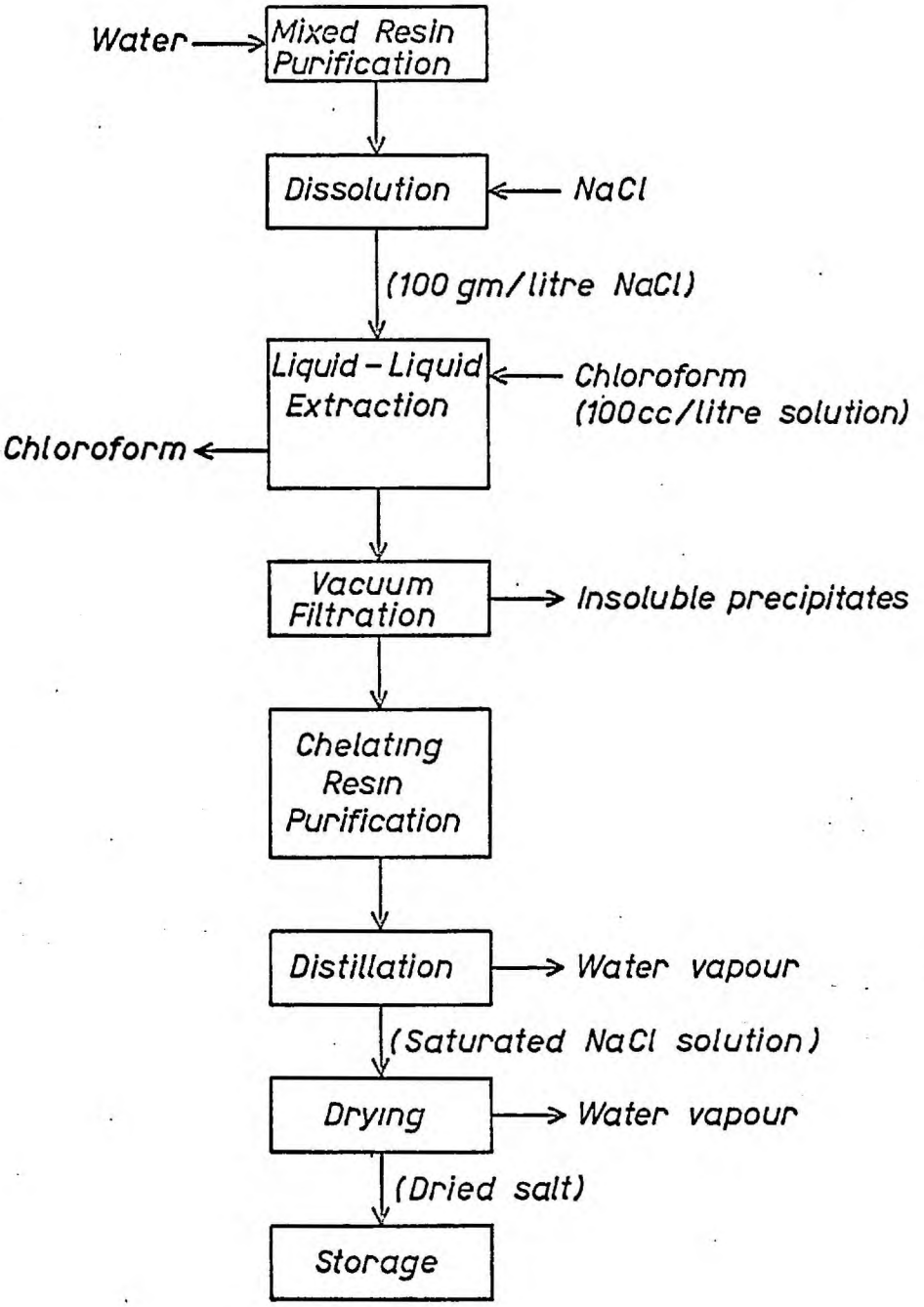

Fig. 13. FLOW CHART FOR PURIFICATION PROCESS

aqueous solution precipitated and were removed by filtration.

The filtered salt solution was then passed through three consecutive chelating resins. The first resin[94] was prepared by conversion of a weakly basic anion exchange resin (De Acidite E), replacing the tertiary amine groups with monochloroacetic acid radicals. 200 gms. of the moist resin were added to 1.5 litres of 10% NaOH and 100 gms. of monochloroacetic acid. After heating with agitation for 20 hours at 60°C, the solution was decanted from the resin and the resin washed several times, alternately with 1N NaOH and 1N HCl, rinsing between each wash with deionized water. A final rinse of the resin, now in the sodium form, was continued until the rinse water was nearly neutral. The second resin[88] was synthesized from resorcinol and formaldehyde with oxine as the chelating group. 0.2 mole of 8-hydroxyquinoline (oxine) was added to 30 c.c. of 6N NaOH and 100 c.c. of deionized water. The solution was allowed to stand for one hour after slowly adding 40 c.c. of 37% formaldehyde. A solution of 0.2 mole resorcinol in 30 c.c. of 6N NaOH and 100 c.c. of deionized water was then added, followed by a further 40 c.c. of 37% formaldehyde. Upon heating over a steam bath to 100°C for several hours the solution solidified into a rubber-like mass which was ground and screened (-20+35 mesh). The resin was then washed and rinsed as for the first resin, but using 0.1N HCl and 0.1 N NaOH. The third resin[95] was the commercial resin Dowex A1, and was also used in the sodium form.

The filtered salt solution was passed consecutively through one column of each of the synthesized resins and two columns of Dowex A1 resin. All the columns were 2 cm. in diameter and 60 cm. in length, with a 250 c.c. reservoir at

the top and a goose-necked capillary tube at the bottom which prevented air entrainment in the column. The resin bed, supported on a porous, sintered glass disc was 55 cm. in height. The flow rate through all columns was 25 c.c. per minute.

To recover the salt from the aqueous phase, 2 litre portions were boiled under vacuum in a distilling flask until saturated. A small air bleed was found necessary to keep the solution boiling, presumably due to the absence of surface irregularities or contaminants in the flask which normally act as nucleation sites. The saturated solution was then evaporated to dryness in an oven at 80°C, and the recovered salt was stored in polyethylene containers until needed.

Results of Purification

As shown in Table 5 the purification process was effective for the removal of cation impurities. Conductivity measurements on single crystals grown from the purified salt however, did not show any appreciable decrease in the 'knee' temperature compared with that of crystals grown from Analar grade salt. The analysis of melt grown crystals indicated that contamination during crystal growth was not unduly large, although the magnesium concentration in the purified salt was significantly higher after crystal growth. This could be contamination from the silica beaker but could also conceivably be due to inaccuracies of the analysis. The important point is that the purified material had less impurity than Analar material irregardless of its absolute concentration.

Impurity	Before Crystal Growth		After Crystal Growth	
	Analar	Purified	Analar	Purified
Ca	30 ppm	< 5 ppm	50 ppm	< 5 ppm
Mg	10	< 1	20	~ 5
Fe[a]	5		1	1
Al	< 2			
Cu	< 0.5			
Cr			< 4	< 4
Ni[b]			4	3

Analysis by Atomic Absorption or Emission Spectroscopy except as indicated.

a) colorimetric thiocyanate.

b) " dimethyglyoxine

Materials analysed before and after growth were not from the same batch.

Table 5 Impurities after Purification

2-2 Growth of Bicrystals

Introduction

Many investigators have dealt with the problems of growth of alkali halide crystals. Dreyfus[80] has reviewed the methods in 'The Art and Science of Crystal Growing'. Rosenberger[96] summarized the basic parameters of crystal growth on the bases of recent publications and his own experience. One of the earliest techniques was the Bridgeman[97] (also Stockbarger) method. Salt, in a sealed silica tube with a conical shaped end, was passed slowly through the natural temperature gradient of a tubular furnace. The conical point tended to nucleate growth of a single crystal as it passed through the hot zone (where the salt just melted) and into the cooler zone. With any luck, at least a polycrystal of very large grain size was produced. A recent technique has been devised by Gruzensky[90] who grew large, very pure single crystals from an aqueous solution. Solution grown crystals are not new in themselves, but crystals as large as 2 cm. along an edge are. Nucleation sites in a relatively large volume of solution must be kept to an absolute minimum. Great purity and absolute cleanliness are necessary. A common method for producing single crystals of NaCl is the Kyropoulos[98] (also Czochralski) method. This method involves the growth from a melt onto a cooled, single crystal 'seed'. The melt is maintained just above the melting point and once growth has begun, the seed and the resulting single crystal are withdrawn slowly from the melt, the crystal continuing its growth at the solid-melt interface.

Several methods have been devised to form bicrystals. Hosoya, Satake and Takagi[99] have investigated small angle tilt boundaries produced by polygonization in crystals under bending loads. Cabane[28] hot pressed two suitably cleaved crystals together to form a grain boundary. Martin, Fehr and McGee[60] used a hot wire technique developed by Long and McGee[64]. In this latter method, a resistance heated platinum wire, a few degrees hotter than the melting point of the salt, is passed down the surface between two crystals held together. A little of each crystal melts, and resolidifies to form a boundary. Fuschillo, Gimpl and McMaster[63] produced bicrystals of NaCl by the Kyropoulos method. They found that in order to grow planar boundaries the following conditions must prevail;

1. The two seeds must be spaced slightly apart and must be immersed into the melt about 20°C above the melting point in order to establish a temperature equilibrium and to allow the removal of polycrystalline overgrowth formed on the seeds when first immersed.
2. Each seed must enter the melt surface at exactly one-half the desired angle of misorientation.
3. The melt temperature must be lowered slowly until the seeds grow together and form a boundary before the pulling motion is initiated.

Crystal Growth Apparatus and Procedure

Many refinements have been made to the original Kyropoulos technique and some are incorporated into the crystal growing apparatus shown in Figure 14, 15 and 16. Some of the features of this apparatus are;

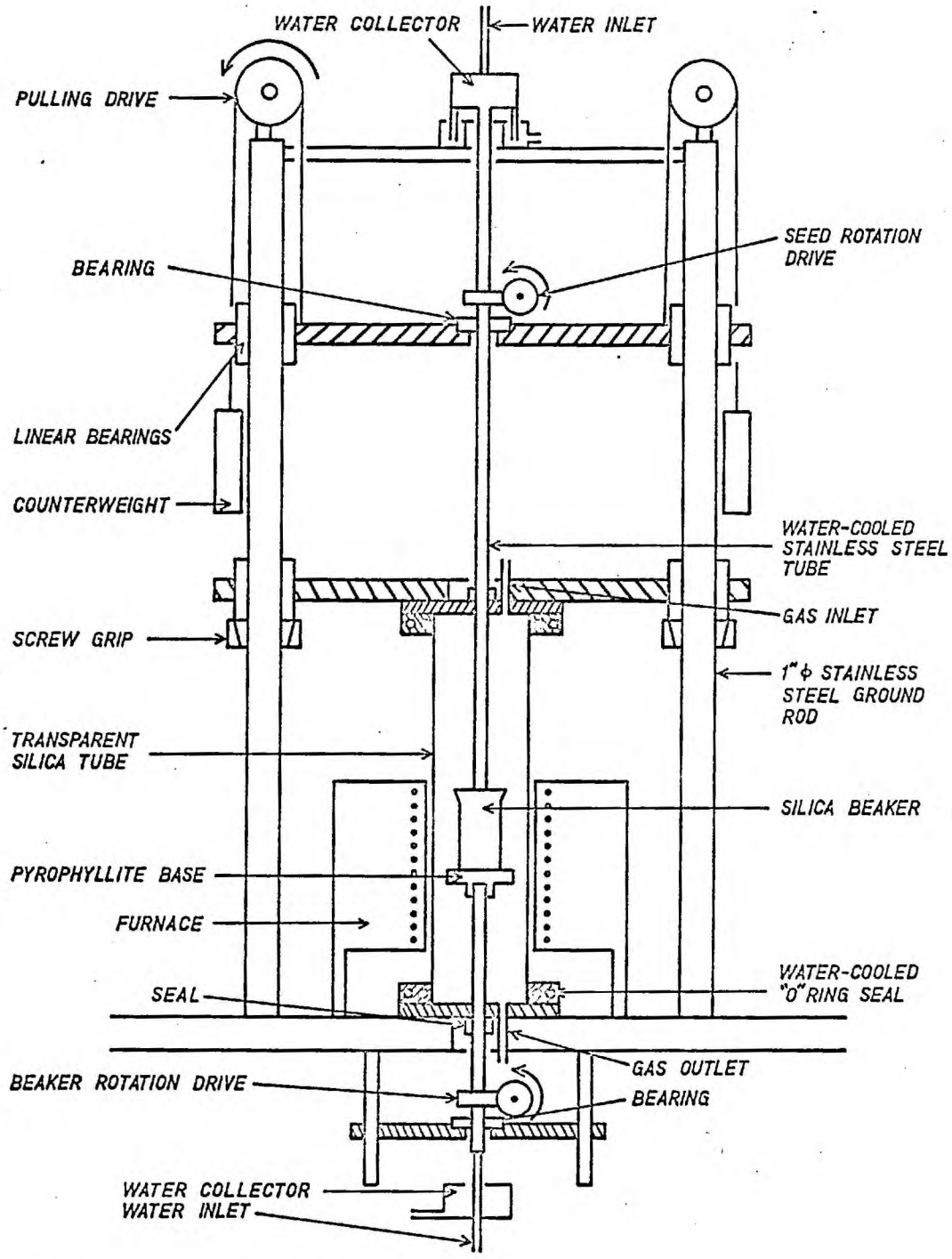

Fig. 14. CRYSTAL GROWING APPARATUS

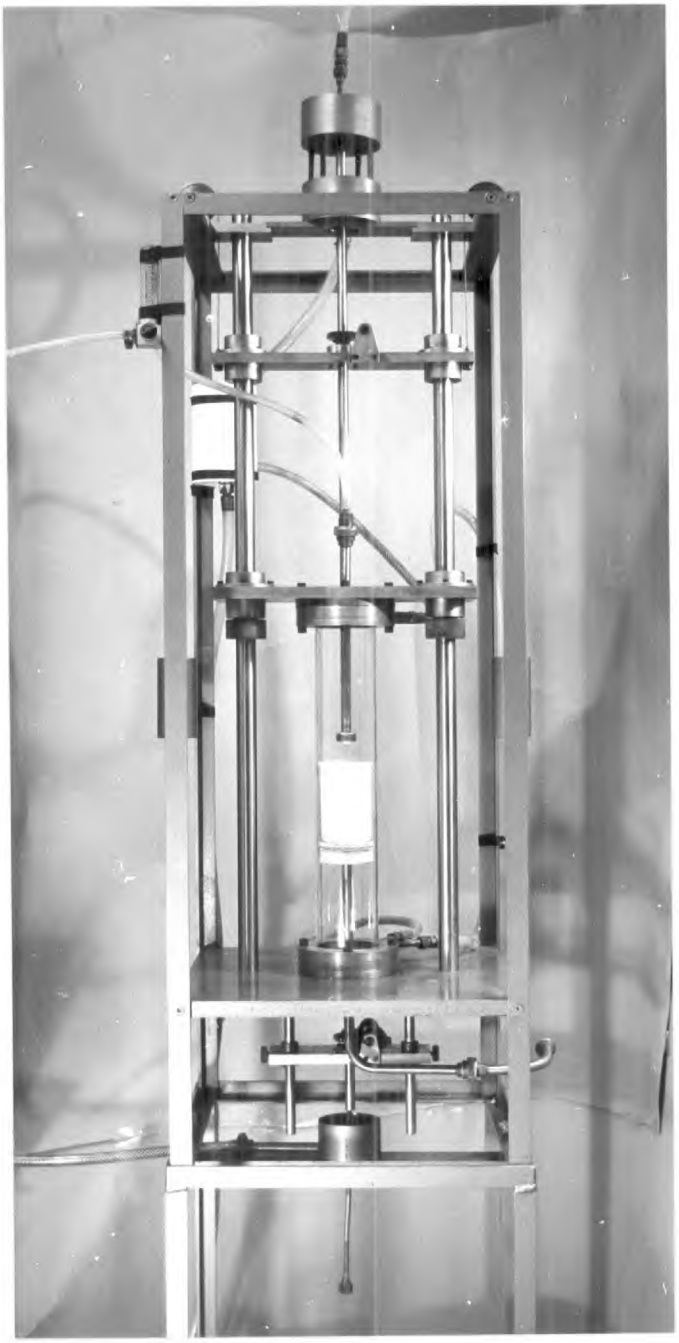

Fig. 15 General View of the Crystal Grower

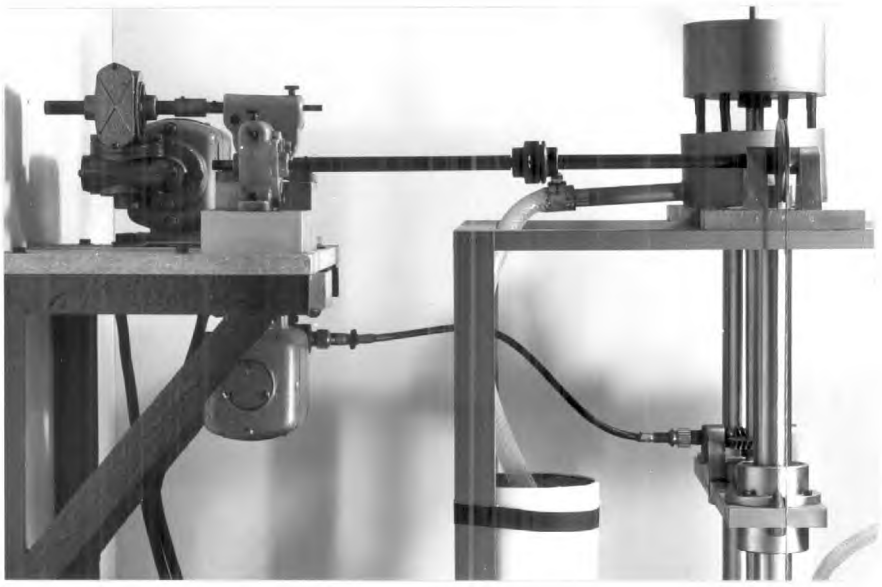

Fig. 16 Drive Mechanism of the Crystal Grower

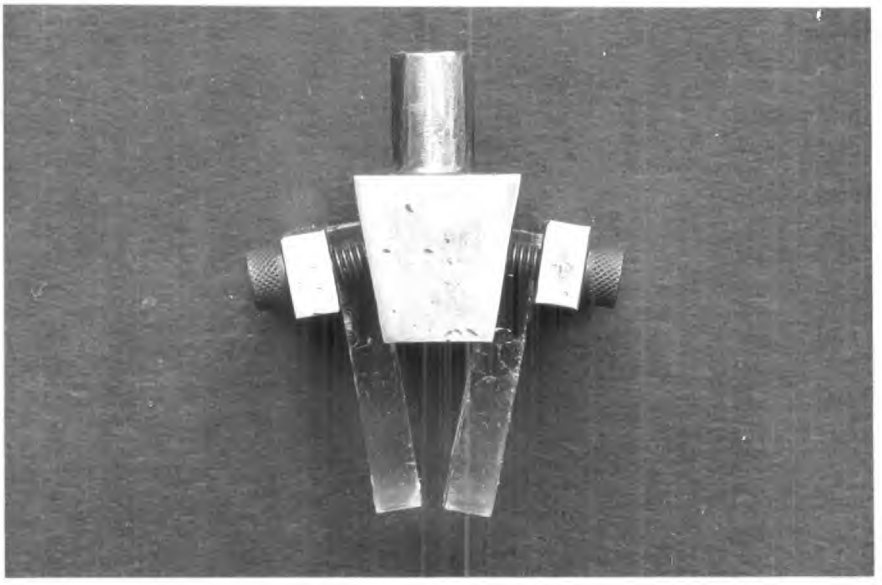

Fig. 17 Seed Chuck with Seeds

1. A transparent, fused silica tube maintaining an inert atmosphere and allowing good visibility of the growing crystal.
2. A furnace situated outside the tube to minimize contamination of the melt.
3. Water-cooled, stainless steel parts within the tube to minimize contamination and to prevent corrosion.
4. A rotating melt beaker to eliminate circumferential temperature gradients.
5. An asymetrically wound furnace to maintain an even temperature profile along the length of the furnace.
6. A cooled base for the melt beaker to minimize vertical temperature gradients in the melt.
7. A variable speed seed-withdrawal rate which permits small corrections to the growth rates.
8. Independent, variable speed rotation of the seed which permits good visibility of the growing boule and which gives a stirring action that helps to remove unwanted parasitic growth in the initial stages.

Seed chucks for the crystal grower were made from stainless steel similar to those of Fuschillo et al., the desired angle of misorientation being machined into the chucks to ensure correct alignment of the seeds (Figure 17).

Seed crystals were cleaved from pure single crystals of NaCl (2 cm. X 1 cm. X 3 mm.) and carefully aligned in the seed chuck. When the melt temperature had reached 820°C, the seeds were immersed and rotated at 10 r.p.m. for 15 minutes. The temperature was then lowered and the seeds allowed to grow together after a visual inspection confirmed the removal of overgrowth. Once they had grown together, the seeds were

withdrawn at between 0.3 and 0.4 inch per hour. The boule grew to about 1 inch in diameter and, to maintain this size, the temperature of the melt was lowered by 3 to 4°C approximately every two hours. All the crystals were grown in a dry argon atmosphere and then slowly cooled in argon over a period of 30 hours.

Seed chucks with angles up to 40° total angle were machined. Bicrystals of greater than 40° of tilt misorientation were grown using the same set of chucks. The seeds in these cases were cut on a diamond saw at an angle of 20° to the (100) cleavage planes.

Observations on Bicrystal Growth

With this apparatus, bicrystals with simple symmetrical tilt misorientations of 10, 20, 30, 40, 50, 60, 70 and 80 degrees were grown. Although the angle of the boundary with (100) planes is one-half the total misorientation, this thesis will always refer to bicrystals by the angle between corresponding (100) planes in either half. Thus a boundary at 10° to the cleavage faces will be referred to as a 20° boundary.

Planar boundaries resulted if the following three additional conditions were met;

1. The seeds must be similar in size and shape and must have equal contact area with the seed chuck to avoid differences in the cooling rates. Otherwise, the boundary will curve toward the lesser cooled seed.
2. For tilt boundaries there must be no net twist component of angle between the two seeds. Otherwise the boundary will curve into an 'S' shape along the line of the growth.

3. The bicrystal must be allowed to grow at the maximum temperature possible. Large amounts of subgrain boundaries and meandering grain boundaries result from too rapid crystal growth.

Figures 18 and 19 show the planarity of the grain boundaries. The shape of the solid-melt interface during growth can also be seen. The boundaries in bicrystals of less than 10 degrees total misorientation were never planar and rapidly grew out the side of the crystal. In general, fewer attempts were necessary to grow planar high angle boundaries than to grow low angle boundaries.

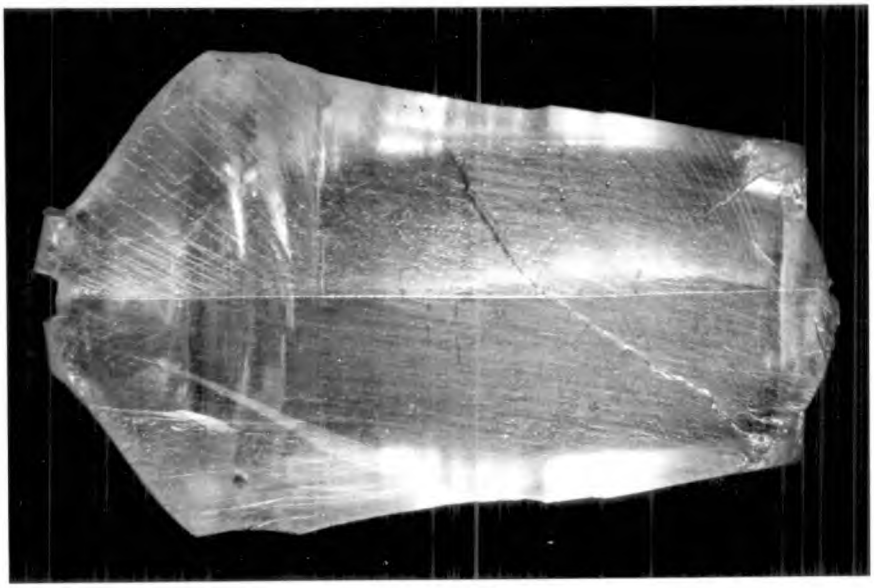

Fig. 18 20° Cleaved Bicrystal X 2

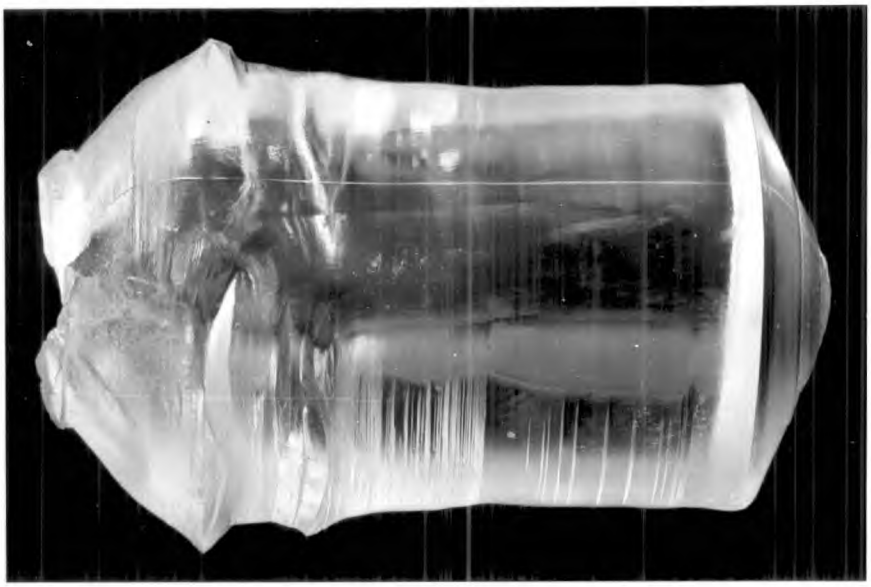

Fig. 19 70° Bicrystal X 2

CHAPTER 3

EXPERIMENTAL METHODS

3-1 Grain Boundary Conductivity Measurements

Specimen Preparation

The method of Moment and Gordon[29] was used to investigate the conductivity of ions 'injected' into grain boundaries. A small spot of material containing the 'dopant' species was vapour deposited onto a specimen surface directly over a grain boundary. The dopant ions were injected into the boundary by applying a large d.c. field across the specimen. The a.c. conductivity was measured with a small probe placed over the boundary on the face opposite the deposited spot. Most specimens were cleaved but some were cut to give surfaces that were orthogonal to the common cleavage plane of bicrystals. Pieces were mounted with Durafix and specimens were cut with a Capco diamond wheel slitter. The cut faces were orientated orthogonally to both the plane of the boundary and to the common cleavage plane. Cut specimens were thicker than the cleaved ones, being between 0.9 and 1.1 mm., because of the tendency to break during the slitting operation. The specimens were removed from the base by soaking in acetone to dissolve the Durafix. A rinse in ethanol was followed by a brief polish in distilled water to make the boundary visible on the cut surface.

The vapour deposition apparatus (without the vacuum system) is shown schematically in Figure 20. The specimen was mounted as shown upon a disc of platinum foil having a central hole of 0.5 mm. diameter. To ensure correct alignment, the specimen was viewed through the hole under oblique light with the aid of a microscope. The silica boat was filled with the appropriate alkali halide which had previously been dried

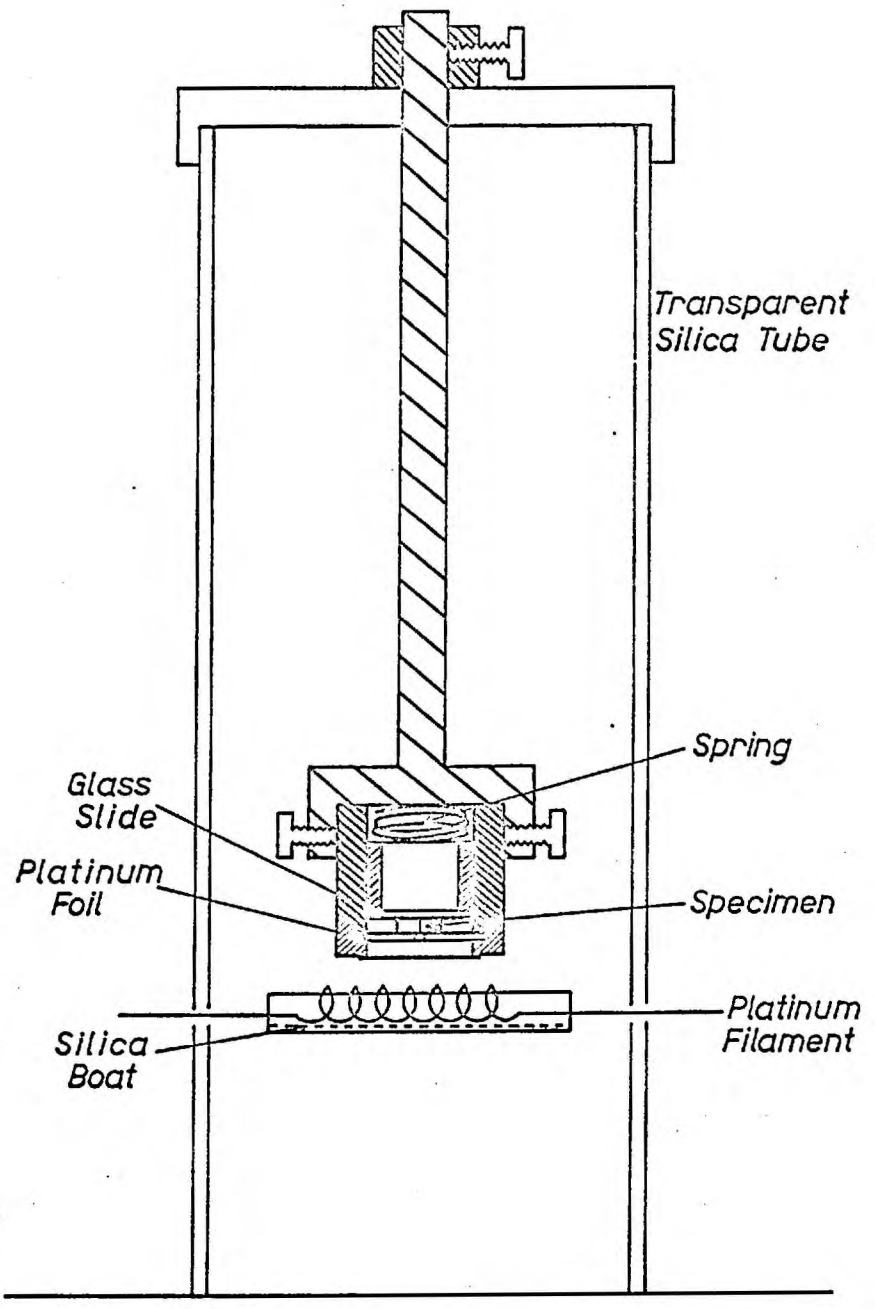

Fig. 20. VAPOUR DEPOSITION APPARATUS (inside bell jar)

and ground in a mortar. The system was evacuated to less than 5×10^{-5} torr and the current in the platinum filament, supplied by a Variac autotransformer, was raised in stages to 2.7 amps, whereupon evaporation took place in approximately 15 minutes. Because of the platinum foil mask, only a spot 0.5 mm. in diameter was actually deposited on the specimen.

Apparatus

The conductivity rig is shown in Figures 21 and 22. The large nickel electrode (1 cm. x 1.5 cm. dia.) helped to even out temperature gradients in the short length (3 in. x 1.5 in. dia.) of the furnace. The probe electrode was a nickel-tipped stainless steel rod fitted through a gas-cooled vacuum seal located centrally in the optically flat, quartz glass window. The end of the probe in contact with the specimen was flat and was rectangular in shape, being approximately 0.31 mm. by 0.11 mm. in size. Positioning of the probe was accomplished by the movement of the window manipulated by two calibrated micrometer screws as shown in Figure 23. The springs ensured positive movement in any direction. The probe was positioned over the boundary with the aid of oblique light and a long focal length microscope. The pressure exerted by the probe upon the specimen could be altered by adjusting the pressure of the vacuum seals on the probe shaft.

The furnace consisted of a nichrome wire element wound onto a silica tube core and was insulated with a porous fire brick. It was powered with smoothed, 220 volt mains direct current ensuring minimum a.c. pickup by the measuring circuit. The temperature was controlled by an Ether Transitrol Controller to better than $\pm$ 1°C, using a chromel-alumel thermo-

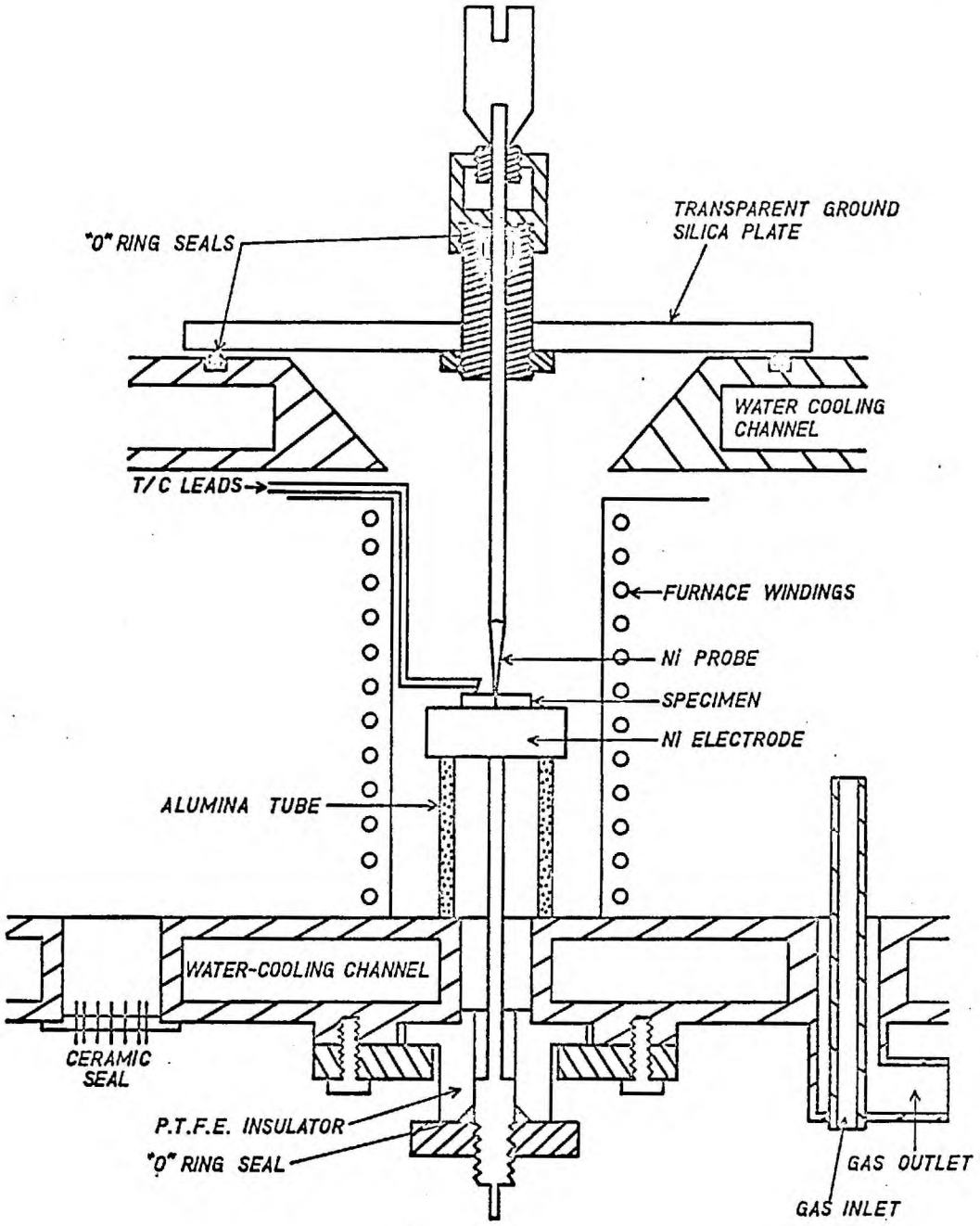

Fig. 21. GRAIN BOUNDARY CONDUCTIVITY APPARATUS

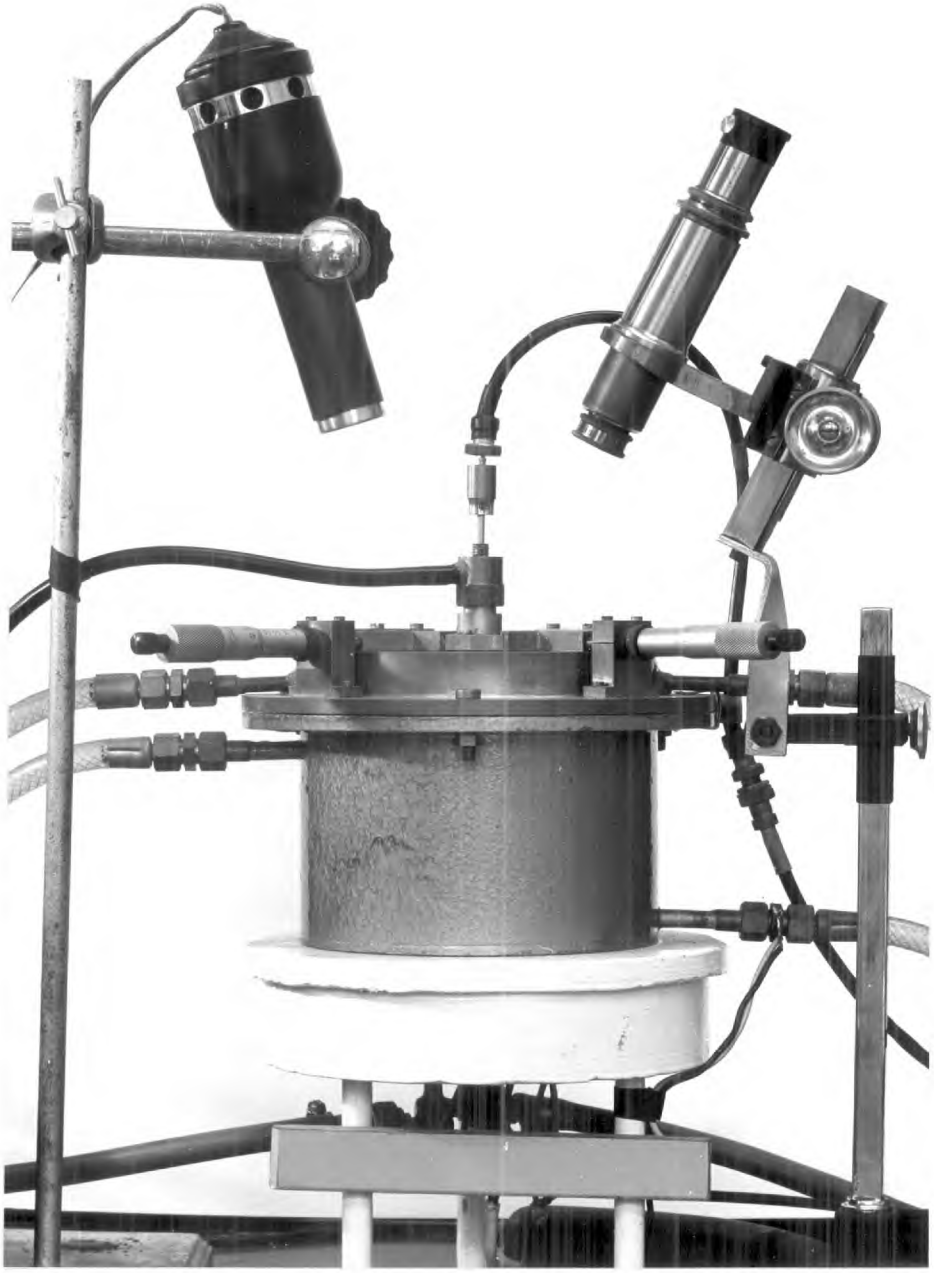

Fig. 22 General View of the Grain Boundary Conductivity Apparatus

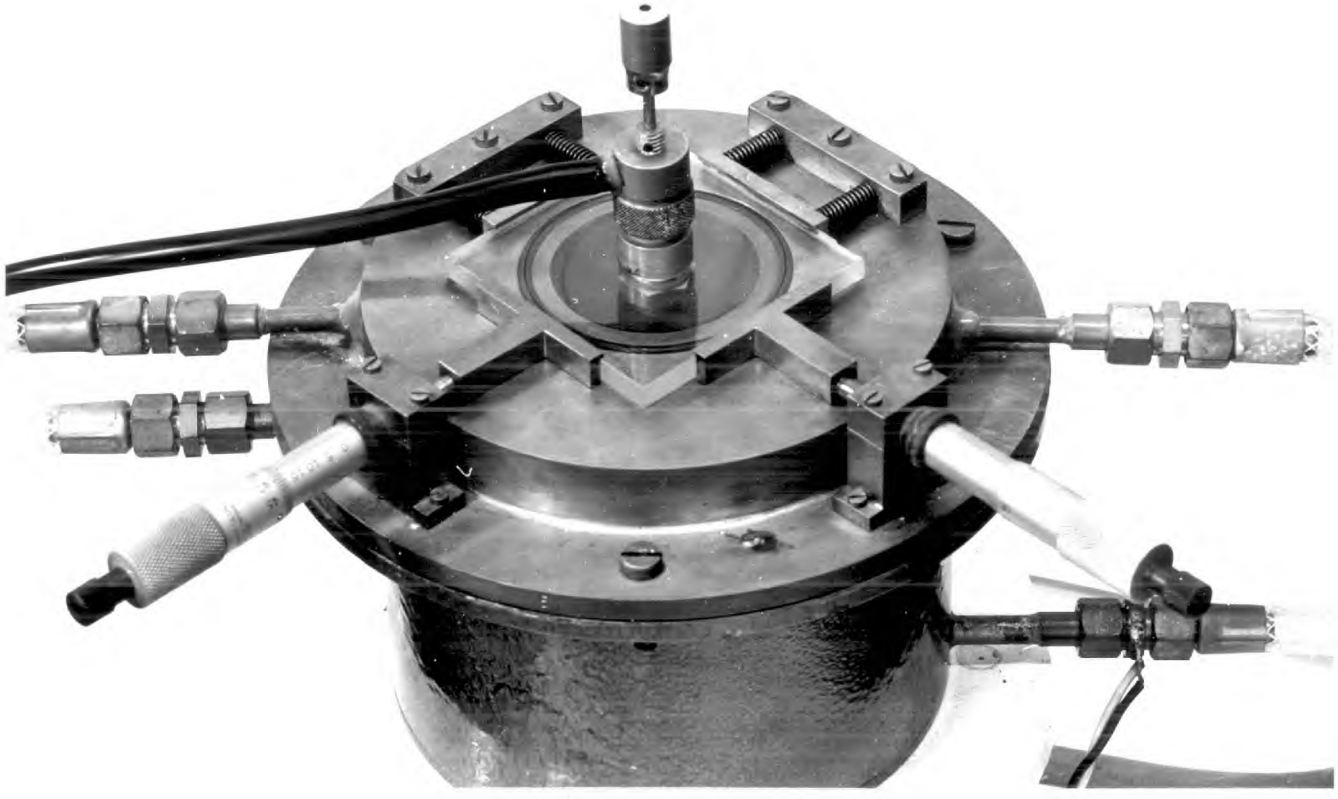

Fig. 23 Top View of the Grain Boundary Conductivity Apparatus

couple touching the inside of the core tube. A variable resistor in series with the furnace windings allowed an approximate power setting. The assembly could be evacuated to better than 10^{-4} torr in the normal operating condition.

Initial conductance measurements indicated large temperature gradients, both vertical and horizontal, on and near the electrode. To eliminate the vertical gradients the position of the lower electrode was varied until the temperature remained the same at a position 1 mm. above the electrode as it was immediately below on the electrode. During actual experiments, the probe was positioned near the specimen thermocouple but at the same radius from the electrode centre point. These precautions achieved greater consistency of the results.

A diagram of the measuring circuit is shown in Figure 24. The three way switch had ceramic insulators to maintain a high insulation resistance throughout the circuit. The PTFE plug in the casing and the quartz glass window were kept clean and dry to inhibit paths of leakage current. All external leads were made with coaxial cable, the screening being at earth potential. The insulation resistance of the complete circuit was thus maintained at over 10^{10} ohms. The noise level on the measuring circuit was negligible.

The electric field necessary for the 'injecting' operation was supplied by three 120 volt drycell batteries in series. The full potential was dropped across a 100K ohm potentiometer and the potential across the specimen could be varied continuously by means of the wiper arm. The potential across the specimen was measured by a Solartron Digital Voltmeter. The current flowing through the specimen was measured by switching the voltmeter into parallel with a known resistance in series

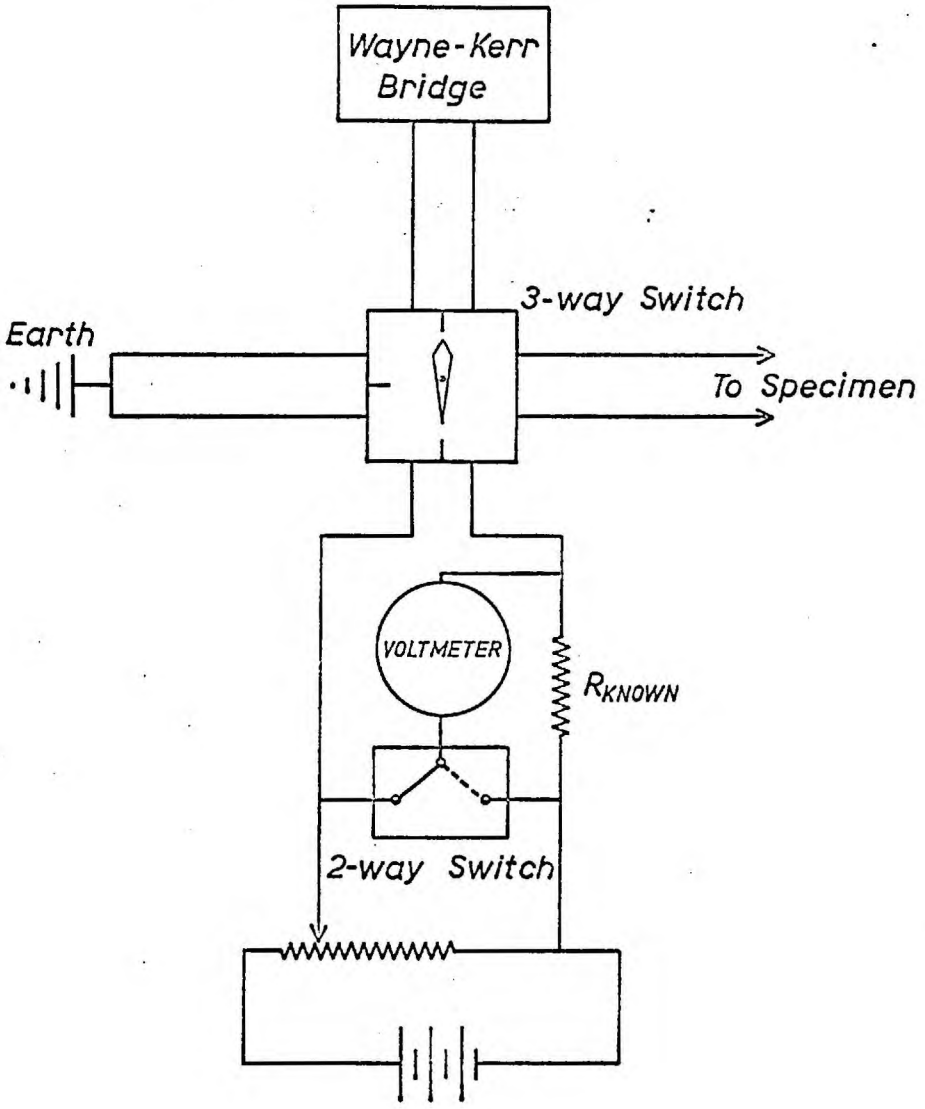

Fig. 24. CIRCUIT DIAGRAM FOR GRAIN BOUNDARY CONDUCTIVITY

with the specimen.

A Wayne Kerr Universal Bridge was used to measure the a.c. conductance. This bridge, altered on the conductance circuit to read down to 10^{-10} ohm^{-1}, operates on the transformer ratio arm principle, balancing unknown impedances against standards of resistance and capacitance. Transformer tappings connected to decade controls permit accurate readings over a wide range of impedance. Zero trim controls, to eliminate stray capacitances or conductances, were generally set with all the components in the circuit except the specimen. The procedure was especially critical when measuring on the most sensitive instrument ranges. The frequency of the applied signal was 1592 cycles per second, the root mean square voltage being approximately 30 millivolts on the two most sensitive ranges.

Procedure

A prepared specimen was placed on the electrode inside the furnace with the spot of vapour deposited alkali halide in contact with the electrode. A chromel-alumel thermocouple was placed on top of the specimen, insulation being provided by a thin flake of alumina cut from a solid polycrystalline rod. The probe was fixed a short distance above the specimen with a grub screw, and the system was evacuated to about 100 microns of mercury and flushed with high purity argon. This step was repeated four to five times before the furnace was heated to 450°C. After achieving equilibrium, the probe was released and positioned over the grain boundary directly above the deposited spot. Both the spot and the grain boundary line were visible under the correct lighting conditions. The vacuum seal was

adjusted to a pressure at which the probe would just slide through the seal under its own weight. Again waiting for the temperature to equilibrate (as indicated by the conductance) before proceeding, conductance measurements were made at 15 to 20 degree intervals down to 380°C. At this point, a d.c. field was applied across the specimen. The potential of about 250 volts was applied for approximately 20 minutes. The electrodes were then earthed briefly before switching the bridge back into the circuit. The temperature was held constant until a steady conductance was observed, and measurements were resumed at 10 to 20 degree intervals down to at least 300°C.

The measurements were made under descending temperature conditions for two reasons. Firstly, annealing the specimens at 450°C removed surface damage caused by placing the probe on the specimen, as evidenced by a change in the conductance at constant temperature. Secondly, a contraction of the probe length occurred during cooling cycles. By allowing the probe to slip through the vacuum seals under its own weight, the contraction did not affect the nature of the probe-specimen contact. During heating cycles, expansion of the probe length severely indented the specimen. Surface damage was thus minimized while retaining good contact even though the probe length changed during an experiment.

3-2 Surface Potential Profile Measurements

Apparatus

The experimental apparatus is shown in Figures 25 to 27. A specimen was heated while in a d.c. field and the potential profile across the edge surface between the electrodes was recorded using a small diameter probe which traversed the specimen surface at a slow speed. The furnace was supplied by a Variac autotransformer driven by mains alternating current and the temperature was controlled to $\pm$ 1°C by an Ether Transitrol Controller operated by a chromel-alumel thermocouple placed on the furnace windings. The inside surface of the core and the top plate of the furnace were painted with a suspension of silver paste in alcohol to form a monolithic conducting layer which, when earthed, screened the specimen and electrodes from a.c. pickup.

The specimen was held by slight spring pressure between platinum foil electrodes, each with its own platinum wire lead. The stainless steel retainers were mounted on an alumina disc which in turn was suspended into the hot zone by stainless steel rods fixed at the top of the furnace. The whole arrangement was quite rigid inside the furnace.

The probe was made by suspending a length of 0.008 in. diameter tungsten wire vertically into a mixture of nitric and hydrofluoric acids, which dissolved the immersed tungsten to form a pointed end of approximately 10 microns diameter. The wire was sheathed in a small bore alumina tube (Degussit Al23) which was clamped to the end of a balanced rod. The balanced rod was pivoted on jewelled points mounted on a movable platform, and was counterbalanced to allow for adjustments in the

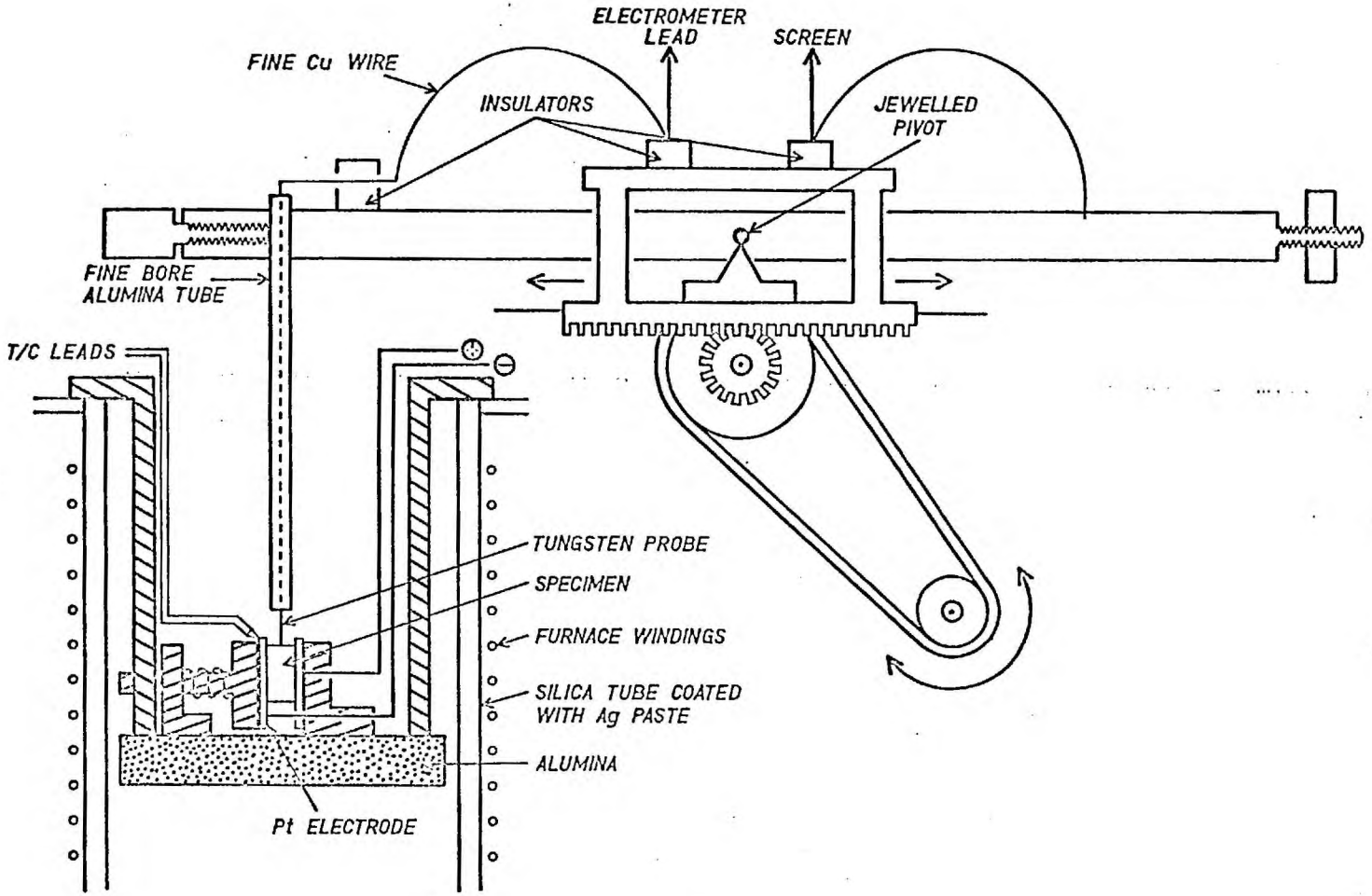

Fig. 25. POTENTIAL PROFILE APPARATUS

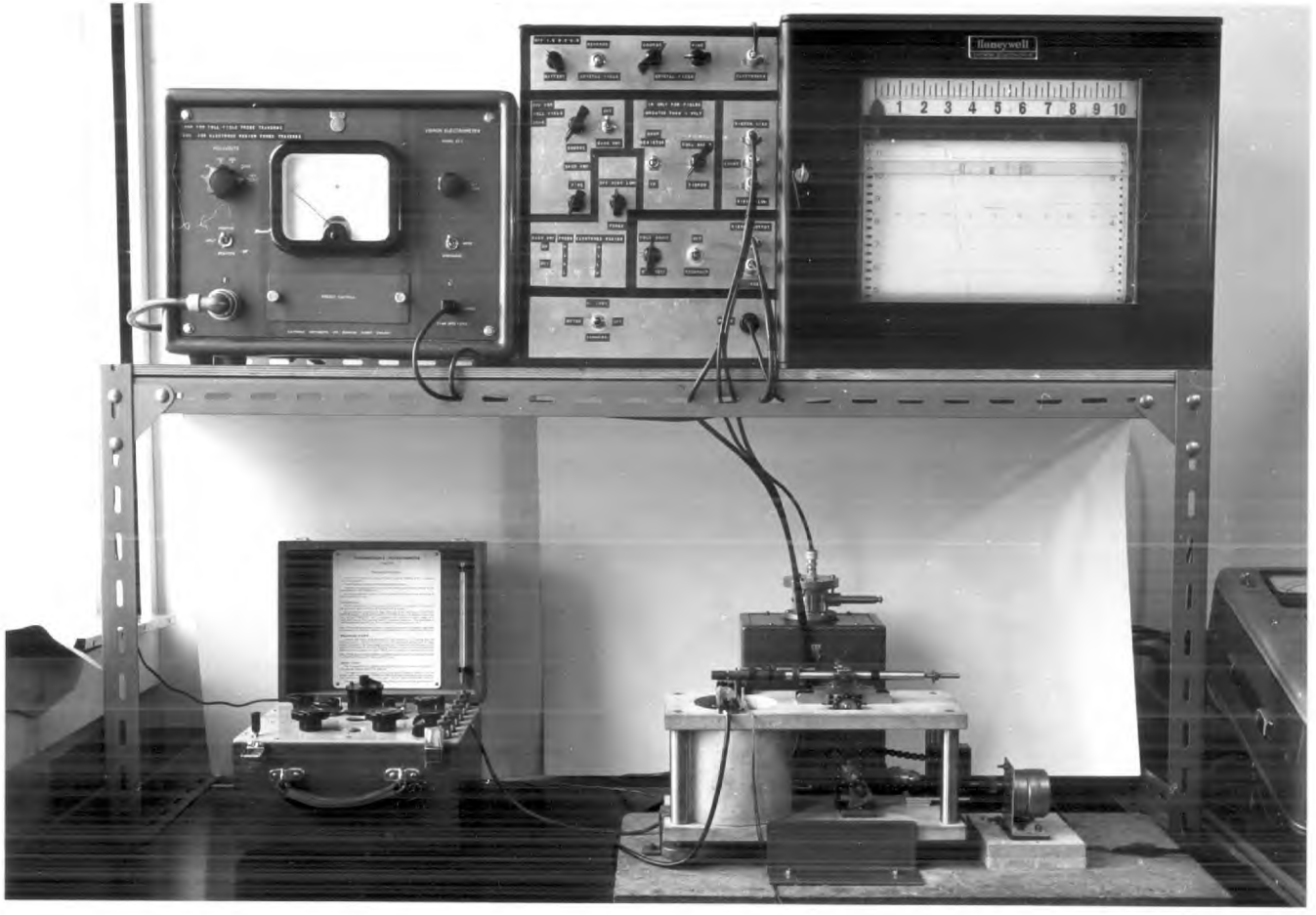

Fig. 26 General View of the Potential Profile Apparatus

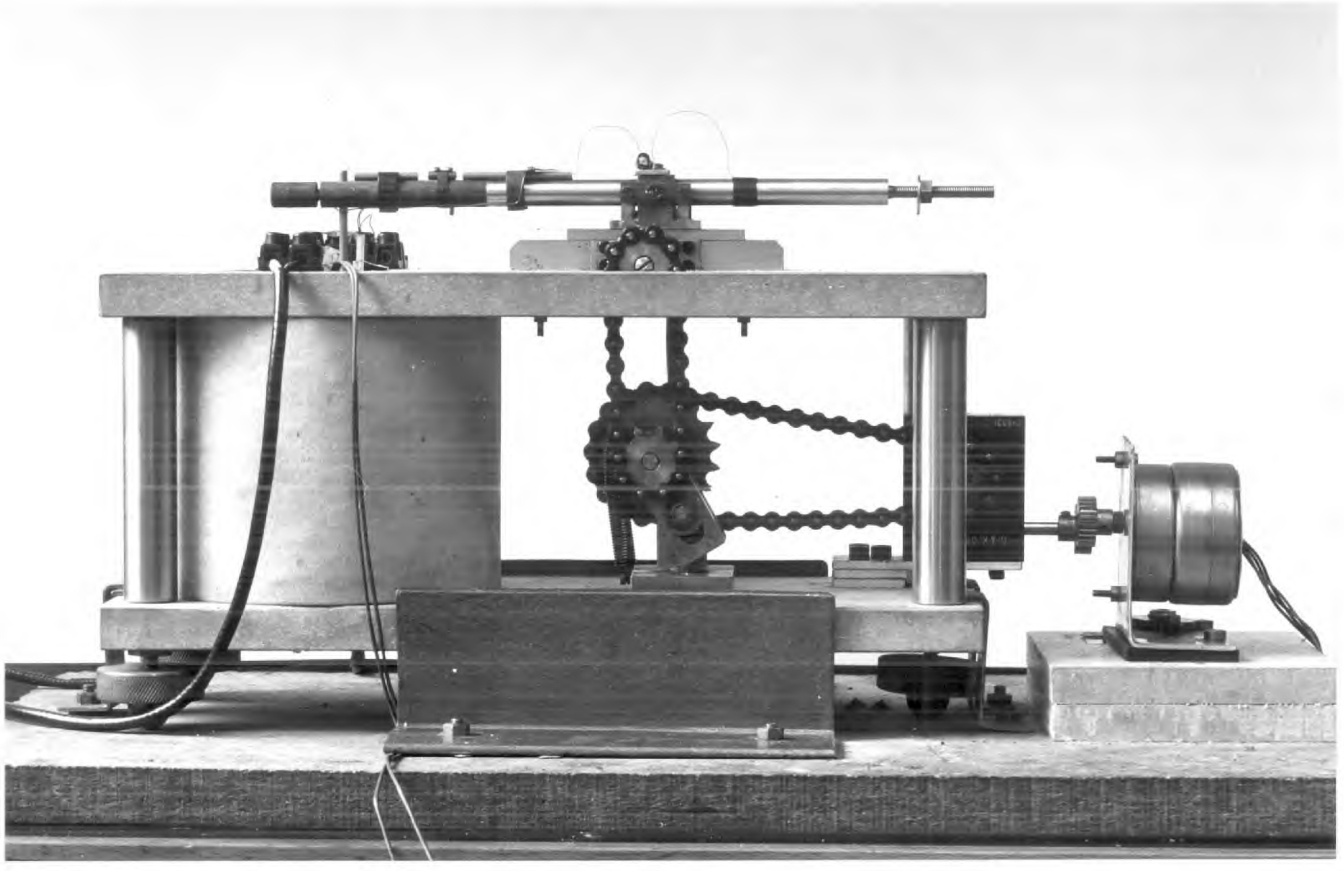

Fig. 27 Potential Probe

probe contact pressure. The metallic part of the rod was earthed to remove induced stray currents that could affect the electrometer leads nearby. The end holding the probe was made of Tufnol for added insulation resistance. The platform and pivot point could be driven forwards or in reverse by a constant speed motor via a reduction worm gear and a rack and pinion. Generally, the probe was 'pulled' rather than 'pushed' across the surface as the inherent springiness and sharp point of the fine probe otherwise tended to pierce the specimen. The probe traversed the surface at 43.75 microns per minute.

A diagram of the measuring circuit is shown in Figure 28. The source of the field across the specimen was three 1.5 volt dry cells. The full potential was dropped through the variable potentiometers of differing total resistance, giving a course and fine control to the voltage appearing across the wipers and thus across the specimen. The low or reference terminal of the electrometer could be connected to the wiper of either potentiometer, thus acquiring the same potential as either one of the specimen electrodes. Reversing the specimen field did not alter the reference potential to the electrometer and vice versa. The high terminal of the electrometer was connected to the probe. This terminal is extremely sensitive to induced currents and to static charges. Ideally, connections should be rigid but as this was not possible, non-microphonic coaxial cable was used. Only the probe and a short length of the lead to the high terminal were not screened. This unscreened lead was necessary to make the connection between the moving probe and the stationary electrometer. The cable screening was maintained at the reference potential which was pinned to earth potential. All metallic parts near the unscreened

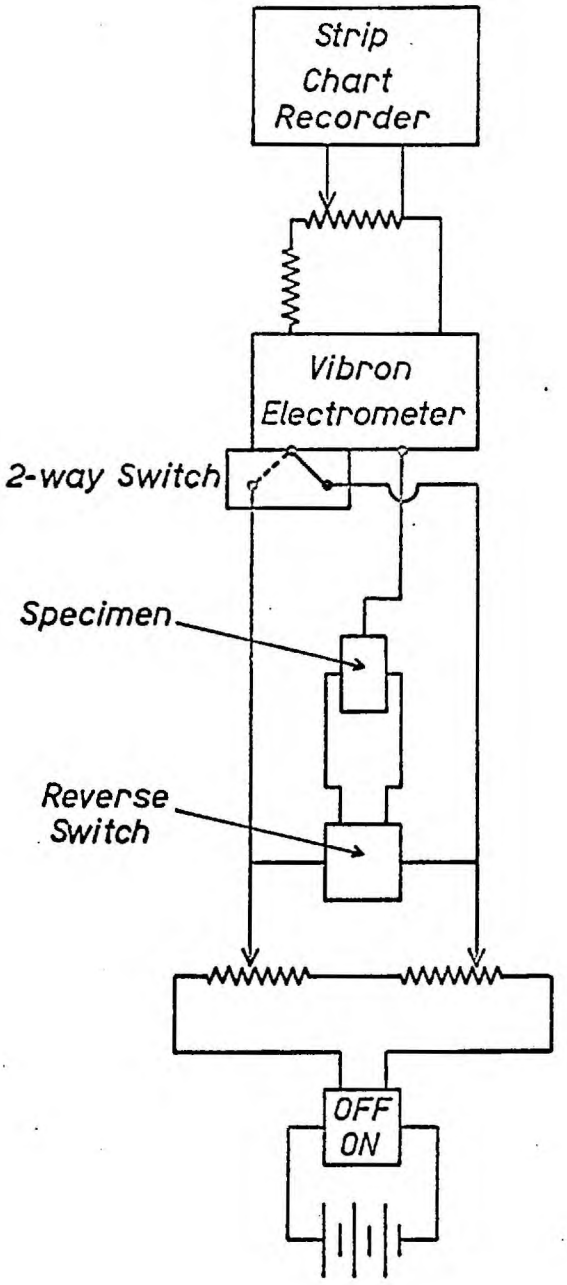

Fig. 28. CIRCUIT DIAGRAM FOR POTENTIAL PROFILE APPARATUS

portion were also earthed at the same point in order to eliminate stray currents arising from earth loops. With the circuit completed and with all the power consuming apparatus switched on, the noise level on the measuring circuit was negligible providing the operator kept well away from the apparatus. The insulation resistance of the complete circuit was better than 5×10^{14} ohms.

The potential profile across the specimens was measured with a Vibron Model 33C Electrometer. The operation of this instrument depends on a vibrating capacitor modulator, consisting of two flat parallel discs. One of the plates is mechanically vibrated so that the spacing varies sinusoidally, generating an alternating potential proportional to the static charge on the plates. This component can be applied to a conventional a.c. amplifier and, as there are no d.c. paths across the capacitor, no power is removed from the source connected across the high and low terminals. The electrometer is capable of measuring d.c. potentials from 0.5 to 1000 millivolts directly from sources of internal impedance of 0 to 10^{12} ohms. However, as the response time of the instrument becomes sluggish at high internal impedances, measurements could only be obtained when the specimen temperature was greater than 300°C. A Honeywell Electronik strip chart recorder plotted the potential profiles.

Procedure

Specimens were cleaved from pieces of single crystal or cut from bicrystals (8 mm. x 8 mm. x 1-2 mm. thick) and electrodes were painted on as a suspension of silver paste in alcohol. The edges of the specimens were then cleaved off to ensure good surface resistance. After loading into the rig,

a chromel-alumel thermocouple was placed on the top edge of the specimen but was insulated from it by a thin flake of alumina. The specimen was heated to between 300°C and 500°C and the probe was placed on the edge of the silver electrode, the balanced rod being positioned by hand. Care was taken to previously adjust the counterweight so that the probe exerted only slight pressure on the specimen. The positioning of the probe was aided by a long focal length microscope. The probe drive assembly was then connected and a one volt potential applied across the specimen. The probe drive was switched on simultaneously with the strip chart recorder and the complete profile from one electrode to the other recorded.

Most experiments were done in an atmosphere of air. One experiment was carried out with the whole of the apparatus enclosed in a glove box previously purged for 70 hours with dried, high purity argon. The application of the electrodes and the cleaving of fresh faces were also carried out in the glove box immediately prior to the experiment.

3-3 Bulk Conductivity Measurements

A.C. Technique

The rig used for bulk conductivity measurements is shown schematically in Figure 29. The furnace was supplied by smoothed direct current from the mains. The electrodes were covered with platinum foil, and one was spring loaded to ensure a small but positive contact pressure. After cleaving or cutting specimens, electrodes of graphite or silver paste were applied from an alcohol suspension. The edges of the specimens were then cleaved off. The conductance was measured with a Wayne Kerr Universal Bridge in the temperature region 730°C to 250°C, successive readings being taken with steps of descending temperature.

D.C. Technique

The same rig and furnace was used. The current flowing through the specimen was determined by measuring the potential drop across a known, fixed resistance in series with the specimen. A Vibron Electrometer was used to detect the potential drop and the output was recorded with a Bryan X-Y Recorder. The fixed resistance was interchangeable so that its value could be kept to a fraction of the specimen resistance. The initial conductivity was calculated from the potential found by extrapolating the voltage versus time curve to time zero. The final conductivity was calculated from the essentially steady-state potential. D.c. conductivity was measured in single and bicrystals below the knee temperature. Both a.c. and d.c. measurements could be taken almost simultaneously.

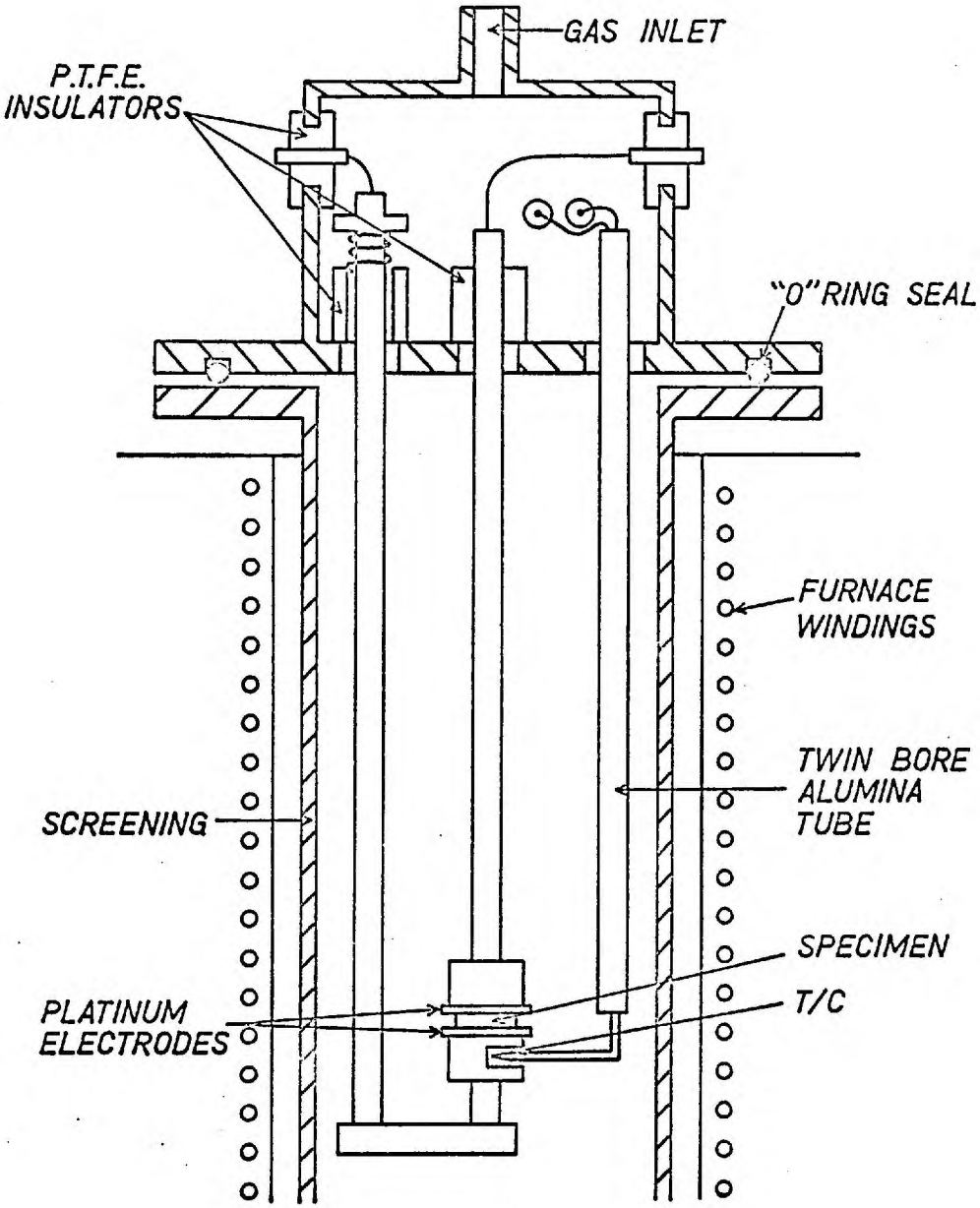

Fig. 29. BULK CONDUCTIVITY APPARATUS.

3-4 F-Centre Formation Rate Measurements

Single and bicrystal specimens were irradiated with gamma rays from a cobalt^{60} source, the source strength being approximately 10^6 rads per hour. The specimens were of similar size, had undergone the same preparation procedure and were irradiated at the same temperature. The optical density of the specimens was measured with a Parkin-Elmer 450 Spectrophotometer, using the F-band absorption peak at 465 mμ wavelength (visible range). The specimens were at all times protected from stray light sources and measurements were made at equal time intervals after irradiation. The growth curve of the optical density was followed from about 30 seconds to 10 hours.

CHAPTER 4

RESULTS AND DISCUSSION

4-1 A.C. Bulk Conductivity in Single Crystals

An Arrhenius plot of the conductivity for a single crystal specimen is shown in Figure 30. The activation energies of 1.84 ± 0.02 eV in the intrinsic region and 0.71 ± 0.02 eV in the extrinsic region are in good agreement with the results of Kirk[8]. The deviations at high and at low temperatures indicate an anion contribution and an association of cation vacancies with divalent impurities respectively.

The knee temperature was at approximately 495°C which also agreed with that found by Kirk for pure single crystals. Kirk noted however, that a chemical analysis of his pure single crystals revealed 30 molar ppm divalent cation impurity while the knee temperature of 493°C indicated only 2 ppm. The majority of impurity cations obviously did not affect the conductivity and must have been neutralized by anion impurities. Quin[75] suggested that a large fraction of Ca^{++} ions was neutralized by complexes formed with OH^- ions in doped specimens. Kirk and others, by doping with NaOH, lowered the knee temperature of pure crystals to 457°C which indicated less than one molar ppm effective divalent cation concentration. Clearly, the knee temperature is highly sensitive to both anion and cation impurities in the region 450°C to 500°C. The position of the knee temperature of specimens for the present studies can then be explained in terms of lower cation and lower anion impurity levels arising from the purification process and the improved crystal growing conditions.

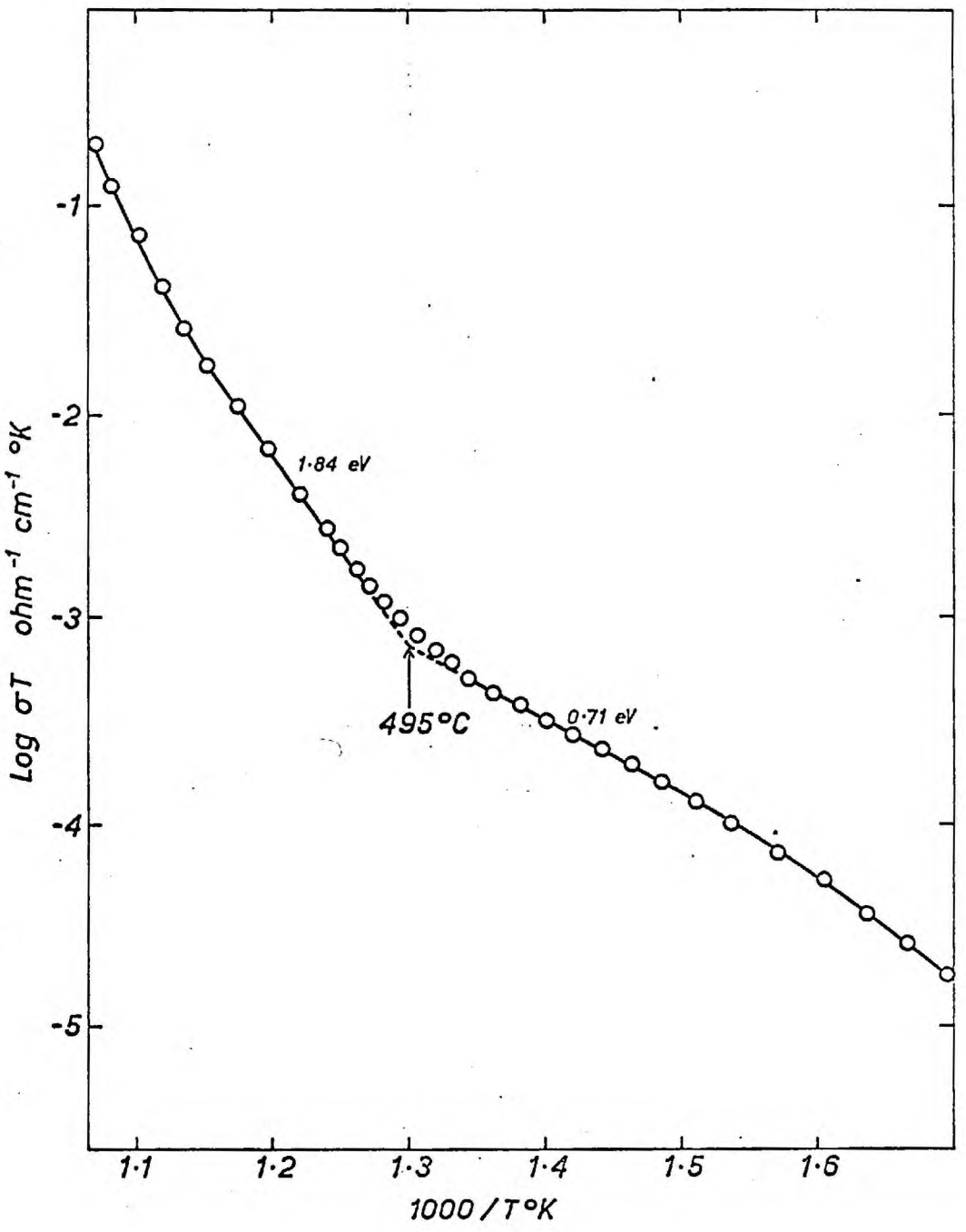

Fig.30. BULK CONDUCTIVITY OF PURIFIED NaCl

4-2 Grain Boundary Conductivity

Selection of 'Dopant' Material

Sodium ions were chosen for the previous investigations[29] of grain boundary conductivity in LiF because it was believed that the large ionic radius of Na^+ with respect to the normal lattice cation would preclude any diffusion into the bulk material. Arai and Mullen[104] found however, that relatively large Rb^+ ions diffuse at least as readily as Na^+ ions in the intrinsic region in NaCl.

A more important consideration than ion size is the mobility of the species. A diffusion coefficient of 10^{-5} cm^2/sec for Na^+ diffusion in dislocations in LiF may be calculated from the results of Tucker, Laskar and Thomson[70]. Assuming a similar value for the system considered here, the diffusion coefficient of monovalent cations in the bulk would be 7 or 8 orders of magnitude smaller. Bulk diffusion could then be neglected with respect to boundary diffusion over a relatively short period of time.

The dc conductivity experiments of Tucker et al. involved the use of radioactive $Na^{24}Cl$. The sections for counting were taken from the top surface of the specimen where metallic dendrites formed (under dc field conditions). Further, the deposited layer of NaCl was on the bottom of the specimen while the probe, which was the negative electrode, was placed on the top. This evidence led them to believe that the metallic dendrites were in fact sodium metal, and had been transported as ions through the dislocations.

For the present experiments divalent cations were not used because of their high diffusivity in the bulk[105-107] and because of the double charge on each ion. The alkali metals seemed to

be the best choice of monovalent cations and the choice is enhanced by the full outer shell configuration of electrons of these ions. Sodium ions were also used as there was no reason for supposing that the effect could only arise from an impurity ion.

Effects of the Probe on the Measured Conductivity

Conductivity measurements are usually made with large flat electrodes to give a uniform electric field. To determine the effect of the small area of the probe on the measured activation energies, experiments were done on single crystals. The activation energy in region II varied between 0.71 and 0.78 eV, the most consistent value being 0.73 eV. The scatter in the results could be due to temperature gradients, the imprecision involved in calculating the energy from measurements over a relatively short temperature range, or to variation in the probe contact pressure, which may vary with temperature if the probe is fixed either too loosly or too rigidly in the vacuum seals.

A more significant feature of the conductance measured by the probe was, that by using the measured probe area to determine the conductivity, the magnitude was about 4 times that measured by large plate electrodes. A large part of this enhanced conductance must arise from the shape of the electric field inside the crystal, giving a larger 'effective' area in which the conductance was measured. Hersh and Bronstein[108] demonstrated this point when injecting electrons into alkali halides by applying a large potential to a pointed electrode. The volume of coloured crystal containing F-centres was conical in shape, the apex being at the pointed electrode.

Fig. 31 Typical Specimen

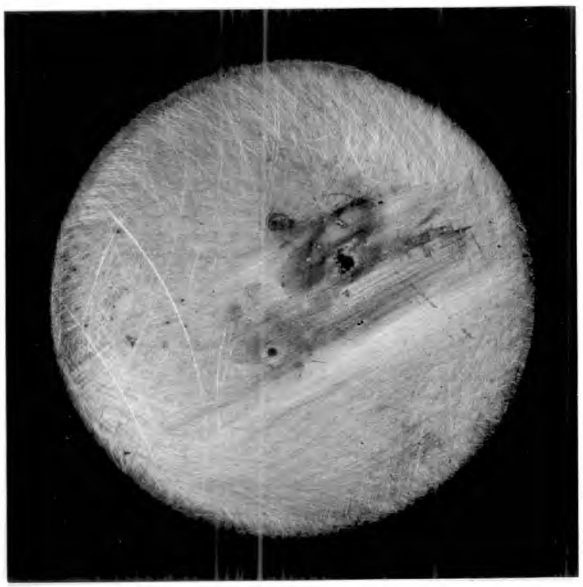

Fig. 32 Electrode Showing Corrosion

Conductance of Cation Dopants in Grain Boundaries

A significant increase in the ac conductance and a decrease in the activation energy was found after a dc potential of 250 volts had been applied across a grain boundary specimen with a vapour deposited alkali halide spot. The field was applied for about 20 minutes, and the application of the field for longer periods of time did not enhance the conductance further. Larger dc potentials often caused crack discharge along the boundary whilst applying the potential at higher temperatures often melted the specimen due to resistance heating. For the most part, experiments were confined to applying 250 volts for 10 to 20 minutes at 380°C.

As the temperature dependence and the magnitude of the background specimen conductance varied, it was first measured between 450 and 380°C before the dc potential was applied. The difference in the slope of the conductivity plot before and after applying the field was generally constant for a given dopant material, even though the slopes varied from specimen to specimen.

Several possible mechanisms may have caused the enhanced conductivity under the experimental conditions used. Hersh and Bronstein[108] and Wild[109] injected electrons into single crystals to form F-centres by using a similar experimental technique. Electron motion in the conduction band of the bulk crystal could cause enhanced conductivity. Jain and Sootha[110] point out however, that contributions to electronic conduction from ionized F-centres are negligible at lower temperatures. They interpreted the enhancement of conductivity in additively coloured KCl crystals to be the result of thermionic emission into the conduction band from metallic colloid particles, which are formed at about 400°C from F-centres and excess metal ions introduced

at higher temperatures. Tucker et al. pointed out that a measureable effect could arise from electronic conduction in metallic dendrites, should the conditions lead to their formation.

Impurity diffusion in the bulk, or diffusion into the boundaries, of ionic species other than the main constituents of the dopant material may also cause enhanced conductivity. Large cations may diffuse rapidly in the bulk because they associate with vacancies in order to minimize local stress concentrations. Divalent cations are known to diffuse very rapidly in the bulk crystal, and the extra charge per ion could give an enhanced effect. Although the specimens themselves were quite pure, the impurity concentration in the dopant material was unknown. Another possible source of divalent cations was the nickel electrode. Certainly some reaction took place between the deposited spot and the electrode as evidenced in Figure 32 showing the corrosion of the electrode face. Further, this chemical reaction only occurred when the electrode was the positive electrode, indicating that the halogen was responsible. Anion impurity diffusion into the bulk or into the boundary region was another possible mechanism of the enhancement.

Preliminary experiments, after applying a dc potential to a single crystal specimen with a vapour deposited spot of KCl, showed no difference in the conductance to those measurements involving the probe alone. Thus the enhancement noted for grain boundary specimens did not arise from any of the mechanisms discussed above operating in the <u>bulk</u> regions near the boundary. Conductivity measurements, with the probe placed over a grain boundary in specimens with a deposited KCl spot, <u>or</u> in specimens having had a dc potential applied, were the same as measurements on specimens without the spot or the dc potential. Only when <u>both</u> the spot was present on the surface over a boundary and a potential had been applied was any enhancement observed.

After the 'injection' process, the enhancement remained even when the deposited spot was removed. The results of some of the preliminary experiments are shown in Figure 33.

Typical results of the ac conductance measurements before and after applying the dc potential (the probe being the negative terminal) are shown in Figures 34 and 35, for specimens with a variety of alkali halides deposited on a surface over a grain boundary. In these figures, the conductance rather than the conductivity is plotted because of the problems associated with determining the effective thickness and area of specimen involved. The full results are given in Table 6. No results were obtained for attempts to dope the boundary with Rb^+ ions as the vapour pressure of RbI was too small to achieve a satisfactory deposit. The activation energy for the enhanced conductance was 0.32 ± 0.03, 0.55 ± 0.03 and 0.65 ± 0.03 eV when the dopant material was the halide of sodium, potassium and cæsium respectively.

Many of the specimens were examined optically for evidence of metallic dendrites, colloid particles and F-centres but none was observed. Further experiments were performed using higher temperatures, larger injection potentials and longer doping times but again, no direct optical evidence was found. As the colloid particles that are stable in additively coloured crystals at 400°C can be converted to F-centres upon heating[110], a few of the specimens used for conductivity experiments were annealed at 650°C in air and then quenched. Again, there was no visible evidence of colour centres.

The current flowing under the action of the injection potential was also measured for a few specimens. In Figure 36 the lower curve is from the work of Taylor[100], and demonstrates the ohmic nature of NaCl at 162°C. The current measured by the

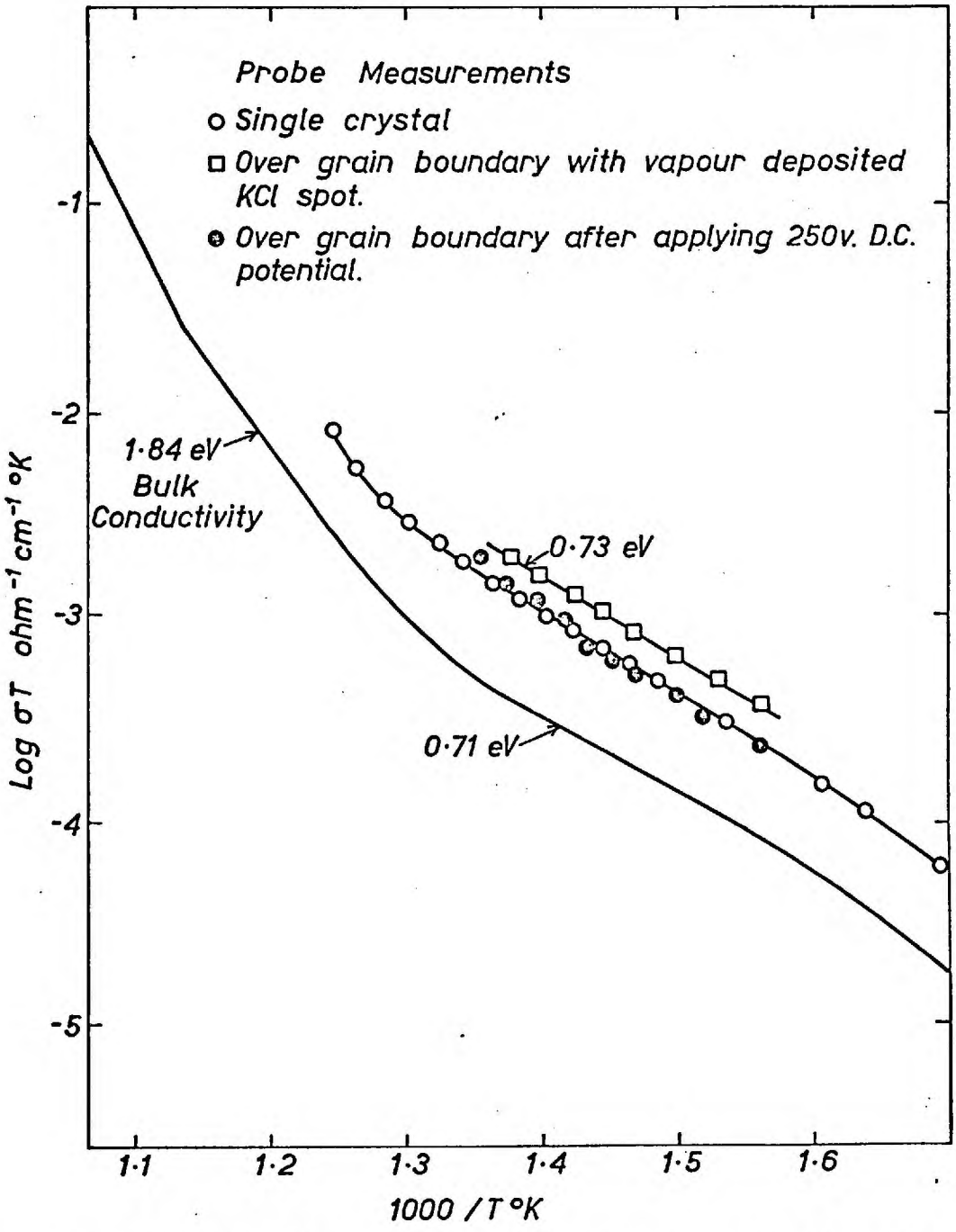

Fig. 33. CONDUCTIVITY MEASURED WITH PLATE ELECTRODES AND WITH A SMALL DIAMETER PROBE

probe on single crystal specimens could be ohmic at lower voltages but a logarithmic relationship is more appropriate at higher fields and temperatures, possibly due to the increase in the 'effective' area through which current occurred as the field increased. For a grain boundary specimen with a vapour deposited NaI spot, the curve showed a slight but significant increase at high field strengths, indicating the presence of another mechanism contributing to the current.

Although the results of the preliminary experiments indicated that the enhanced conductance did not arise from the bulk regions near the boundary, nor from the vapour deposited spot, the mechanisms possible in the boundary are not as easily excluded. However, anion diffusion is not considered likely as the dc field was such as to repel anions. Further, with the field reversed to attract anions into the boundary no enhancement was observed.

Although motion of electrons in the conduction band of of the bulk crystal was negligible, electronic conduction could occur in the boundary region by virtue of the band 'bending' to lower energy levels near crystal surfaces. But presumably this effect would have been observed in specimens without a vapour deposited spot. For overall charge balance, an injection of electrons into the crystal would necessitate either a loss of cation vacancies[111] or a simultaneous injection of cations. The former effect may decrease the background conductance due to the loss of mobile charge carriers, while the latter effect may cause colloids or dendrites to form. Neither of these effects is observed however, in the present experiments.

Another way in which to preserve overall charge balance is to inject cations and remove anion vacancies. If the

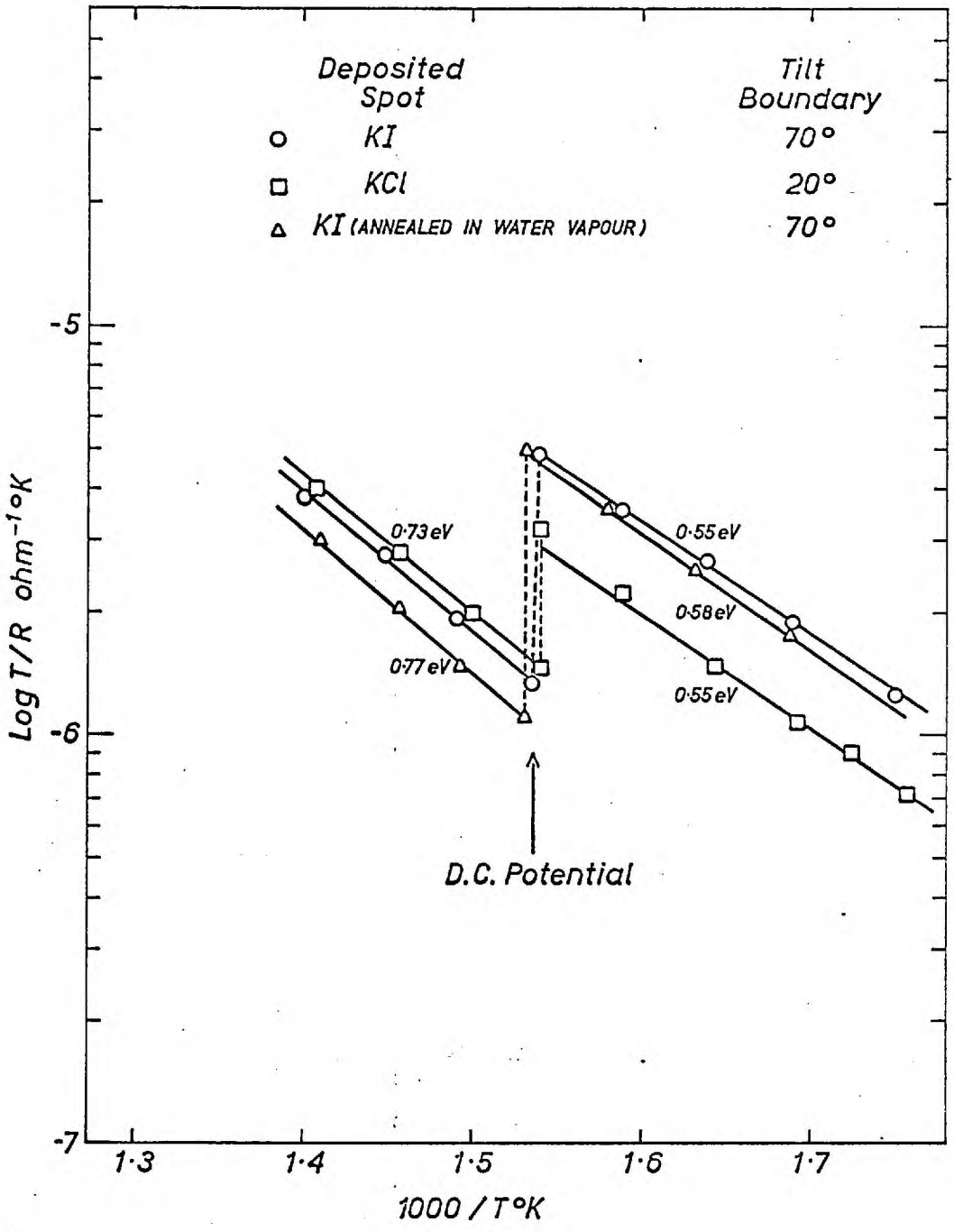

Fig. 34. GRAIN BOUNDARY CONDUCTANCE OF K^+

Specimen	Boundary Angle	'Dislocation Spacing'	Dopant Ion	Increase in Conductance	Activation Energy
10-1	5°	5.7a	K^+(KCL)	3.59×10^{-9} mho	0.52eV
20-7*	10	2.9	"	2.95 "	0.54
30-3*	15	1.9	"	3.13 "	0.55
40-4*	20	1.5	"	2.22 "	0.55
50-1	25	1.2	K^+(KI)	9.3 "	0.54
60-1	30	1.0	"	8.2 "	0.58
70-1	35	0.9	"	5.39 "	0.55
80-1	40	0.8	"	6.73 "	0.56
10-3	5	5.7	Na^+(NaI)	9.7 "	0.31
20-10*	10	2.9	"	13.1 "	0.31
40-6*	20	1.5	"	8.8 "	0.36
50-3	25	1.2	"	25.5 "	0.32
70-2	35	0.9	"	11.1 "	0.33
30-5	15	1.9	Cs^+(CsI)	3.08 "	0.64
50-5	25	1.2	"	2.66 "	0.66
80-2	40	0.8	"	3.45 "	0.65
10[b]	5	5.7	K^+(KI)	-	0.56
70[b]	35	0.9	"	-	0.54
10[b]	5	5.7	Na^+(NaI)	-	0.33
70[b]	35	0.9	"	-	0.30
10-6*c	5	-	"	-	-
20-15*c	10	-	"	-	-
30-11c	15	-	"	4.45 "	0.37
60-4c	30	-	"	17.8 "	0.32
70-5c	35	-	"	8.7 "	0.34

*- more than one specimen. a- interionic spacing.

b- this series annealed 2 hours at 700°C in water vapour.

c- direction of measurement perpendicular to 'dislocation direction'.

Table 6 Results of Experiments

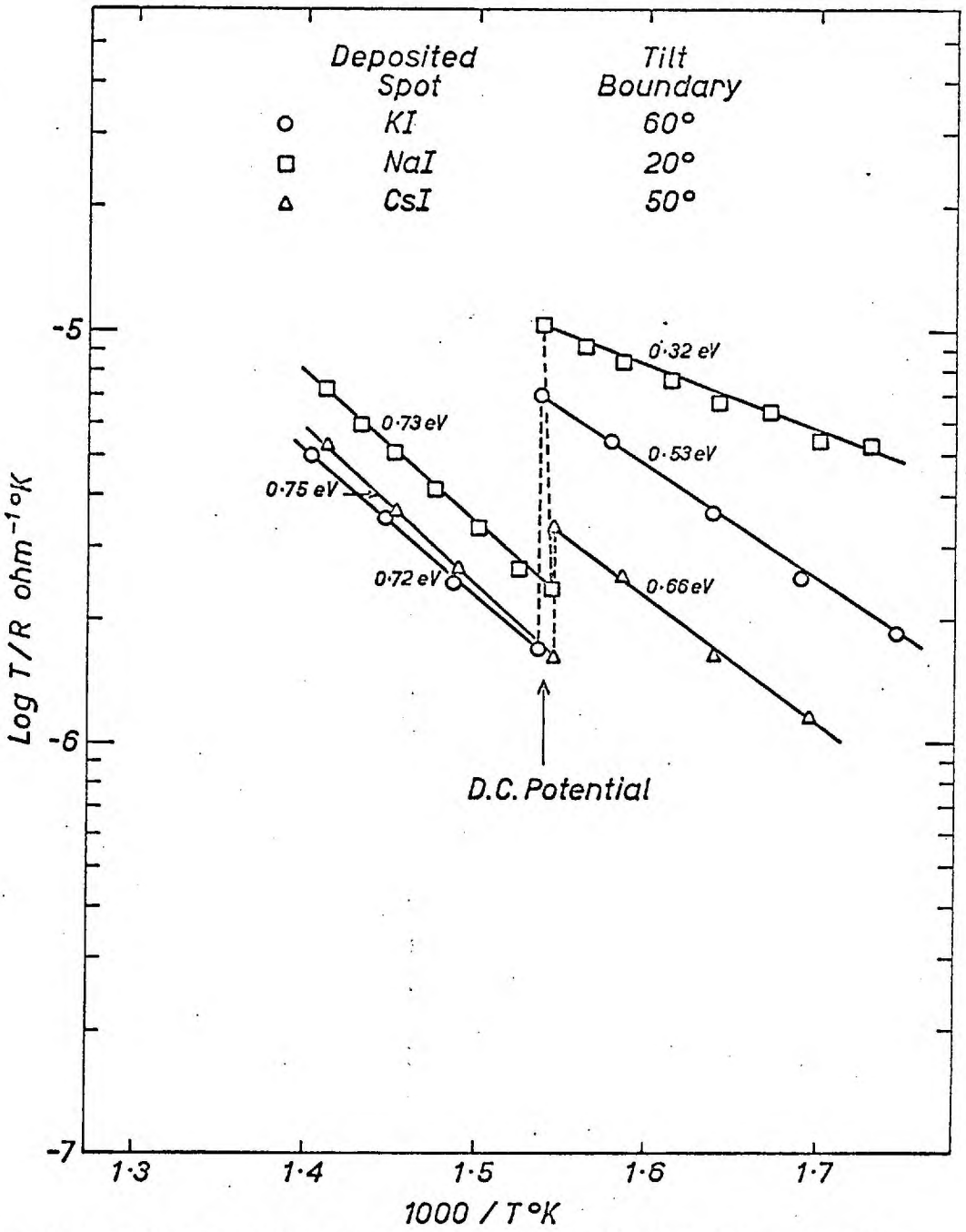

Fig. 35. GRAIN BOUNDARY CONDUCTANCE OF Na^+, K^+ and Cs^+

injected ions remain in the boundary region, the net positive charge could attract to the boundary some of the cation vacancies from the bulk crystal. Whether the observed enhancement was due to the motion of the ions in the boundary or to the increased number of mobile vacancies in the boundary region is difficult to determine. However, the simple analysis presented above and the observed behaviour of the conductivity suggests that injection of some cation species was necessary.

The enhancement of the conductance was in the order of 10^{-8} mhos. Assuming a boundary width of 5 or 6 atomic spacings and a diffusion coefficient in the boundary similar to that reported by Tucker et al. for dislocations (this assumption is not unrealistic as D can be 10^{-8} cm^2/sec for divalent cations in bulk NaCl), one can show that the number of ions contributing to the enhancement is approximately 10^{11}. More than this amount is readily available for injection and can be injected under the conditions of electric field and time used. A similar analysis will show the same to be true for diffusion of nickel ions into the boundary. However, if either nickel ions or an increase in the number of cation vacancies in the boundary region was responsible for the enhancement, one might expect that the activation energy would be the same irregardless of the species present in the dopant material. More experimental evidence of a direct nature will be necessary to fully resolve the operative mechanism. But one may infer from the evidence that injection of ions into the boundary region does occur, and that the measured activation energies could well arise from their motion in the boundary. The lack of dependence of the activation energy with the misorientation angle of the boundary indicates a common mechanism of motion over a wide range of angles.

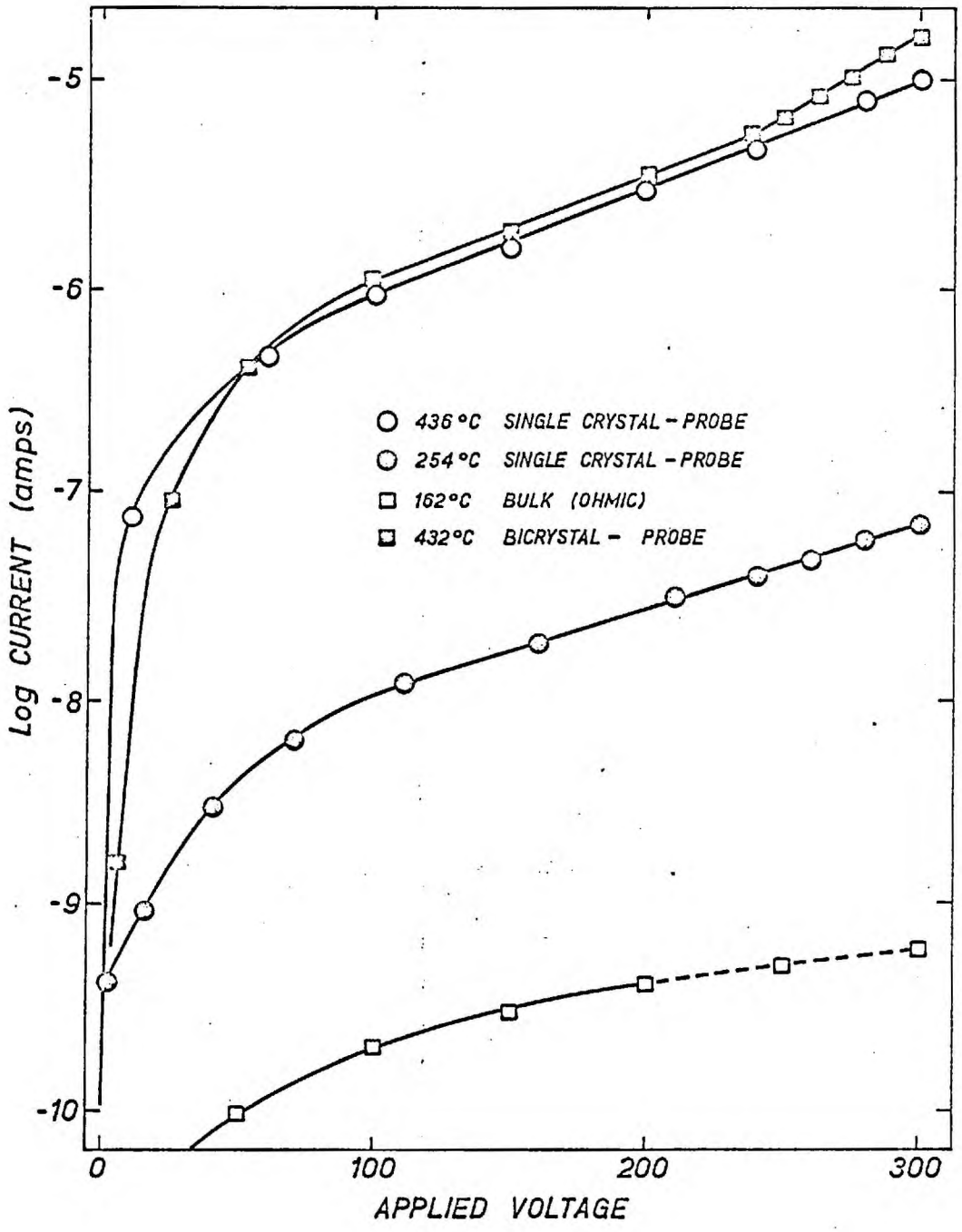

Fig.36. VARIATION OF CURRENT WITH VOLTAGE

Effect of OH^- Ions on the Conductance of Cations

Specimens of 10° and 70° bicrystals were annealed for 2 hours at $700^\circ C$ in an atmosphere containing H_2O vapour. The water vapour had some effect on the specimens as evidenced in Figure 37. The surface was etched with marks similar to dislocation etch pits only larger in size. A comparison of the boundaries shown in the top two photographs indicates some etching of the boundary as well. This treatment had no effect on the conductance of K^+ or Na^+ ions in the boundary. Although Otterson[77] reported this procedure effective for OH^- doping, more recently Kirk[8] reported it ineffective for changing the knee temperature. Doping of the melt before crystal growth with NaOH was found necessary to alter the bulk conductivity. Some doping probably occurred but not in sufficient concentrations to affect the mobility of dopant ions. The results then, are inconclusive, and doping of the melt will be necessary to determine the effect of OH^- ions.

Effect of Directional Orientation on the Conductance of Cations

Specimens were prepared to allow the measurement of grain boundary conductance in the orthogonal direction to that of previous experiments. That is, perpendicular rather than parallel to the 'dislocation direction' in the grain boundary. Figure 38 shows the results for Na^+ ion doped boundaries. For 60° and 70° boundaries, the results were similar to the previous experiments, even in the magnitude of the conductance. For a 30° boundary, a similar activation energy was found but the increase in magnitude was not so large. 10° and 20° boundaries showed no enhancement at all. Repeated efforts

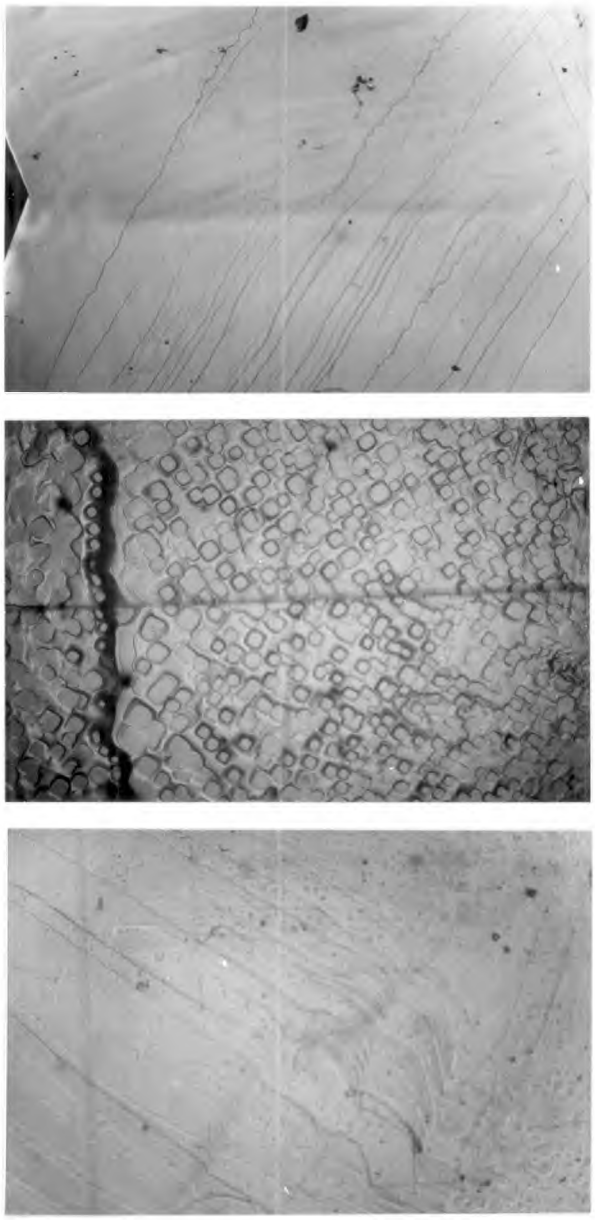

Fig. 37 Specimen Surfaces: top, freshly cleaved; centre, annealed in H_2O vapour; bottom, annealed in air. Approx. X50

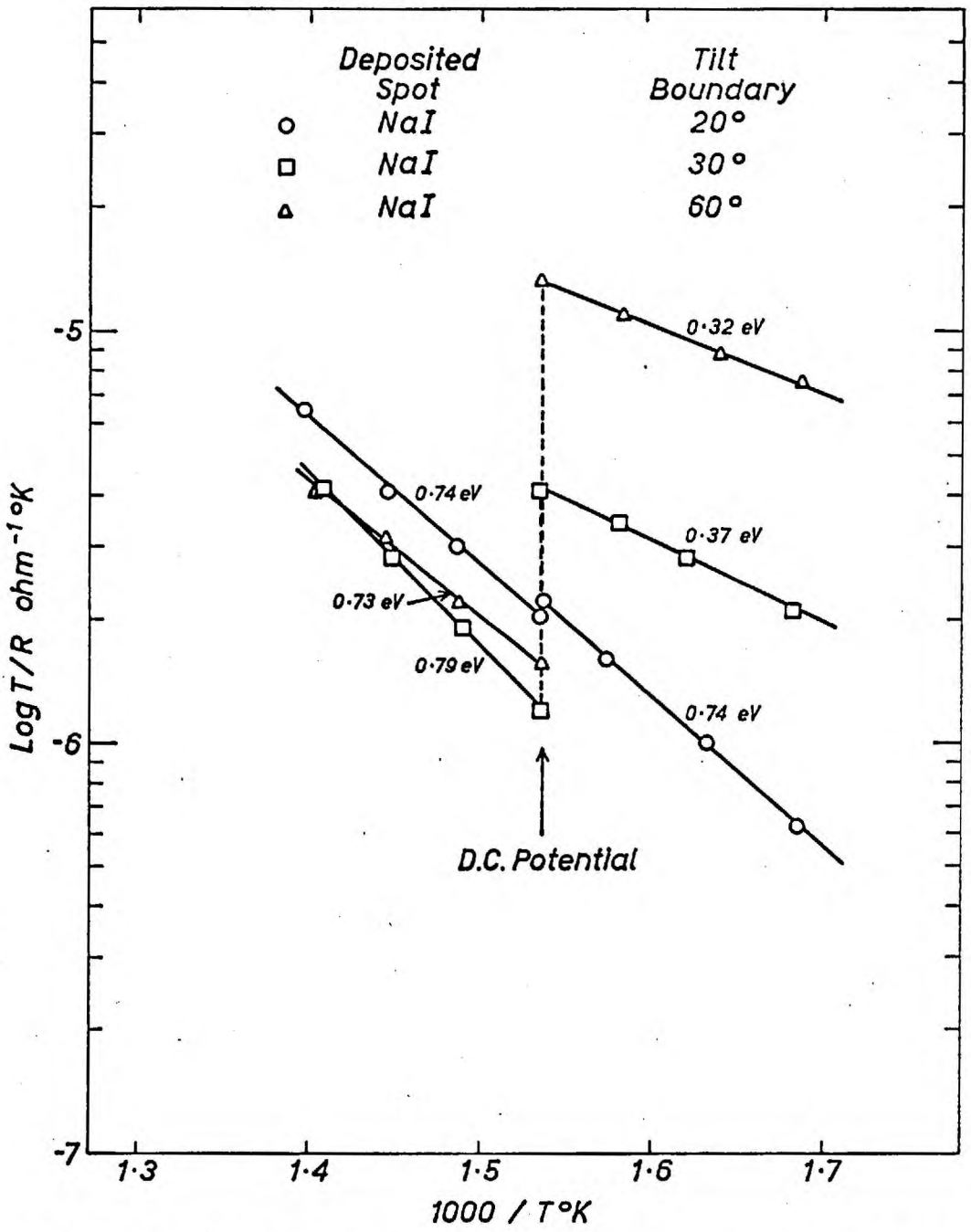

Fig. 38. GRAIN BOUNDARY CONDUCTANCE OF Na^+ PERPENDICULAR TO DISLOCATION DIRECTION

were made with larger potentials and longer doping times but were not effective.

These experiments indicated some 'columnar' grain boundary structure at low angles consistent with a dislocation model. High angle boundaries however, showed no anisotropy of the conductance, indicating an amorphous grain boundary structure.

Conductance of Anion Dopants in Grain Boundaries

Attempts were made to dope the boundaries with anions, but no results could be obtained for Cl^- or I^- ions. Larger fields and longer doping times were again not effective. The works of Laurent and Bénard[27], Cabané[28] and others[30,69] indicate that anions do diffuse more readily in grain boundaries. The problem then, would appear to arise from the injection process. Indeed, when the field was reversed to inject anions rather than cations, the corrosion shown in Figure 32 was notably absent. This fact would seem to indicate that either some necessary electrode reaction was not energetically favourable or that the appreciably lower diffusion coefficients of anions in alkali halides necessitated much longer doping periods. The latter is expected to be the main cause of the difficulty encountered.

4-3 Potential Profiles on Surfaces

Surface Potentials

The experiments of Wimmer and Tallan[24] on interfacial polarization were discussed in Chapter 1. They measured the surface potential profile between electrodes of a specimen in a d.c. field and found that 25 percent of the potential was dissipated in 30 micron thick layers at each electrode. The interpretation of the results of these experiments in terms of the presence of increased resistivity depended on the assumption that the surface profile was representative of the potential gradient in the bulk of the specimen. An experiment was devised to test this assumption. If surface conduction gives rise to the surface profile, the profile should be linear between two surface electrodes (i.e. electrodes on the same surface) as the current will be constant. But if the probe is more sensitive to bulk currents, the profile on the surface will not be linear as the current density at the near edges of the surface electrodes will be larger. The results of this experiment are presented in Figure 39 and indicate that the probe was sensitive to the bulk potential gradient.

The experiments of Wimmer and Tallan were repeated in the present study to verify the increased surface resistivity and to ascertain if the same effect existed at grain boundaries. Figure 40 shows the results on single crystal specimens, representing three general observations. Sometimes the profile fell rapidly at the positive electrode but this was always accompanied by a more negative reading near the negative electrode. Often the situation was reversed and in some cases, the profile was linear from one electrode to the other. The

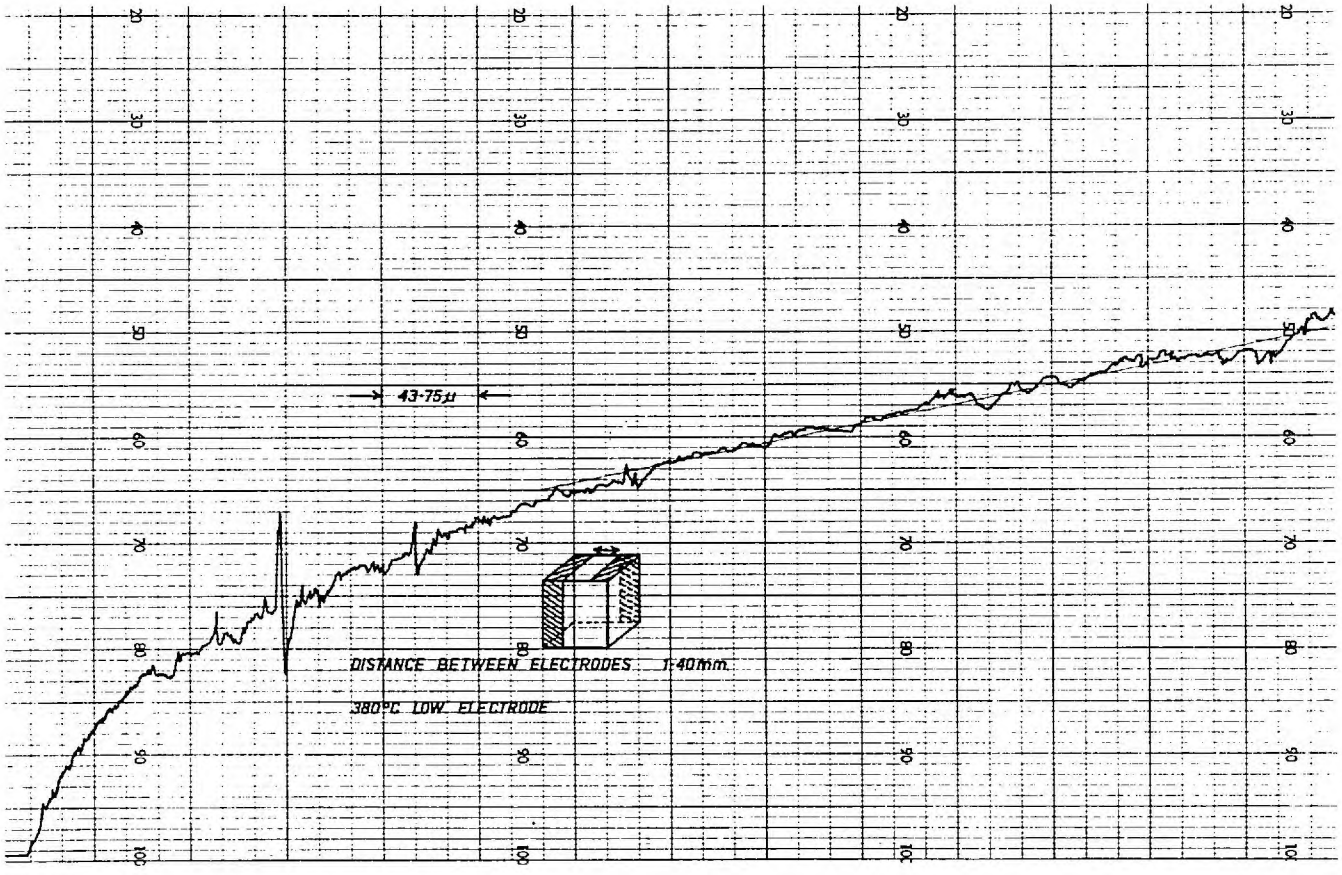

Fig. 39 Profile Between Surface Electrodes

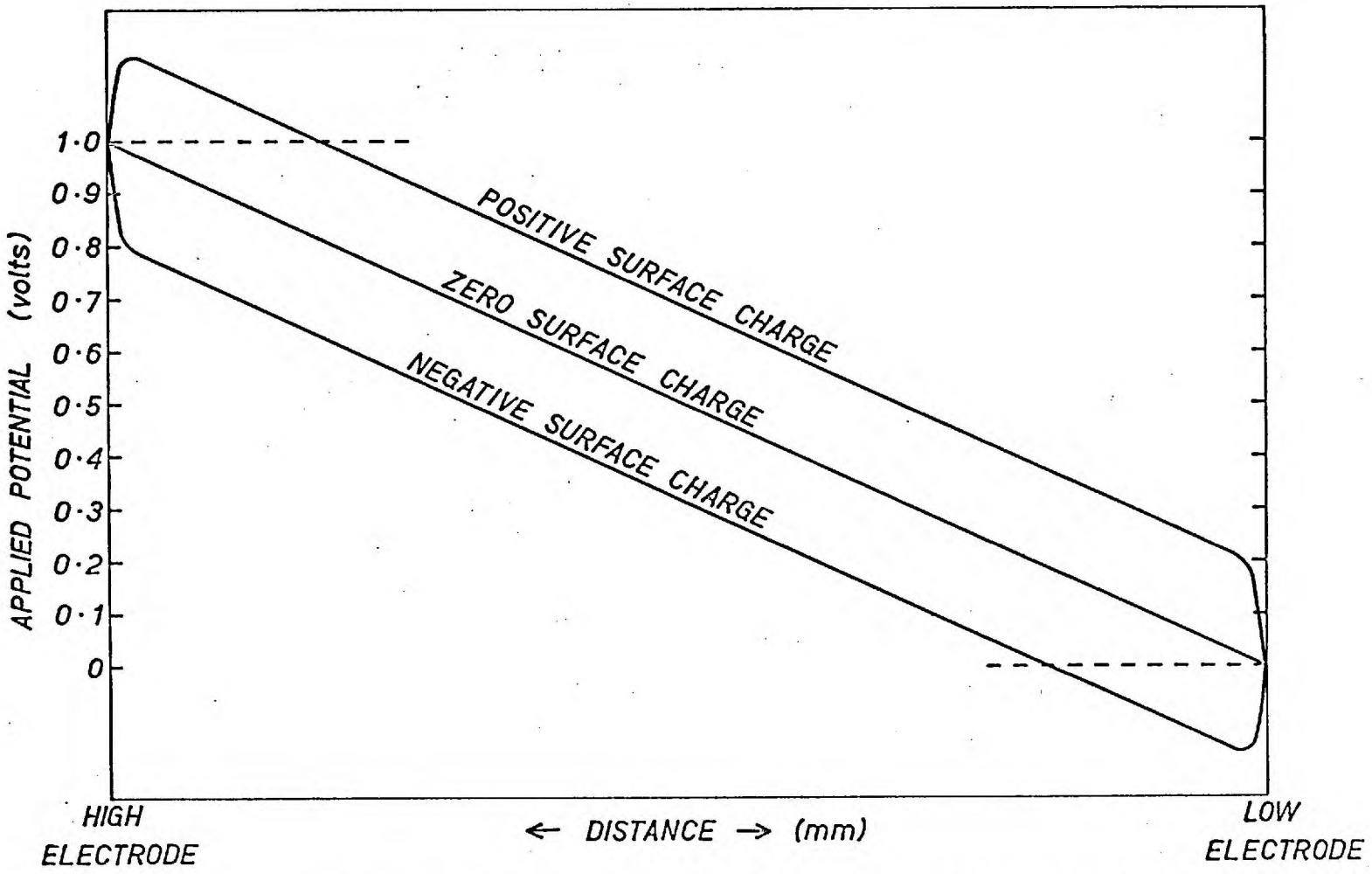

Fig.40. SHAPE OF POTENTIAL PROFILE SHOWING THE EFFECT OF SURFACE CHARGE

important point is that the slope of the linear regions in all three cases was the same, being just that to give the full applied potential across the measured thickness of the specimen. The behaviour near the electrodes was found to be a surface potential (referred to as surface charge in some diagrams) which was invariant over the top surface of the specimen. Thus the curves of Figure 40 represent the effect of a constant surface potential superimposed on a linear potential gradient.

The magnitude and sign of this surface potential varied considerably from specimen to specimen, and often changed over a period of time from -200 to +200 mV. No temperature or impurity dependence was obvious and the potential appeared to vary quite randomly. A freshly prepared probe tended to make the potential more negative but again no consistent effect was observed. The surface potential could be a measure of the surface charge arising from the distribution of vacancies and impurities near the specimen surfaces. The magnitude and sign of such a surface charge is known[35] to be highly dependent on surface conditions. More likely however, this potential was a contact potential arising from the electronic considerations[101] of the relative energy distribution of electrons in a metal in contact with an insulator. This explanation can also account for the inconsistency of the surface potential. As the experiments were carried out in air, both the specimen and the probe are subject to oxidation, changing the materials in contact and thus the contact potential. A tracing from the strip chart recorder for a specimen with zero surface potential is shown in Figure 41.

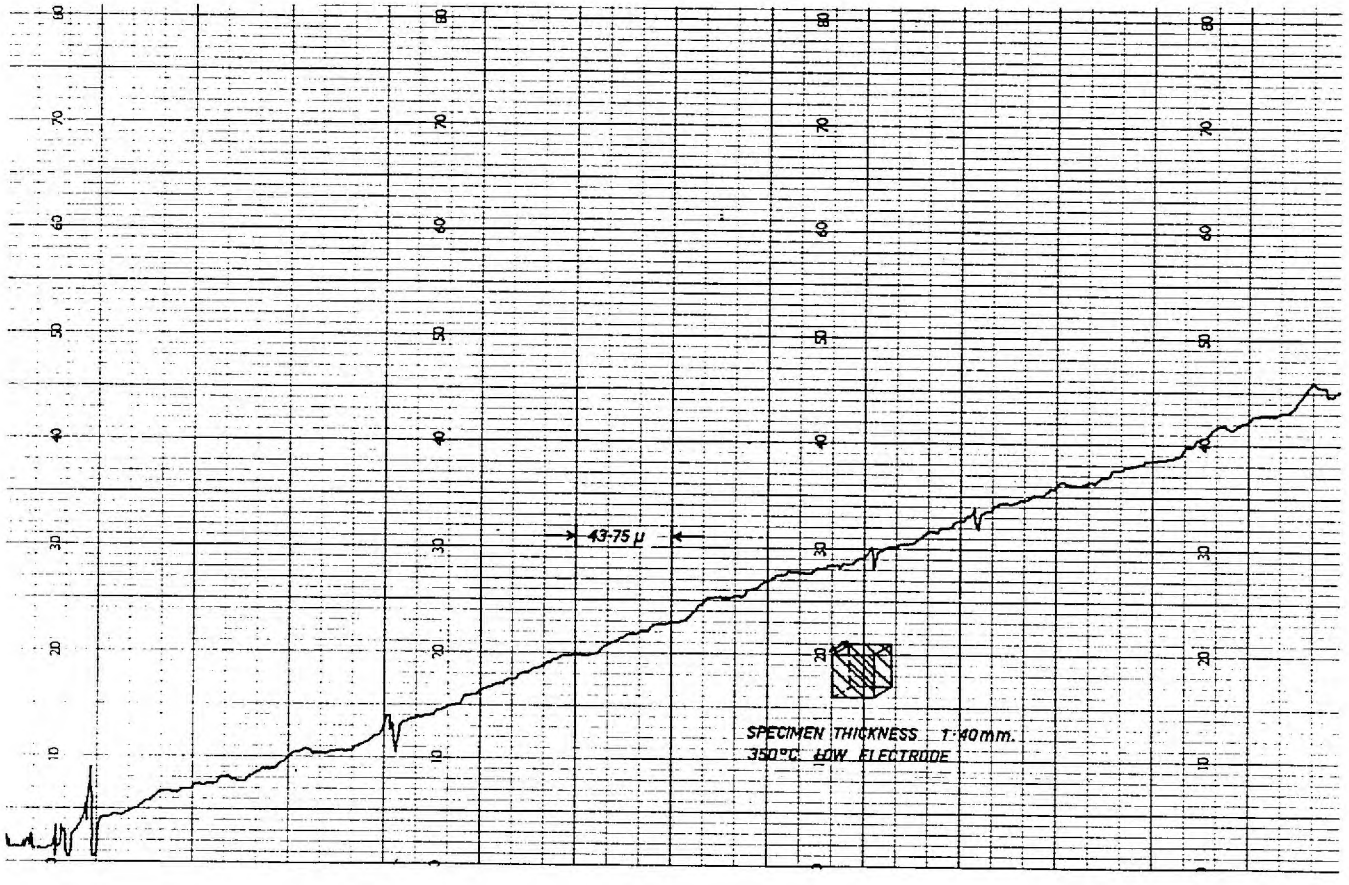

Fig. 41 Profile with Zero Surface Potential

Extrinsic Effects on the Profile

The results of the present experiments then, contradicted the work of Wimmer and Tallan in that no increase in the resistivity of surface regions was found. As their experiments were conducted on specimens previously used for other measurements, specimens were annealed for various times in air (some with the silver electrodes applied) to simulate specimen conditions that could possibly have led to the surface phenomenum. Other specimens were air quenched from 500°C or cut on a diamond slitting wheel to initiate surface strain. These specimens, and an annealed doped specimen showed no signs of increased surface resistivity. Figure 42 shows the birefringence associated with the strained surfaces of the cut specimen and Figure 43 shows the segregation of calcium to free surfaces. Impurity diffusion, impurity segregation or surface strain then, cannot account for the results of Wimmer and Tallan.

An Explanation of the Results of Wimmer and Tallan

As the result of Wimmer and Tallan did not seem to arise from the specimen itself the effects of the electrodes and of the circuitry were investigated. A specimen was prepared by applying graphite electrodes to the surfaces before the silver electrodes. Graphite is a partially blocking electrode material that can cause space charge polarization due to the blocking of charge carriers. Within the limits of detection, the profile was again linear. As the effect is not large between 300°C and 400°C, the resultant polarization could have been too small to detect. In any case, electrode blocking

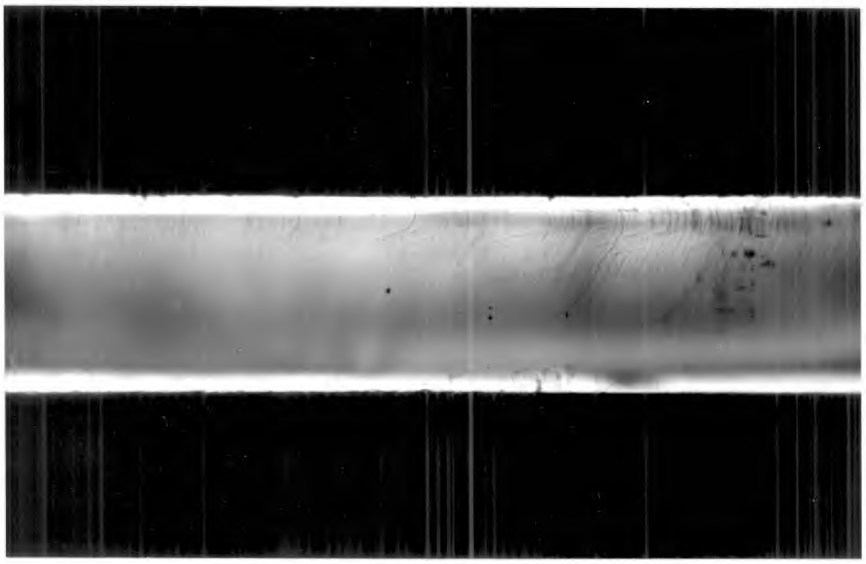

Fig. 42 Birefringence in a Cut Specimen

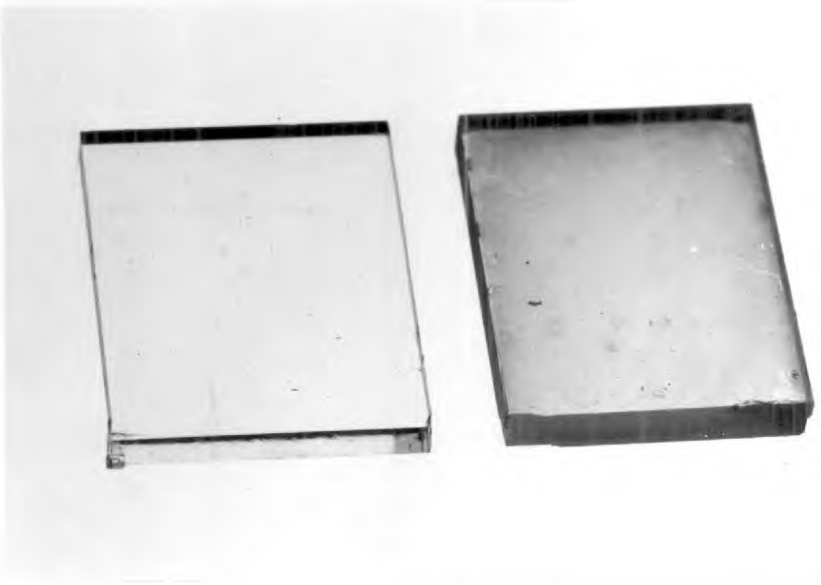

Fig. 43 Pure and Doped Specimens Annealed in Air

effects do not appear to have caused the results of Wimmer and Tallan.

From previous discussion in this chapter a contact potential is seen to develop when the metallic probe touches the specimen. A contact resistance, associated with the effective resistance between two conductors of differing charge carriers will also be involved. Considering the circuit shown in part A of Figure 44, the contact resistance is negligible when the probe is in contact with the electrode. Even if the insulation resistance is low the leakage current in parallel with the meter can easily be supplied by the dry cells through the small resistance of the probe contact. Thus the leakage current will not alter the potential between the electrodes and the electrometer will give a correct reading of the applied potential. Considering now part B of Figure 44, a contact resistance must appear when the probe is on the specimen. As the electrometer draws no current, a large insulation resistance will not affect the meter reading. But a smaller insulation resistance will reduce the potential between the reference electrode and the probe because the specimen resistance and contact resistance do not allow sufficient electronic current to the insulation resistance. Further, the measuring circuit acts as a potential divider, some of the potential appearing across the contact resistance and some across the insulation resistance. The meter will then read some value less than the true potential. In summary, when $R_{ins} \gg R_{cont}$, the circuit has no effect on the meter reading. But when $R_{cont} \gg R_{ins}$, the potential across the meter approaches zero. When $R_{cont} \sim R_{ins}$, the meter will read approximately one-half the true value.

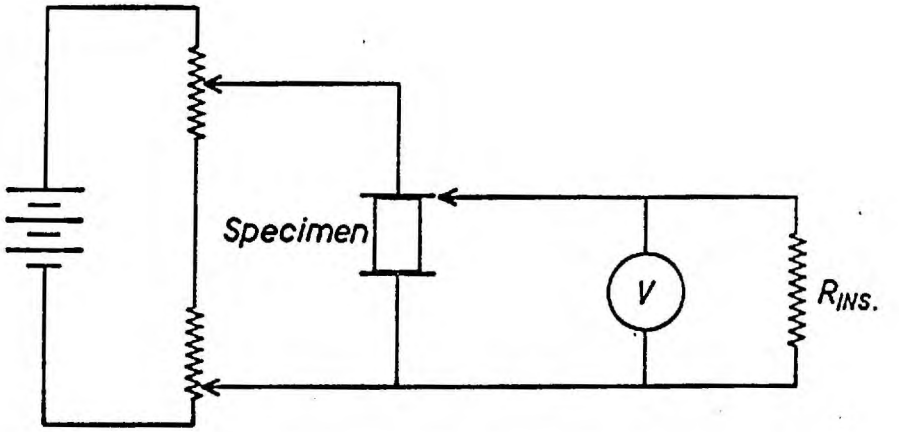

A.

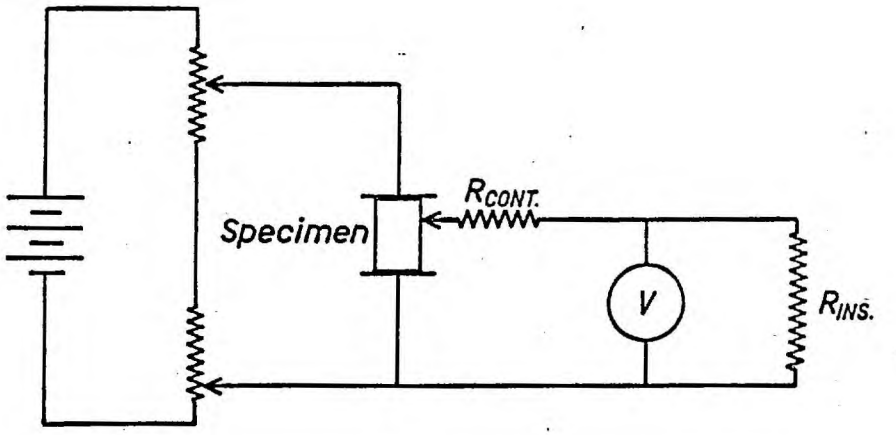

B.

Fig.44. CIRCUIT DIAGRAMS SHOWING INSULATION RESISTANCE AND CONTACT RESISTANCE

Figure 45 shows the value of resistors inserted in parallel with the meter necessary to divide the true potential in half. The temperature was varied until the reading with the normal insulation resistance ($>10^{14}$ ohm) was twice that when the resistor was in the circuit. The method was very approximate but the curve shows a large temperature dependence, especially for lower temperatures. Thus at 250°C where Wimmer and Tallan obtained their results, an insulation resistance as large as 10^{12} ohms could still give erroneous results.

The combined effect of insulation resistance, contact and specimen resistance and contact potential complicates the measured profile. Figure 46 shows the results obtained in the present work for a specimen with a positive contact potential and a circuit insulation resistance of 10^{11} ohms at 350°C. The result is very similar to that of Wimmer and Tallan.

Profiles on Bicrystals

To determine if grain boundaries had any effect on the potential profiles, surfaces of high angle boundary specimens were cut parallel to the boundary. Two specimens, tested in air, showed no anomalous effects. The third specimen was prepared, cleaved and tested in an atmosphere of dried, high purity argon, and the recorder tracing of this experiment is shown in Figure 47. No major effect was observed at the boundary although the specimen had a 100 mV positive contact potential. The slight difference in the slope for each half of the bicrystal is not thought to be important, although it could indicate some slight polarization due to blocking of negative charge carriers at the boundary.

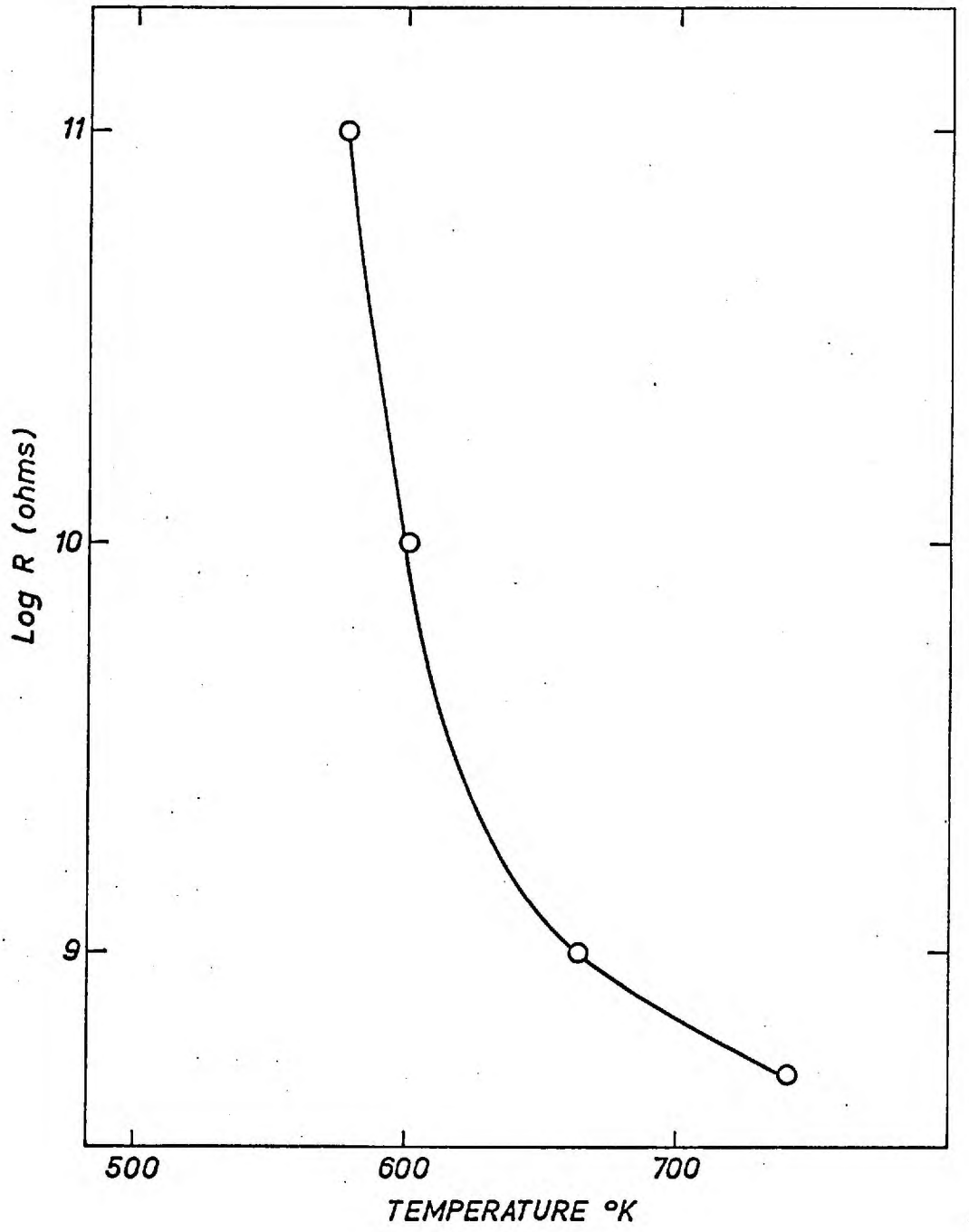

Fig.45. INSULATION RESISTANCE EQUAL TO CONTACT RESISTANCE

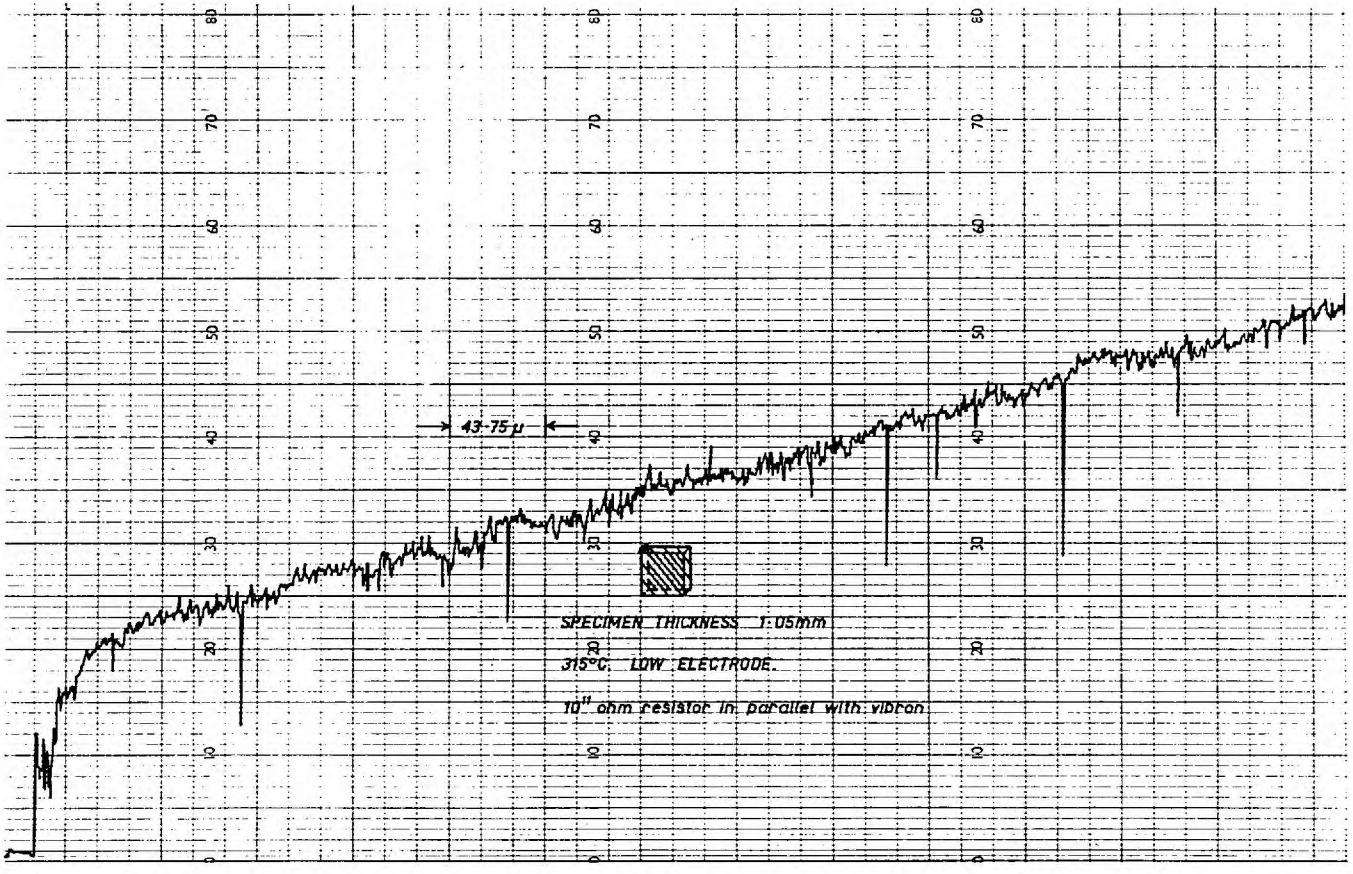

Fig. 46 Profile with Surface Potential and Circuit Leakage

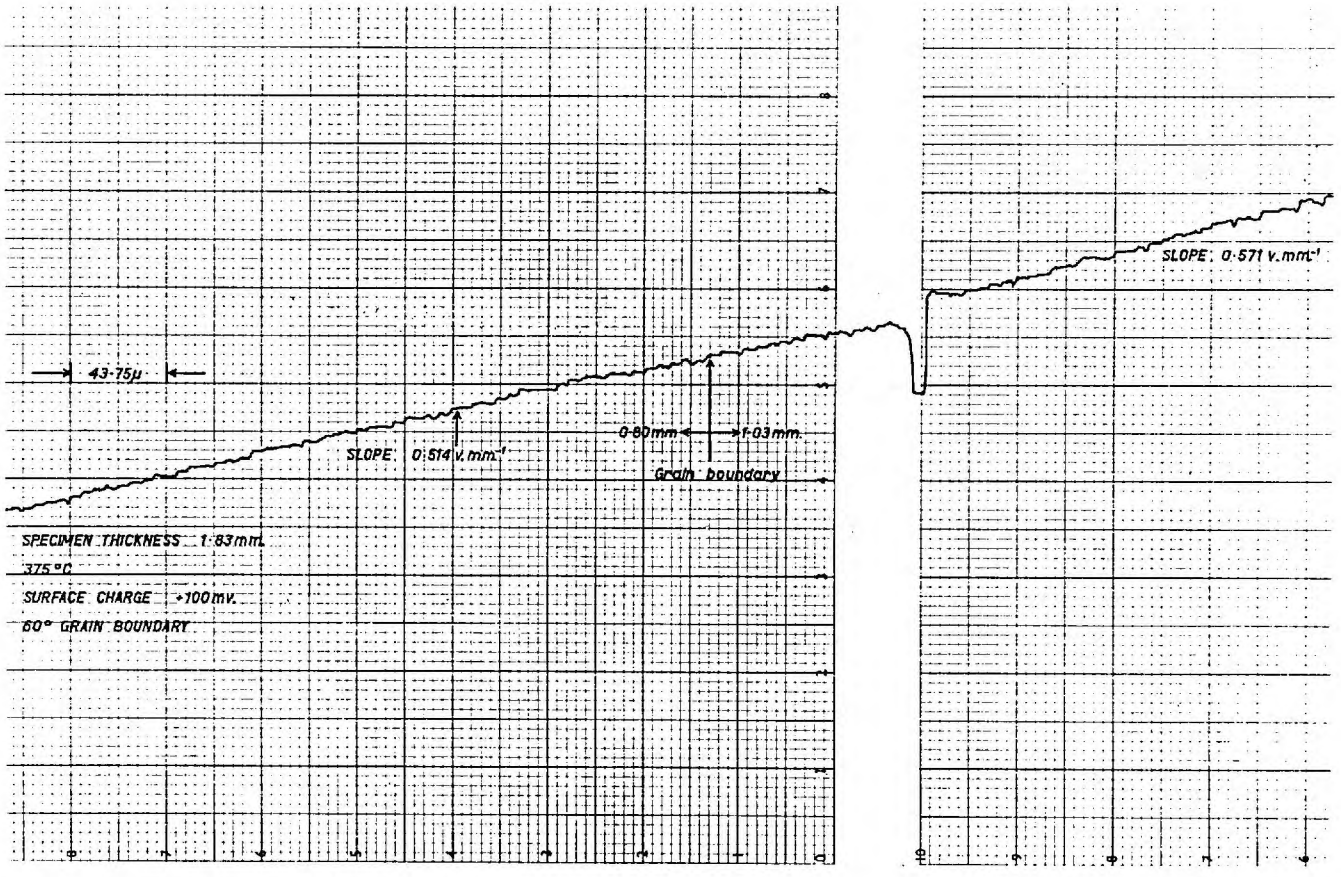

Fig. 47 Profile Across a Grain Boundary

4-4 D.C. Conductivity in Bicrystals

If as previously suggested, high angle boundaries cause some polarization due to the blocking of charge carriers, then some effect may be seen in the d.c. conductivity of bicrystals. Accordingly, specimens were prepared by cutting surfaces parallel to the plane of the boundary in 60° bicrystals. For comparison a section of single crystal was cut from near the boundary at the same time. Figure 48 shows the results obtained using graphite electrodes. The agreement between the a.c. conductivity ($\sigma_{a.c.}$) and the initial d.c. conductivity (σ_o) was good. The long term d.c. conductivity (σ_∞) dropped to about 10 percent of σ_o, but as σ_∞ was the same for the single and bicrystal specimens, the effect must be due to the blocking characteristics of the graphite electrodes. The experiments were repeated (see Figure 49) using silver paste electrodes. Again, $\sigma_{a.c.}$ agreed well with σ_o for both specimens. In these experiments however, σ_∞ was only 10 percent less than σ_o for both specimens. Obviously, silver electrodes are less blocking than graphite electrodes.

The agreement of results for single and bicrystal specimens indicated that no measurable space charge polarization occurred at large angle boundaries, at least for the temperature range investigated. The relative blocking behaviour of silver and graphite electrodes can presumably be explained in terms of electrode reactions with ions. Unless some reaction affects surface states, there is no apparent reason why electrode material should affect vacancy discharge or formation.

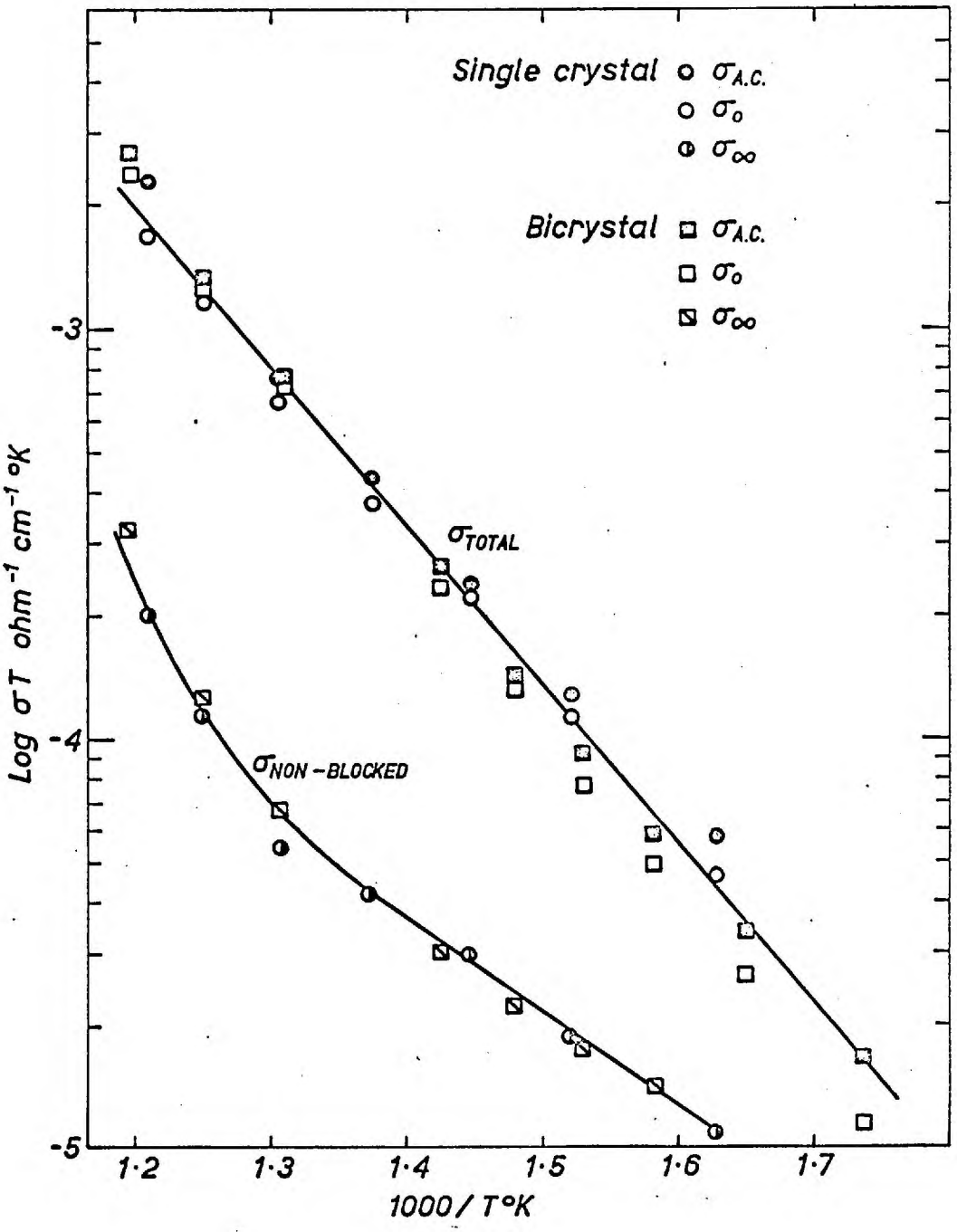

Fig.48. BULK CONDUCTIVITY WITH GRAPHITE ELECTRODES

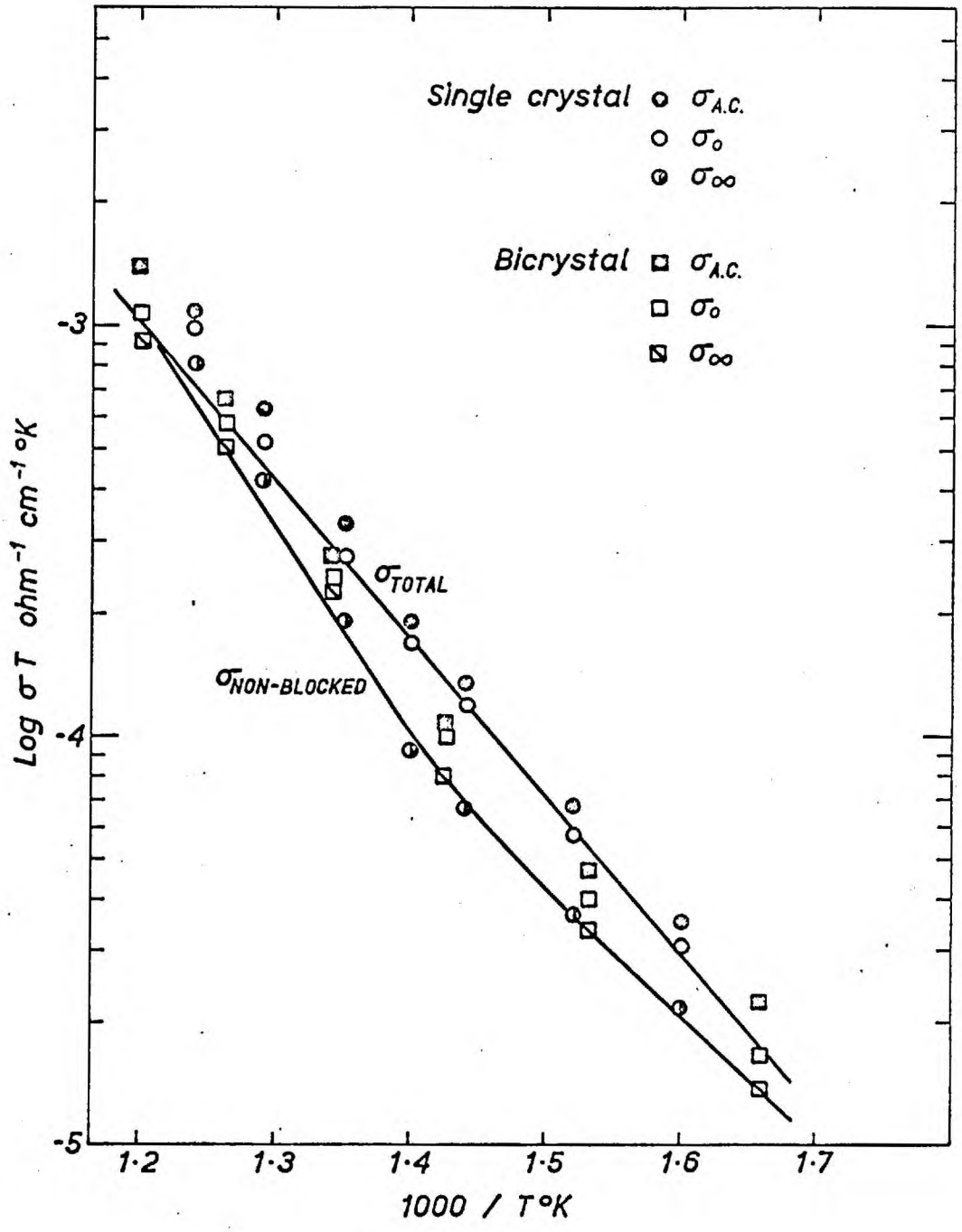

Fig.49. BULK CONDUCTIVITY WITH SILVER ELECTRODES

4-5 Rate of F-centre Formation in Bicrystals

The initial rate of F-centre formation in alkali halides is known to be structure sensitive. Some impurities retard and others enhance the rate while dislocations are known to increase the rate of formation. When all the sites of low energy requirements have been used, the irradiation produces new vacancies and a secondary mechanism is evident in the growth rate curves. Chang[102] proposed a model for the deformation enhancement, based on the earlier work of Davidge and Pratt[103], consisting of low energy sites near the 'vacancy sheet' formed between dislocation dipoles.

Figure 50 compares the optical density of F-centres in a single and bicrystal specimen. The nominally pure single crystal exhibited a similar time dependence to that found in the literature. The bicrystal specimen showed an increase in the optical density and, as the two specimens were similar in every respect excepting the boundary, the boundary itself (60°) must be responsible. As only one experiment was done and as the data points are few, concrete conclusions are difficult to draw. With the help of Chang's model however, the results could be indicative of high vacancy densities in the boundary region. This interpretation corroborates the evidence of the grain boundary conductivity experiments.

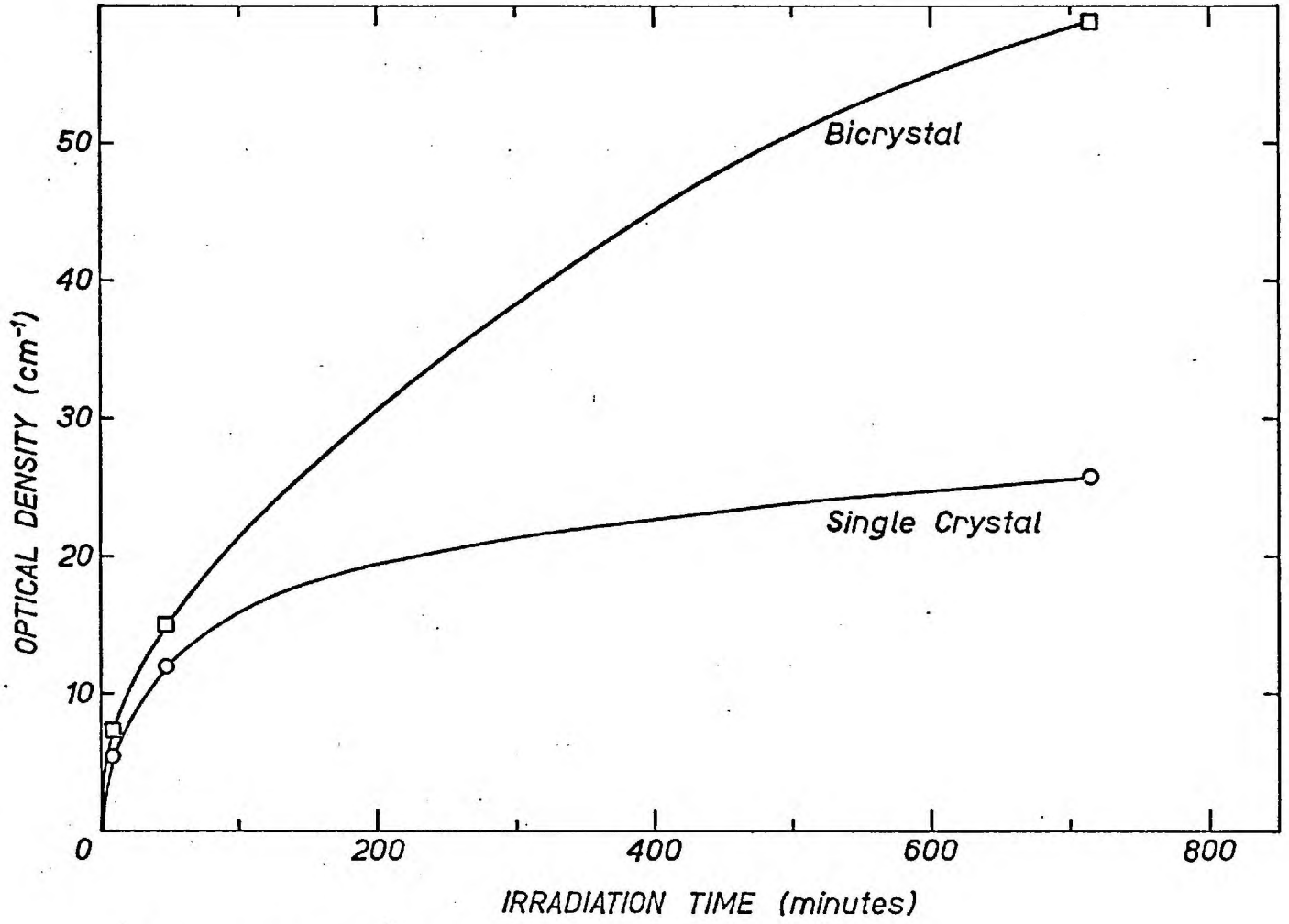

Fig. 50. F-CENTRE FORMATION RATES

CHAPTER 5

CONCLUSIONS AND SUGGESTIONS FOR FUTURE WORK

5-1 Conclusions

Activation energies of motion for cations 'injected' into tilt boundaries in NaCl can be calculated from the enhanced conductance measured in the boundary region. The experiments yield activation energies for Na^+, K^+ and Cs^+ ions of 0.32 ± .03 eV, 0.55 ± .03 eV and 0.65 ± .03 eV respectively. These results indicate that the energy of motion is dependent on the ionic radius of the diffusing species, smaller ions having lower activation energies. The summary of Stoebe[9] on bulk diffusion of impurity ions (see Table 2) shows a similar dependence for the divalent cations, Zn^{++}, Mn^{++}, Ca^{++} and Sr^{++}. However, the energies of motion for ions in grain boundaries are lower than for ions of equivalent radius in the bulk material.

The dependence on ionic radius of the relative ease of motion would seem to indicate the presence of discrete sites in the boundary, diffusing cations having to be thermally activated into an adjacent site. Further, the fact that the activation energy is not dependent on the boundary angle indicates that the same mechanism of motion prevails over a wide range of tilt misorientations. The large enhancement in the conductance of ions in the boundary region can be interpreted in terms of a high density of vacancies, and a vacancy mechanism could be responsible for ion motion. An interpretation of the enhanced F-centre formation rate in bicrystals, based on Chang's model[102] of the stress interaction of dislocation dipoles and the associated 'vacancy sheet', supports the hypothesis of high densities of vacancies in boundary regions. Unfortunately, due to the scatter of the

data in the conductivity experiments, arising partially from the rate controlling injection process, an analysis of the relative number of available sites in the boundaries is impossible.

The anisotropic behaviour of the enhanced conductance in the boundary region indicates some columnar dislocation structure for tilt boundaries up to 20° of grain misorientation, while boundaries over 30° indicate a more amorphous structure. The dislocation structure of tilt boundaries up to 12° has previously been observed by Martin, Fehr and McGee[60]. Electrostatic charge considerations and the evidence of discrete grain boundary sites cannot be reconciled with a viscous fluid or liquid model of high angle boundaries in NaCl. The island model, as proposed by Mott[50] and extended by Gifkins[58], is probably more suitable in ionic compounds than the dislocation core 'slab' model of Li[53] or the extended coincidence model of Brandon[56].

The previous experiments[29,70] on the motion of Na^+ ions in grain boundaries and dislocations in LiF gave an activation energy for motion of 0.32 ± .02 eV. The agreement with the present study on NaCl is difficult to explain, and perhaps is the result of coincidence. Experiments on a wider range of alkali halides are necessary before adequate comparisons can be made.

The energy for motion (0.61 eV) of Na^+ ions in edge dislocations in NaCl, as reported by Geguzin and Dobrovinskaya[71], does not agree with the present results. Turner and Whitworth[41] reported that edge dislocations have a charge equivalent to one cation vacancy for every eight sites in the core at room temperature. The number of vacancies in equilibrium with a

dislocation is thermally dependent[39], and thus the activation energy measured by Geguzin et al. could include an energy of association as well as of motion for vacancies in the region of a dislocation. Unfortunately, as no results were obtained for enhanced anion motion, a comparison with previous results[26-28] for enhanced anion motion in grain boundaries cannot be made.

The surface potential profile experiments indicate that surface layers of enhanced resistivity do not exist at free surfaces or at grain boundaries. The observations of Wimmer and Tallan[24] of these layers can be explained in terms of the external circuitry, the specimen, contact and insulation resistance and the contact potential all contributing to give the reported result. D.C. conductivity experiments on bicrystals indicate no measurable polarization at grain boundaries arising from the blocking of charge carriers, at least below 500°C. Thus the interfacial polarization model does not appear to apply in NaCl. The agreement of dielectric loss measurements by Wimmer and Tallan with Volger's model[25] of interfacial polarization, could conceivably be explained in terms of two operative relaxation mechanisms existing throughout the bulk of the material. Each can be assigned an 'effective' width or volume according to its relative contribution to the total effect.

5-2 Suggestions for Future Work

Greater accuracy in the determination of the enhanced conductance of ions in grain boundaries or dislocations can give a value of D'_o as well as of the energy of motion[70], from which a diffusion coefficient (D') for the region may be calculated. Tracer diffusion experiments[28] on polycrystals can give a value of $D'\delta$, where δ is the boundary width. Combining the two experiments then, could give a reasonable estimate of the width of boundary regions.

The surface charge arising from a vacancy distribution or from the mobility of charged dislocations is usually measured with metal electrodes in contact with the specimen. Lamb[101] has pointed out that contact potentials arise from the metal-insulator contact, and that a more accurate determination of surface charge can be made with a Kelvin probe, which operates on the same principle as the Vibron Electrometer and thus avoids direct contact. Using this method to determine surface charge profiles could give evidence of high vacancy concentrations in the near surface or grain boundary region which may give rise to an interfacial polarization mechanism.

A further and more rigorous investigation on the formation rate of colour centres in bicrystals of varying misorientation could yield some information on the interaction of dislocation stresses in boundaries and thus of the structure of grain boundaries. Chang's model[102] for dislocation dipoles would have to be extended to interpret the interaction of stresses from dislocations in grain boundaries.

Acknowledgements

I wish to thank my supervisor, Professor P.L. Pratt, for his initial guidance into the present work and for his continued contributions and stimulus. I would also like to express my gratitude to H. Haddow and A. Lloyd for the quality of the experimental apparatus and to B. Dalgleish and N. Souster for their valuable assistance with the experiments.

The financial assistance of the Athlone Fellowship Committee and the Imperial College of Science and Technology is greatly appreciated. The provision of departmental facilities by Professor Ball and the provision of the cobalt ^{60} source in the Department of Nuclear Technology by Professor Hall are gratefully acknowledged.

Finally, I wish to thank my wife, Diana, for her encouragement, devotion and assistance.

References

1. W. George, Colloquium on Surface Conductivity, (unpublished), University of Leeds, (1969)
2. O.T. Özkan, Colloquium on Surface Conductivity, (unpublished), University of Leeds, (1969)
3. H.G. Van Bueren, 'Imperfections in Crystals', North Holland Publishing Co., Amsterdam, (1961)
4. W.T. Read, Jr., 'Dislocations in Crystals', McGraw-Hill Book Co., N.Y., (1953)
5. J.P. Hirth and J. Lothe, 'Theory of Dislocations', McGraw-Hill Book Co., N.Y., (1968)
6. P.G. Shewmon, 'Diffusion in Solids', McGraw-Hill Book Co., N.Y., (1963)
7. A.B. Lidiard, 'Handbuch de Physik', 20, part 2, Springer-Verlag, Berlin, (1957)
8. D.L. Kirk, Ph.D. Thesis, University of London, (1968)
9. T.G. Stoebe, Ph.D. Thesis, Stanford University, (1965)
10. A.R. Allnatt and P.W.M. Jacobs, Trans. Faraday Soc., 58, 116, (1962)
11. R.G. Fuller and M.H. Reilly, Phys. Rev. Letters, 19, 113, (1967)
12. R.W. Dreyfus and A.S. Nowick, J. Appl. Phys., 33 Supp. 1, 473 (1962)
13. D. Mapother, H.N. Crooks and R.J. Maurer, J. Chem. Phys., 18, 1231, (1950)
14. R. Guccione, M.P. Tosi and M Asdente, J. Phys. Chem. Sol., 10, 162, (1959)
15. F.G. Fumi and M.P. Tosi, Disc. Faraday Soc., 23, 92, (1957)
16. I.M. Boswarva and A.B. Lidiard, Phil. Mag., 16, 805 (1967)
17. L.W. Barr, J.A. Morrison and P.A. Schroeder, J. Appl. Phys., 36, 624, (1965)
18. K.C. Kao, L.J. Giles and J.H. Calderwood, J. Appl. Phys., 39, 3955, (1968)

References

19. A.F. Joffé, 'The Physics of Crystals', McGraw-Hill Book Co., N.Y., (1928)

20. A.R. Allnatt and P.W.M. Jacobs, J. Phys. Chem. Sol., 19, 281, (1961)

21. P.W.M. Jacobs and J.N. Maycock, J. Chem. Phys., 39, 757, (1963)

22. P.H. Sutter and A.S. Nowick, J. Appl. Phys., 34, 734, (1963)

23. R.W. Dreyfus, Phys. Rev., 121, 1675, (1961)

24. J.M. Wimmer and N.M. Tallan, J. Appl. Phys., 37, 3728, (1966)

25. J. Volger, 'Progress in Semiconductors', Vol. 4, John Wiley and Sons, N.Y., (1960)

26. J.F. Laurent and J. Bénard, Comptes Rendus de L'Academie des Sciences (Paris), 241, 1204, (1955)

27. J.F. Laurent and J. Bénard, J. Chem. Phys., 21, 218, (1958)

28. J. Cabané, J. Chim. Phys., 59, 1135, (1962)

29. R.L. Moment and R.B. Gordon, J. Appl. Phys., 35, 2489, (1964)

30. H.C. Graham, N.M. Tallan and R. Russell, J. Amer. Ceram. Soc., 50, 156, (1967)

31. I.I. Frenkel, 'Kinetic Theory of Liquids', Clarendon Press, Oxford, (1946)

32. K. Lehovec, J. Chem. Phys., 21, 1123, (1953)

33. J.D. Eshelby, C.W.A. Newey, P.L. Pratt and A.B. Lidiard, Phil. Mag., 3, 75, (1958)

34. R.J. Schwensfeir and C. Elbaum, J. Phys. Chem. Sol., 26, 781, (1965)

35. I.M. Lifshits and Ya.E. Geguzin, Sov. Phys.-Sol. Stat., 7, 44, (1965)

36. I.M. Lifshits, A.M. Kosevich and Ya.E. Geguzin, J. Phys. Chem. Sol., 28, 783, (1967)

37. R.W. Whitworth, Phil. Mag., 11, 83, (1965)

References

38. R.W. Whitworth, Phil. Mag., 15, 305, (1967)

39. R.W. Whitworth, Phil. Mag., 17, 1207, (1968)

40. N.V. Zagoruiko, Sov. Phys.-Crystal., 11, 375, (1966)

41. R.M. Turner and R.W. Whitworth, Phil. Mag., 18, 531, (1968)

42. A. Hikata, C. Elbaum, B. Chick and R. Truell, J. Appl. Phys., 34, 2154, (1963)

43. J.R. Macdonald, J. Chem. Phys., 23, 275, (1955)

44. J.M. Burgers, Proc. Phys. Soc. (London), A52, 23, (1940)

45. W.L. Bragg, Proc. Phys. Soc. (London), A52, 54, (1940)

46. W. Shockley and W.T. Read, Phys. Rev., 75, 692, (1949)

47. J.H. Van der Merwe, Proc. Phys. Soc. (London), A63, 616, (1950)

48. S. Amelinckx and W. Dekeyser, 'Solid State Physics', Vol. 8, Academic Press, London, (1959)

49. G.T. Beilby, 'Aggregation and Flow of Solids', Macmillan Book Co., London, (1921)

50. N.F. Mott, Proc. Phys. Soc. (London), 60, 391, (1948)

51. W. Shockley, L'Etat Solide, 9th Int'l Solvey Confer., Brussels, (1951)

52. B. Chalmers, Progr. Metal Phys., 3,293, (1952)

53. J.C.M. Li, J. Appl. Phys., 32, 525, (1961)

54. T.D. McGee, 'Material Science Research', Volume 2, Plenum Press, N.Y., (1965)

55. M.L. Kronberg and F.H. Wilson, Trans. Amer. Inst. Min. Metal. Engrs., 185, 501, (1949)

56. D.G. Brandon, Acta Met., 14, 1479, (1966)

57. W.T. Read and W. Shockley, Phys. Rev., 78, 275, (1950)

58. R.C. Gifkins, Mat. Sci. Eng., 2, 181, (1967)

59. G.F. Bolling, Acta Met., 16, 1147, (1968)

60. D.M. Martin, G.K. Fehr and T.D. McGee, 'Material Science Research', Vol. 3, Plenum Press, N.Y., (1966)

References

61. M.L. Gimpl, A.D. McMaster and N. Fuschillo, 'Material Science Research', Vol. 3, Plenum Press, N.Y., (1966)

62. M.L. Gimpl, A.D. McMaster and N. Fuschillo, J. Amer. Ceram. Soc., 51, 655, (1968)

63. N. Fuschillo, M.L. Gimpl and A.D. McMaster, J. Appl. Phys., 37, 2044, (1966)

64. S.A. Long and T.D. McGee, J. Amer. Ceram. Soc., 46, 583, (1963)

65. D. Turnbull and R.E. Hoffman, Acta Met., 2, 419, (1954)

66. B.J. Wuensch and T. Vasilos, 'Grain Boundary Diffusion in MgO', Office of U.S. Naval Research, Report No. NONR 4267 (00)

67. J.C. Fisher, J. Appl. Phys., 22, 74, (1951)

68. R.T.P. Whipple, Phil. Mag., 45, 1225, (1954)

69. L.W. Barr, I.M. Hoodless, J.A. Morrison and R. Rudham, Trans. Faraday Soc., 56, 697, (1960)

70. R. Tucker, A. Laskar and R. Thompson, J. Appl. Phys., 34, 445, (1963)

71. Ya.E. Geguzin and E.R. Dobrovinskaya, Sov. Phys.-Sol. Stat., 7, 2826, (1966)

72. E.W. Hart, Acta Met., 5, 597, (1957)

73. R. Smoluchowski, Phys. Rev., 87, 482, (1952)

74. J.H. Westbrook, Met. Rev., 9, 415, (1964)

75. J. Quin, Ph.D. Thesis, University of London, (1967)

76. H.W. Etzel and D.A. Patterson, Phys. Rev., 112, 1112, (1958)

77. D.A. Otterson, J. Chem. Phys., 34, 1849, (1961)

78. L.W. Barr, F.P. Koffyberg and J.A. Morrison, J. Appl. Phys., 33, 225, (1962)

79. S.K. Agarwal and A.P. Kulshreshtha, Indian J. Pure Appl. Phys., 5, 535, (1967)

80. R.W. Dreyfus, 'The Art and Science of Crystal Growing', John Wiley and Sons, N.Y., (1963)

References

81. R.W. Warren, Rev. Sci. Instr., 36, 731, (1965)

82. O. Samuelson, 'Ion Exchange Separations in Analytical Chemistry', John Wiley and Sons, N.Y., (1963)

83. F.C. Nachod and W. Wood, J. Amer. Chem. Soc., 66, 1380, (1944)

84. J. Beukenkamp and W. Rieman, Anal. Chem., 22, 582, (1950)

85. O. Samuelson and E. Sjöström, Anal. Chem., 26, 1908, (1954)

86. E.D. Olsen and H.R. Sobel, Talanta, 12, 81, (1965)

87. R. Turse and W. Rieman, J. Phys. Chem., 65, 1821, (1961)

88. L.D. Pennington and M.B. Williams, Ind. Eng. Chem., 51, 759, (1959)

89. H.P. Gregor, M. Taifer, L. Citarel and E.I. Becker, Ind. Eng. Chem., 44, 2834, (1952)

90. P.M. Gruzensky, J. Chem. Phys., 43, 3808, (1965)

91. C.T. Butler, L.R. Russell, R.B. Quincy and D.E. LaValle, J. Chem. Phys., 45, 968, (1966)

92. E. Sandell, 'Colorimetric Metal Analysis', Interscience Publishers, N.Y., (1959)

93. L. Alders, 'Liquid-Liquid Extractions', Elsevier Publishing Co., Amsterdam, (1955)

94. T. Takagi and H. Imoto, Japan Analyst, 7, 565, (1958)
Japan Analyst, 8, 782, (1959)

95. Circular Number 164-280, Dow Chemical Corp., (1959)

96. F. Rosenberger, Mat. Res. Bull., 1, 55, (1966)

97. P.W. Bridgeman, Proc. Amer. Acad. Sci., 60, 306, (1925)

98. S. Kyropoulos, Z. Anorg. Allg. Chem., 154, 308, (1926)

99. S. Hosoya, S. Satake and S. Takagi, J. Phys. Soc. Japan, 11, 1228, (1956)

100. A. Taylor, Ph.D. Thesis, University of Birmingham, (1958)

101. D. Lamb, Southampton University, private communication

102. R. Chang, Phys. Rev., 138, A839, (1965)

103. R.W. Davidge and P.L. Pratt, Phys. Stat. Sol., 3, 665, (1963)

References

104. G. Arai and J.G. Mullen, Phys. Rev., 143, 663, (1966)

105. A. Kessler, E. Mariani and V. Paulíny-Tothová, Czech. J. Phys., B14, 34, (1964)

106. A.N. Murin, S.N. Banasevich and Yu.S. Grushko, Sov. Phys.-Sol. Stat., 3, 1762, (1962)

107. B.G. Lur'e, A.N. Murin and R.F. Brigevich, Sov. Phys. -Sol. Stat., 4, 1432, (1963)

108. H.N. Hersh and L. Bronstein, Amer. J. Phys., 25, 306, (1957)

109. R.L. Wild, Amer. J. Phys., 35, 1023, (1967)

110. S.C. Jain and G.D. Sootha, J. Phys. Chem. Sol., 26, 267, (1965)

111. J.J. Markham, 'F-centres in Alkali Halides', Academic Press, N.Y., (1966).